Hydrodynamic modeling of the Bay of La Rochelle to support the control of accidental oil spills

Fernando de Oliveira Machado

Dissertação para obtenção do Grau de Mestre em

Engenharia do Ambiente

Orientador: Professor Doutor Ramiro Joaquim de Jesus Neves

Co-orientador: Engenheiro Rodrigo Manuel Antunes dos Santos Fernandes

Júri

Presidente: Professor Doutor Tiago Morais Delgado Domingos

Orientador: Professor Doutor Ramiro Joaquim de Jesus Neves

Vogais: Professora Doutora Maria João Correia Colunas Pereira

Dezembro 2014

ABSTRACT

We validate a hydrodynamic system of the Bay of La Rochelle, providing Historical observations and predictions of several atmospheric and water conditions, including hydrodynamic properties.

We characterize the system application area, mainly his circulation patterns. Modeling system framework is explained, as well as main tools involved and developed are described. Different components of data acquisition are analyzed, and water modeling system applied – MOHID – is studied.

The model was implemented by using Mohid Water modelling system. The report describes data used to implement the model and their preprocessing. The hydrodynamic model was implemented by using downscaling technique including nested domains.

We make an analysis of modeling scheme configuration, and main options taken in that subject.

Modeling results are compared with information obtained from automatic stations, monitoring campaigns, acoustic Doppler profilers (ADCP) and empirical data estimated from historical measurements made by tidal gauges.

The hydrodynamic model will provide hydrodynamic forecasts which will be used to assess the best location of oil booms in the occurrence of oil spill. The model is used to predict the movement and dispersion of small patches of oil to support the use of containment barriers. Scenarios are simulated to study most typical consequences of spill occurring on local with more marine traffic.

Key Words: MOHID, modeling, La Rochelle Bay, hydrodynamics, oil spill.

RESUMO

Validamos um sistema hidrodinâmico da Baía de La Rochelle, proporcionando observações históricas e previsões de várias condições atmosféricas e aquáticas, incluindo propriedades hidrodinâmicas.

Caracterizamos a área de aplicação do sistema, principalmente os padrões de circulação. Estrutura do sistema de modelagem é explicada, bem como ferramentas principais envolvidos e desenvolvidos são descritos. Diferentes componentes de aquisição de dados são analisados, e sistema de modelação de água aplicada - MOHID - é estudado.

O modelo foi implementado usando o sistema de modelação MOHID Water. O relatório descreve os dados utilizados para implementar o modelo e seu pré-processamento. O modelo hidrodinâmico foi implementado utilizando downscaling técnica incluindo domínios aninhados.

Fazemos uma análise da configuração do sistema de modelação e principais opções tomadas nesse assunto.

Resultados da modelação operacionais são comparados com informações obtidas de estações automáticas, campanhas de monitoramento, perfiles acústico Doppler (ADCP) e dados empíricos estimativos a partir de medições históricas feitas por medidores de maré.

O modelo hidrodinâmico irá fornecer previsões hidrodinâmicas que serão utilizadas para avaliar a melhor localização de barreiras na ocorrência de derramamento de hidrocarbonetos. O modelo é utilizado para prever o movimento e a dispersão de pequenas manchas de hidrocarbonetos para suportar a utilização de barreiras de contenção. Os cenários são simulados para estudar as consequências mais comuns de derrame que ocorre em local com mais tráfego marítimo.

Palavras-Chave: MOHID, modelação, La Rochelle, hidrodinâmica, derrame de hidrocarbonetos.

ÍNDICE

FIGURES INDEX

TABLE INDEX

1. INTRODUCTION

1.1 Context

The subject for this thesis started off from the ISDAMP (Improvements of Shorelines Defences Against Marine Pollution) project funded by the Directorate General of the European Civil Protection aims the development of an operating system to support the containment of oil spills in port areas. The project involves the use of a behavior model of oil barriers in different regimes of chains and a hydrodynamic model capable of predicting high resolution currents.

The system should run in forecast mode to optimize the tasks to be carried out between the time when the spill occurs and when it is possible to combat it. Combat is done by placing barriers that have to be moved from storage to the place of combat. To optimize this task is necessary to know the expected displacement and dispersion of the plume will occur. The shift is important to know where to move the barriers and extent of stain is required to predict the length of barrier needed.

Spills in ports are usually small and geometry is often complex, including docks and dock mooring. As a result the flow is complex, including recirculation zones whose extent depends on the state of the tide. Under these conditions the system modeling should include a hydrodynamic model for the fine mesh embedded in a harborside global model of the bay.

1.2 Objectives

Validation of a hydrodynamic model of the Bay of la Rochelle and an embedded modelling system able to simulate the flow in the port area with a high resolution spatial step and its use to predict the movement and dispersion of small patches of oil to support the use of containment barriers.

1.3 Methodology

The work will be based on the model implemented in La Rochelle (with MOHID Water modelling system) forced by the tide bordering the sea and the river flow Loire bordering land. The model is implemented with a domain with a mesh step of the order of 500 meters to the La Rochelle zone and the area of the plume. The 500 meter model will be fitted with a model of tidal step of approximately 2.5 km to a zone with a length of around 200 km. The 2.5 km model will be fitted with a model 7x12 km to a zone with a length about 300 km. The 7x12 km model will be fitted with a model 7x12 km to a zone with a length about 400 km to be forced by the tide model FES2004. The system is therefore made up of four models.

In this study we use a 2D hydrodynamic barotropic model to provide boundary conditions (tide) to nested submodels. The nested modelling approach was used because the computation time is not feasible for a full model for the whole domain.

The Gironde river (in particular the parts of the river affected by tidal force) must be inside the modeled zone.

The time period on the test simulation was selected to coincide with available in situ data. The spin up time of the model is on the order of 2 weeks. In order to validate the model using available data, a preliminary simulation of 6 months is carried out from January 1st 2012 to July 1st 2012.

After the initial tests with uniform winds, system was forced with variable wind fields downloaded from NOAA GFS model, and interpolated to mesh the model. The river flow is provided in the form of time series with values obtained from the Water Agency in the region. Once validated the system of hydrodynamic models tests will be conducted with oil spill scenarios.

2. STUDY AREA – LA ROCHELLE

2.1 Context

The Charente coast (**Figure 1**) is located in the middle of the French Atlantic coast along the Bay of Biscay, surrounded by the rocky coastline of South Brittany, in the north, and that of Aquitaine, straight and sandy, the south. It consists of approximately 460 km of coastline, mainly due to the presence of two major islands that are the island of Ré and Oléron Island (about 200 km coastline).

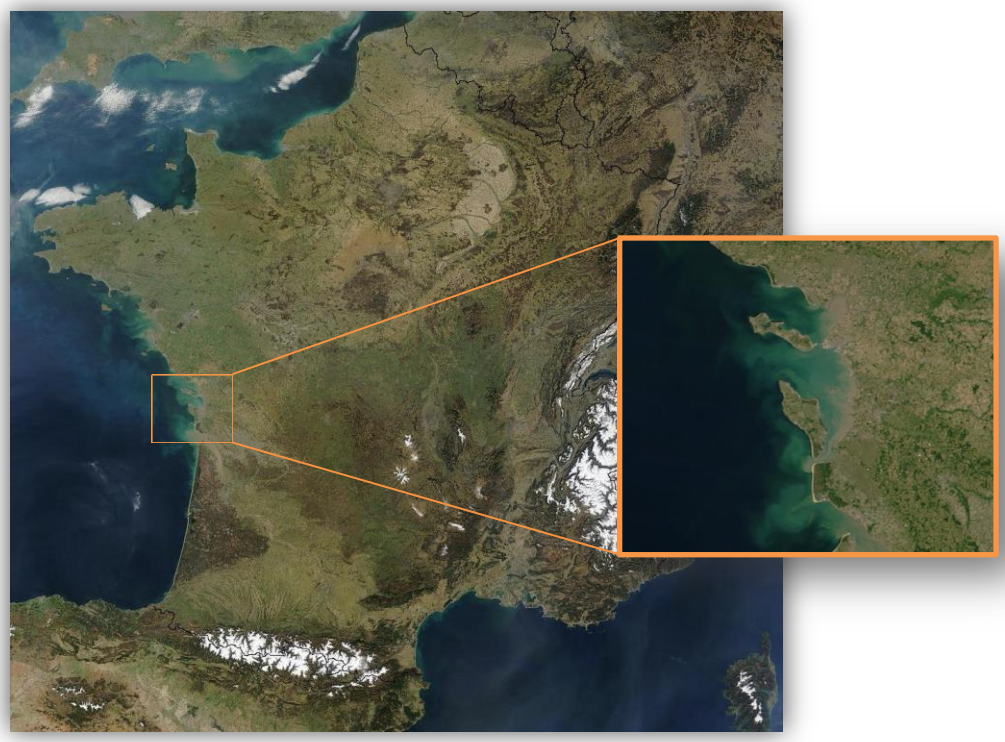

Figure 1 : Study area

These islands are separated from the mainland by maritime areas locally called «Pertuis», which correspond to segments of incised valleys [Chaumillon & Weber, 2006].

From north to south, we can characterize the Pertuis Charentais (**Figure 2**) in three different areas:

- The Pertuis Breton, between the Ile de Ré and the South Vendee coast, represents an area of 360 km^2;

- The Pertuis of Antioch, between the island of Ré and Oléron Island, represents an area of 350 km^2;

- The Pertuis of Maumusson, between the southern tip of the island of Oléron and the coast, represents an area of 260 km^2.

The Pertuis Breton is the incised valley of the Sèvre river and Lay, the Pertuis of Antioch is the one of the Charente river and the Pertuis de Maumusson the one of the Seudre river.

The Pertuis Breton and Pertuis of Antioch communicate with each arm of the sea, locally called "La Pallice".

The Pertuis of Antioch is the largest of the three Pertuis and includes both sites of the harbor of La Rochelle (north) and the island of Aix (south).

Figure 2 : Pertuis Charentais

The two main islands of Ré and Oléron, oriented Northeast / Southwest protect the areas from ocean swell forming tidal bays. The main one is the Bay of Marennes-Oléron (160 km2), located south of the Pertuis of Antioch between Oléron Island and the mainland. It is characterized by numerous and extensive intertidal flats (about 60% of the total area) interspersed with small tidal creeks. This semi-closed environment is identical to estuaries of mixed type dominant tide. [Gouriou,2012].

2.2 Geological and geomorphological setting

The sediments show complex distribution patterns on the seafloor in the Pertuis Charentais (**Figure 3**). According to the synthetic map of sedimentology surface, produced by SHOM (Naval Hydrographic and Oceanographic Service), there are four main types of sediment bedrock, gravel, sand and mud. The bedrock is large reef flats that are found mostly in the western islands of Ré and Oléron where strong currents prevent the deposition of sediments.

The Pertuis Charentais Sea is covered mainly by sandy mud and mud. This mud drape spreads towards the west, infilling the deepest parts of the Chevarache and Antioche Deeps. It is bounded by rocky outcrops covered by discontinuous patches of sand (fine sand to gravel) emplaced on the slopes of the incised valleys. The northern slope of the Chevarache Deep is covered by a vast area of gravel to fine sand, whereas the southern slope is characterized by a complex combination of gravel, sand and muddy sand patches extending within the Breton Inner Domain.

The eastern part of the Pertuis Breton (approximately 25% of its entire surface) is covered by mud. This mud plain is flat without any significant bed ripples or dunes. The central and western parts of the PB are, in contrast, full of sand banks, dunes and ripples [Barusseau, 1973; Schillinger, 2000; Weber *et al.*, 2004]. This transition between the smooth mud flat in the east of the PB to the rippled heterogeneous bed in the middle and in the west suggests the sea bed roughness variations along the PB leading to spatial variability of friction coefficient.

Discontinuous sand patches and rocky outcrops occur in the Antioche Inner Domain. The western part of the Marennes-Oléron Bay is composed of mixed sand and mud flats, whereas the eastern part is covered by the mud drape. Tidal channels in the bay are filled mainly with sand. The interior of the Pertuis is mostly covered by fine sediment type mud, from the Bay of Aiguillon to the Bay of Marennes-Oléron. Other sandbars appear, especially at the Pertuis Maumusson because of strong tidal currents dominating. To the south, the Maumusson Inlet is filled with sand and gravel.

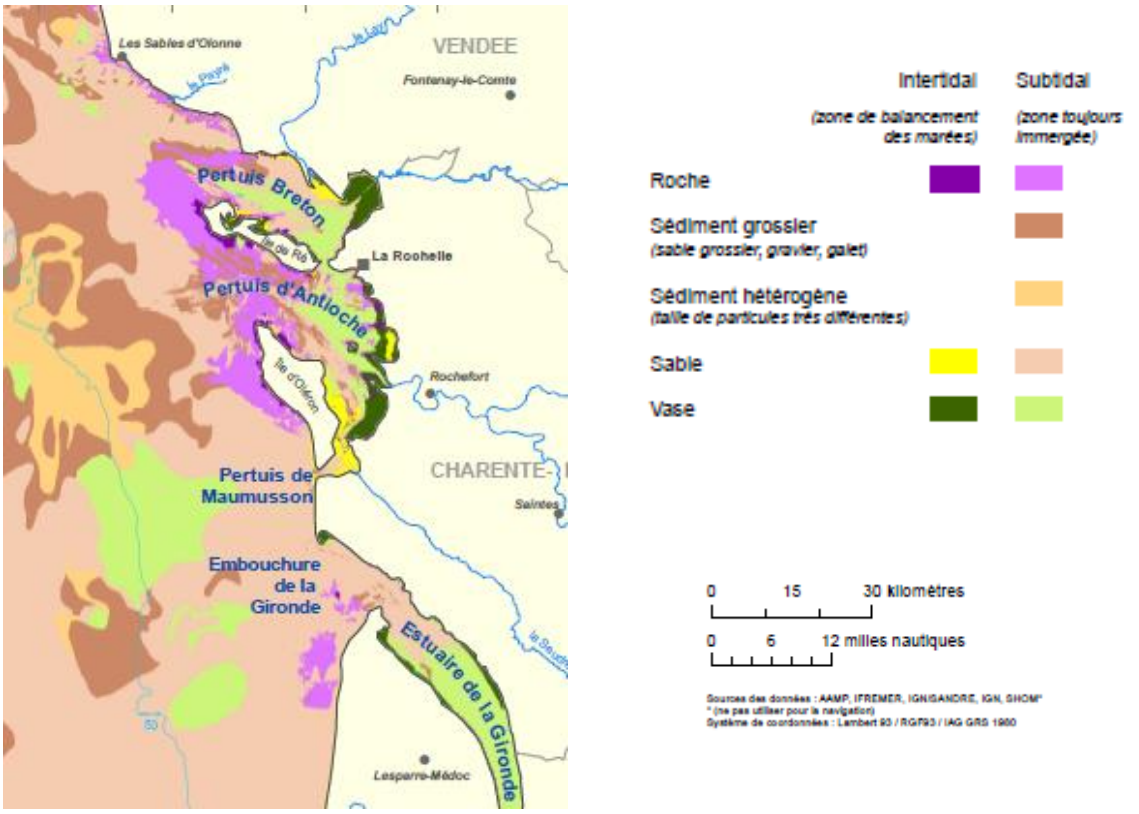

Figure 3 : Sediment map (AAMP, IFREMER, IGN/SANDRE, SHOM) 2011
(roche :bedrock, sediment : sediment, sable : sand and vase : mud)

The bathymetry of the area gradually increases the continent seaward to a maximum of 66 m at the edge of the continental shelf of the Bay of Biscay. The Pertuis Breton and of Antioch both measure about 30 km long and 10 km wide. Overall, the Pertuis Charentais is a shallow area, with the exception of two pits, Chevarache and Antioch Deeps. [Amandine Nicolle, Mikhail Karpytchev,2007]

2.2.1 Geomorphology of the Pertuis Breton

The Pertuis Breton is a coastal embayment, approximately 30km_10 km. The deeper part of the Pertuis Breton is in the west, near the seaward boundary with depth of about 25–30 m, Chevarache deep. The bottom shoals rapidly eastwards where typical depth is about 5m. Extensive tidal flood plains border the Pertuis Breton coasts and are particularly large near the northern and eastern shores. There is no significant fresh water discharge into the Pertuis Breton. Near the city of La Rochelle, the Pertuis Breton is connected to the neighboring basin of the Pertuis of Antioche by a 2km wide passage. In a first approximation, the Pertuis Breton can be seen as an almost rectangular shallow basin with a deeper western part and very shallow eastern flats.

2.2.2 Geomorphology of the Pertuis of Antioch

The inner part of Pertuis of Antioch, called the Basque Roads, is characterized by the fund less deep as it moves towards the mouth of the Charente, Antioch Deep (depth of about 40 m), orientation North-West / South East, isolated western continental shelf by a shoal peaking at - 19 m: the Inter-Islander threshold. [Gouriou, 2012, Poirier, 2010]

It is also characterized by several peaks and rocky peninsulas. Tidal channel, located in the extension of the mouth of the Charente, is bordered by a sandbar lying oriented Northwest / Southeast, locally called loin Boyard, and located at the southern end of the Antioch deep, between the island of Aix and Oléron. This sandbar is approximately 8 km long and 2 km wide and up to 10 m thick [Chaumillon et al., 2008]. It is bordered by two channels, reaching locally up to 15 m depth, which provide communication between the Pertuis and the Bay of Marennes-Oléron.

2.2.3 Geomorphology of the Pertuis of Maumusson

Although it forms part like the other two Pertuis in an incised valley, the Pertuis of Maumusson has a different morphology, characteristic of a tidal estuary [Bertin *et al.*, 2005].

2.3 Hydrological context

Four rivers flow into the Pertuis Charentais: The Lay, the Sèvre river, Charente and Seudre. Flows and watersheds of these rivers are low compared to those of the Gironde estuary, located on the southern edge of the Charente coast, as shown in the

Table 1 below.

River	Watershed (km^2)	Length (km)
Lay	978	55
Sèvre Niortaise	3620	95
Charente	10550	365
Seudre	955	46
Gironde	74000	585

Table 1 : Rivers flow

The annual mean flow of the Charente is about 50 m^3/s [Tesson, 1973] and can reach up to 250 m^3/s during floods. The annual medium flow of Lay and Sèvre river are about 5 m^3/s, while that of the Seudre is extremely low (about 0.5 m^3/s). Even in times of flood, these volumes remain very weak against the volume of water displaced by the tide [Tesson, 1973, Bertin *et al.*, 2005. Chaumillon *et al.*, 2008.]. Forty coasts of lesser importance, which the outlets provide additional freshwater input in Pertuis marshes, are also distributed along the coast [Weber, 2004].

Sediment supply in the Pertuis of Antioch attributed to the Charente would be around 41 000 tons per year [Gonzalez et *al.*, 1991].

Although the largest resort lagoon in Europe is located in Rochefort, 15 km upstream of the mouth of the Charente, its impact on the river represents only an annual mean flow of 0.05 m^3/s, which is negligible [Modéran, 2010].

The Gironde estuary is shared by two rivers: the Garonne and Dordogne, and is the largest estuary in Western Europe, with 75 km long and up to 12 km wide and covers an area of 635 km^2.

The Garonne and Dordogne bring annual medium flow of 800 to 1,000 m^3/s freshwater charged with sediments; at the same time twice a day the tide brings 15 000 to 25 000 m^3 of seawater, which promotes the formation of sandbars and islands of vasards. The encounter of the fresh water rich in alluvial deposits, with salt water flocculated clay particles that form a "silt plug" characteristic of estuarine waters. Gironde carries each year from two to eight million tonnes of suspended particles. Part of suspended solids (1.5 to 3 million tons per year) is deposited, forming sandbars and islands. The Gironde estuary is highly subject to the ebb and flow of the tides. This dynamic tide flows far upstream in the estuary (up to 150 km from the mouth).

2.4 Meteorological context

The Charente coast is subject to an oceanic climate: mild temperatures and moderate rainfall (in relation to the Atlantic disturbances).

2.5 Atmospheric pressure

The few statistics regime atmospheric pressures Charente coastline are calculated from data sets level pressure of the Enet Boyard sea, over the period 1860-1909. There are two classic seasonal periods: winter (November to March) where the differences between the average monthly minimum and maximum are high (above 20 hPa) resulting in significant and rapid weather changes, and summer (May-August) where the differences are small (generally less than 10 hPa), which means that the atmosphere is calmer, and its changes are less important. In general, the values of atmospheric pressure measured in the Charente coast can browse a range of about 85 hPa, 967 hPa to 1050 hPa. [Weber, 2004]

2.6 Wind

The winds of the Charente coast are measured continuously for a little more than fifty years, through the resorts of La Rochelle. The statistics produced by Météo France, from data collected by the National Marine semaphores on the Bay of Biscay, can observe certain homogeneity of wind conditions between the Loire and Gironde. The most prevalent winds are of marine origin from the directions North West South West (50% of observations). In this category, 75% of the wind speedis between 4 and 16 knots throughout the year. The strongest winds (over 25 knots) are recorded from September to April and then up during this period, 25% of the observations [Weber, 2004].

Monthly statistics (**Figure 4**) identify two main seasonal patterns:

• A "winter" feature for months of October to March :

- Very strong winds (> 33 knots, Beaufort 7) blow for nearly 1% of the time Chassiron and 0.5% of the time in La Rochelle. Strong winds (22 to 33 knots, 39 to 61 km/h) blow for more than 10% of the time Chassiron against only 3.3% of the time in La Rochelle, mainly oceanic sector (SW to NW).

- Light winds at Chassiron (1-10 knots) come primarily from the continent, the NE to SE, for a cumulative <48% of the time frequency. At La Rochelle, these light winds also come mostly from the mainland (N sector S) but with a significant proportion of W sector (6% of observations), and a cumulative frequency of more than 57%.

• A "Summer" feature for month from April to September:

- There are no strong winds (> 33 knots, 62 km/h).

- Strong winds (22 to 33 knots, 39 to 61 km/h) blow for 3% of the time Chassiron and 1.7% of the time in La Rochelle, mainly oceanic sector (SW to NW).

- Weak winds near 60% of the time, mainly to West North East (NW 15% of the time Chassiron, N 14% of the time and W 13.5% of the time in La Rochelle).

Statistics on the annual distribution of the wind depending on the direction of La Rochelle were performed by Météo-France from 1991 to 2002. These statistics, conducted over a shorter period, did not show significant differences compared to those outlined above.

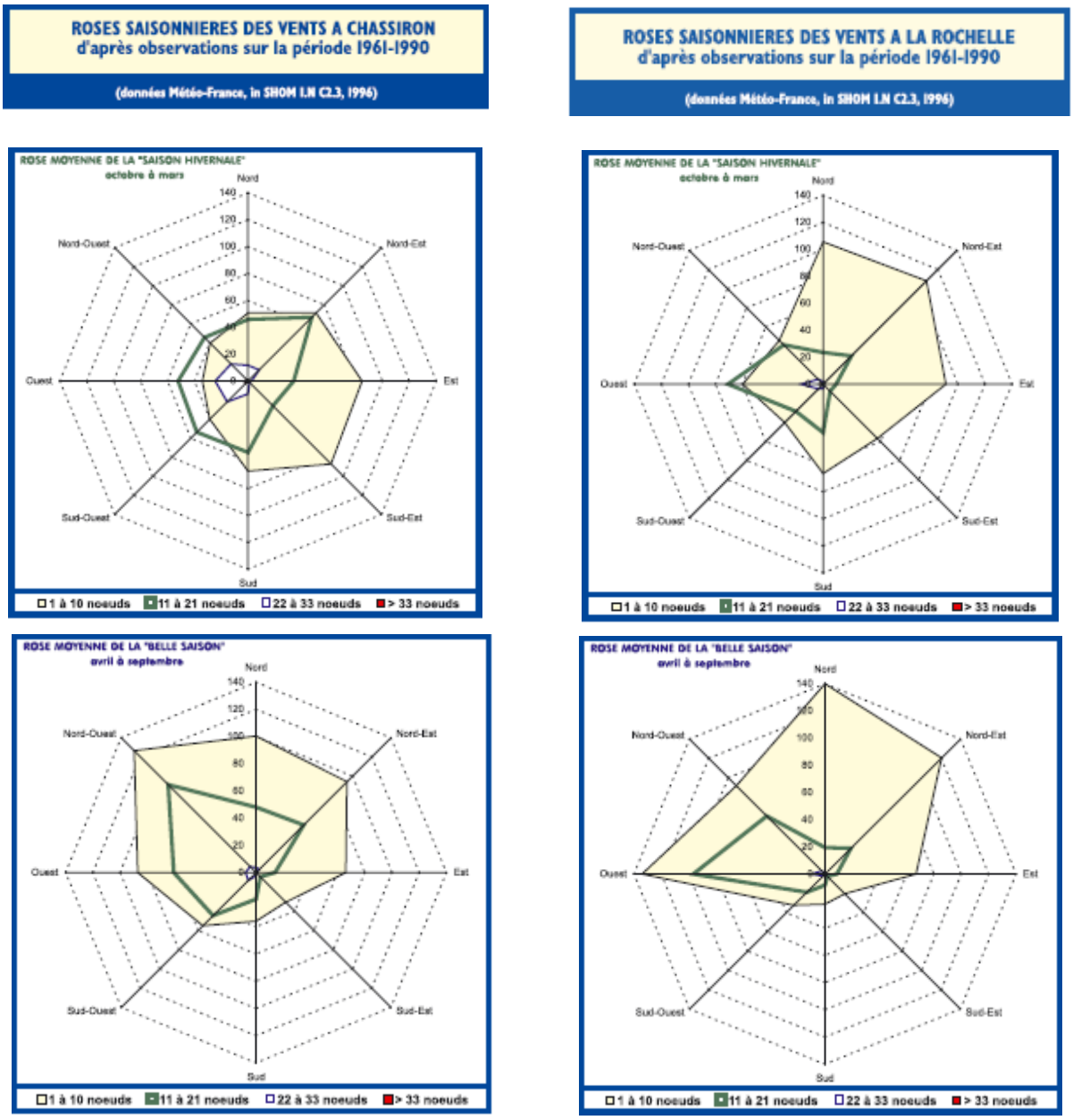

Figure 4 : Seasonal distribution of winds in the direction and intensity for the period 1961-1990 for Chassiron and La Rochelle (Météo France).

(North, South, East, West, wind unit in knots, "saison hivernale": winter, "belle saison": summer).

2.7 Hydrodynamic

Ocean currents are characterized at a given time and a given position by their direction and speed. We can distinguish several types of ocean currents:

- Tidal currents
- Current formed by wave
- Current drift due to wind
- Current slope due to the raised level of the sea near the coast
- Current density related to movements of ocean water masses

2.7.1 Swell

Swell are formed off in the wind, before spreading and reaching the coast. It has a strong seasonal variation in the Bay of Biscay, and more particularly on the Charente coast. The studies of Bertin et *al.* (2008) between 1997 and 2005 recognize two characteristic periods. The summer swells (April to October) that represent about 64% of the wave climate. They are oriented west-northwest, amplitude ranging between 0.8 and 2.5 m and the period between 6 and 12 s. Winter swell (November to March) are more energetic an represent about 21% of the wave climate. They are oriented west, amplitude ranging between 2.5 and 9.4 m and the period between 11 and 15 s.

At the entrance of Pertuis the swell are refracted and attenuated by the sides of the pits Chevarache and Antioch. They reach the coast with a high angle of incidence which induces a longshore drift globally oriented from north to south. The most frequent winds are of oceanic origin, with north-west to south-west direction [data Météo-France, Weber, 2003] that contribute to the littoral drift through the sea wind. The winds of the northeast and to a lesser extent southeast, frequent in late summer, can generate wind waves of short (<5 s) and low amplitude (<0.5 m).

2.7.2 Tide

The Charente coast is characterized by a semi-diurnal tide (two cycles of high and low tide per lunar day 24h50), as the Bay of Biscay. According to official data published by SHOM [SHOM, 2011], the average tidal range of spring tide is 5.10 m in La Rochelle. The coasts of the load are macrotidal types. The average tidal range of neap tide is lower: 2.45 m and 2.50 m La Rochelle to Ile of Aix. The maximum drawdown reached only by astronomical tide is 6.69 m in La Rochelle and 6.68 m in the island of Aix. The tide propagates in the southern Bay of Biscay to the north. Upon entering the Pertuis Charentais, it is amplified and distorted.

As the wave enters the inlet of the Bay it takes 40 minutes after it has passed through the Pertuis of Maumusson in spring tides (Tesson, 1973). Ebb currents which then tend to "dump" the southern part of the bay are accelerated by Flow currents from the north. This generates a current dominance Wot in the northern part of the bay and ebb in the southern part (Allard et al., 2010) and establishes a

residual tidal circulation oriented clockwise around the Oléron island, unless the winds contradict this general trend [Stanisiere *et al.*, 2006].

The residence time of water masses in the Pertuis is short (a few days in the Bay of Marennes-Oléron) [Bacher, 1989] and participates to the mixing of fresh and salt water. Freshening facies (<20 psu) are restricted to estuaries of coastal rivers. In contrast, the salinity in Pertuis reach only rarely values 35 psu, mainly because of the influence of the plume of the Gironde (between 25 and 30 psu) [Le Moine, 2009].

2.7.3 Currents

Due to the weakness of the mainstream in the Bay of Biscay and the Pertuis Charentais appearance, it is the tidal currents govern the circulation of water masses.

Circulation in the Pertuis Breton and Antioch

The tide enters simultaneously in two sluices. The waters from the sluice of Antioch feed the bay of La Rochelle and the Coureau of Pallice and part of the Bay of Aiguillon (also powered by Pertuis Breton). The water from the sluice Breton does not enter the Coureau the Pallice, and therefore does not affect circulation in the bay La Rochelle. Ebb tide waters are returned by the openings which they originate.

Based on the work describing the tidal circulation in the openings Charentais (SHOM, 1993 – [MACUR 1999] Courant de marée de la côte Ouest de France, de St Nazaire à Royan - nº559 - UJA), current velocities in the Bay of La Rochelle stood, outside weather influence, during a tide as follows (**Figure 5**).

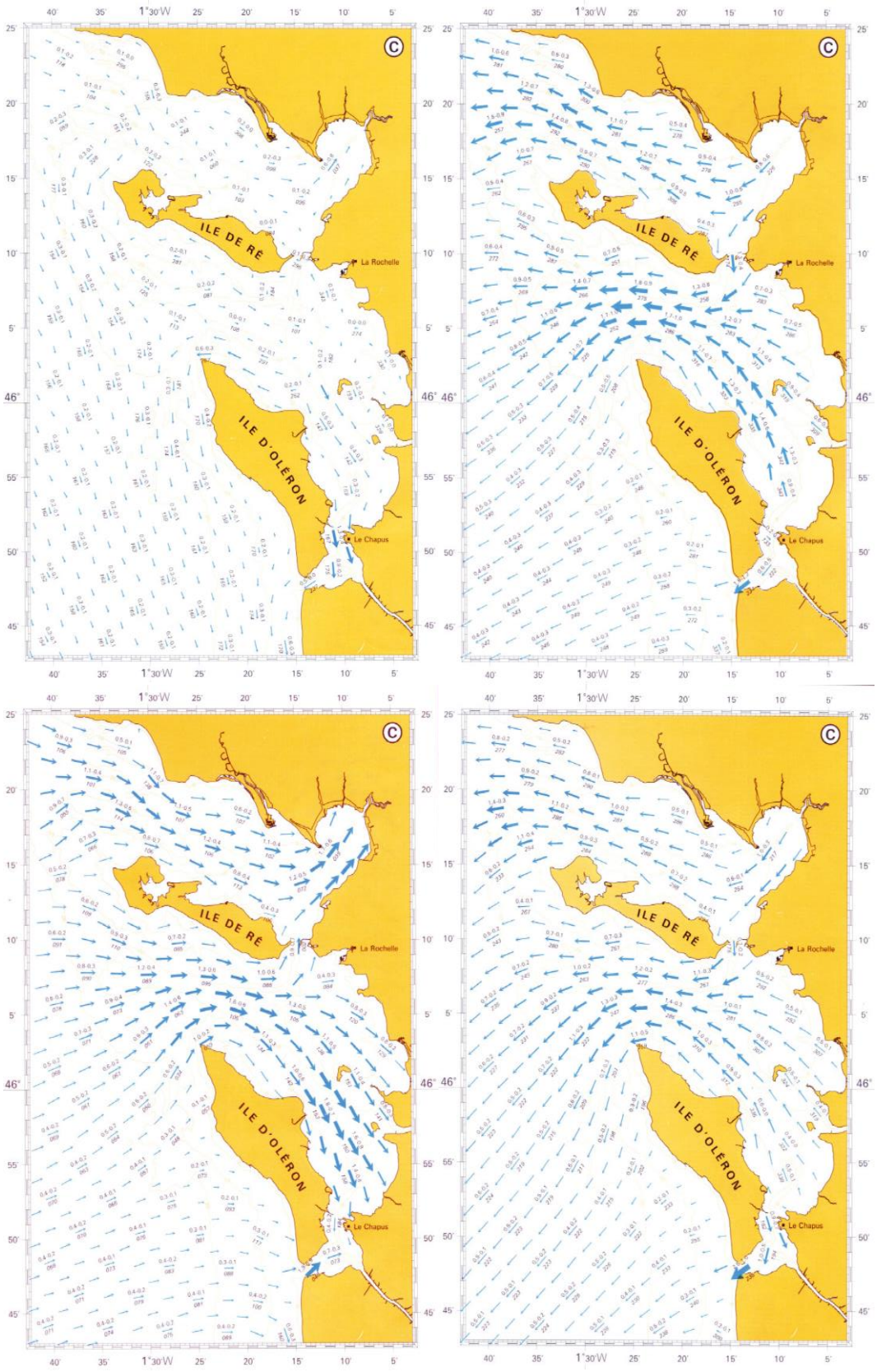
1°30'W
ILE DE RÉ
ILE D'OLÉRON
La Rochelle
Le Chapus
46°

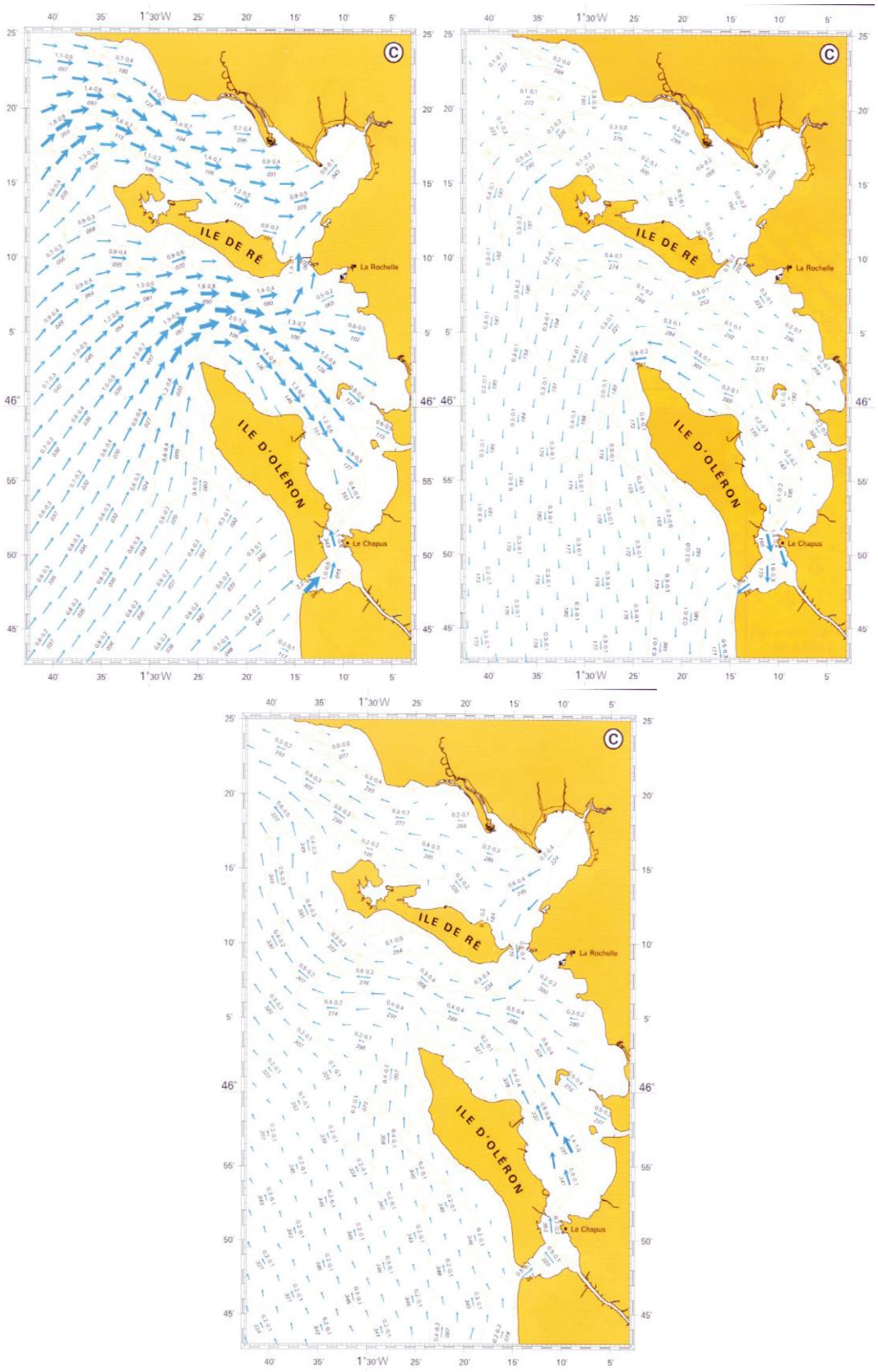

Figure 5 : Maps of tidal currents on the surface for the periods before and three hours after low tide in La Pallice port. (© SHOM – 1993 – Courant de marée de la côte Ouest de France, de St Nazaire à Royan - nº559 - UJA)

Among these various currents, tidal often distinguished by its relatively high speed, especially near the coast and especially along the Charente coast. Maximum speeds are 2 to 3.5 knots and are at both ends of the western islands of Ré and Oléron and at the level the Pertuis Maumusson.

		VIVE EAU (95)		MORTE EAU (45)	
		Partie aval (axe Pte Minimes-Port Neuf)	Partie médiane du chenal	Partie aval (axe Pte Minimes-Port Neuf)	Partie médiane du chenal
Jusant	BM –6h	0.1	0.1	0	0
	BM –5h	0.1	0.1	0.1	0
	BM –4h	0.2	0.1	0.1	0
	BM –3h	0.3	0.1	0.2	0.1
	BM –2h	0.5	0.3	0.1	0.2
	BM –1h	0.6	0.4	0.1	0.1
	BM	0.1	0.1	0	0
Flot	BM +1h	0.6	0.5	0.3	0.1
	BM +2h	0.5	0.4	0.2	0.1
	BM +3h	0.3	0.2	0.2	0.1
	BM +4h	0.2	0.2	0.1	0.1
	BM +5h	0.2	0.1	0.1	0.1
	BM +6h	0.1	0.1	0.1	0

Table 2 : Tidal current La Rochelle

(vive eau 95 : spring tide, morte eau 45 : neap tide, Basse Marée : low tide, jusant : ebb, flot : flood)

Overall, the tidal currents in the Bay of La Rochelle have two main features (**Table 2**):

- They are alternative and regular. They are in the axis of the channel, i.e. to West southwest tide (ebb) and East North East tide rising (flood).
- Their speeds are low or very low (0.6 knots maximum).

The speeds are an increasing gradient from upstream to downstream of the channel.

There are two types of disturbances that can be observed in the Bay of La Rochelle:

- The waves of oceanic origin which are generated off the Pertuis Charentais and are characterized by relatively high periods. The resulting agitation the vicinity of La Rochelle depends essentially on the deformation of the wave in the sluice of Antioch (refraction, damping, and flood).
- Local swell (sea wind, wind waves) are formed under the direct action of the wind and are typically short periods. They depend on the intensity, direction, distance and duration of action (fetch) the wind.

The actual agitation is a complex combination of different types of waves (amplitude ocean swells and wind waves and different periods). Some phenomena (interaction effect of wind on the ocean waves) can locally increase agitation expected theoretically.

2.8 Anthropogenic impacts

The Pertuis Charentais are subjected to strong anthropogenic impacts, especially because it is one of the largest shellfish farming areas in Europe. Cultivated species are non-native as oyster Crassostrea gigas and the Manila clam Ruditapes philippinarum or native mussel Mytilus edulis.

The development of cultures oysters and mussels across the Charente coast begins in the 19th century. Bay of Marennes-Oléron is today one of the most important European centers with an oyster shellfish stock about 95 000 tons with an annual production of about 35 000 to 40 000 tons [Modéran, 2010].

Shellfish farms are distributed throughout the region, mostly on the lower part of the tidal flats, an area of over 175 km2. Mussel areas (38%) are concentrated in the Pertuis Breton while oyster areas (62%) are more abundant in the Bay of Marennes-Oléron [Bertin, 2005].

The Figure **6** show the geographical extend of those cultures.

However, this important economic activity has an impact on the morphological evolution of the bay. Shellfish facilities, which create barriers to tidal currents and sea wind, and the production of pseudo-faeces by oysters promote both the settling of fine sediments. The volume of accumulated sediment in oyster areas since 1824 is estimated to be 35.10^6 m3, or 30% of the total volume of sediment deposited in the bay of Marennes-Oléron since that date (Bertin & Chaumillon, 2006).

These sluices are characterized by a very high natural production. The reduced mixture with sea offshore is highlighted by a lower salinity. This allows the maintenance in these coastal waters, natural production, and this feature explains the development for nearly three centuries of shellfish.

Nearshore zone is used for fishing, boating and water activities. The offshore area is operated by offshore fishing.

These sea activities must also coexist in terrestrial coastal area with tourism, industrial and agricultural activities on the one hand, with the urbanization of the other. Very close to the sea (less than 500 m), 25.5% of the soil is Artificialized. [Observatoir du littoral, 2000].

These activities across multiple functions and uses of water resources are the source of conflicts of use.

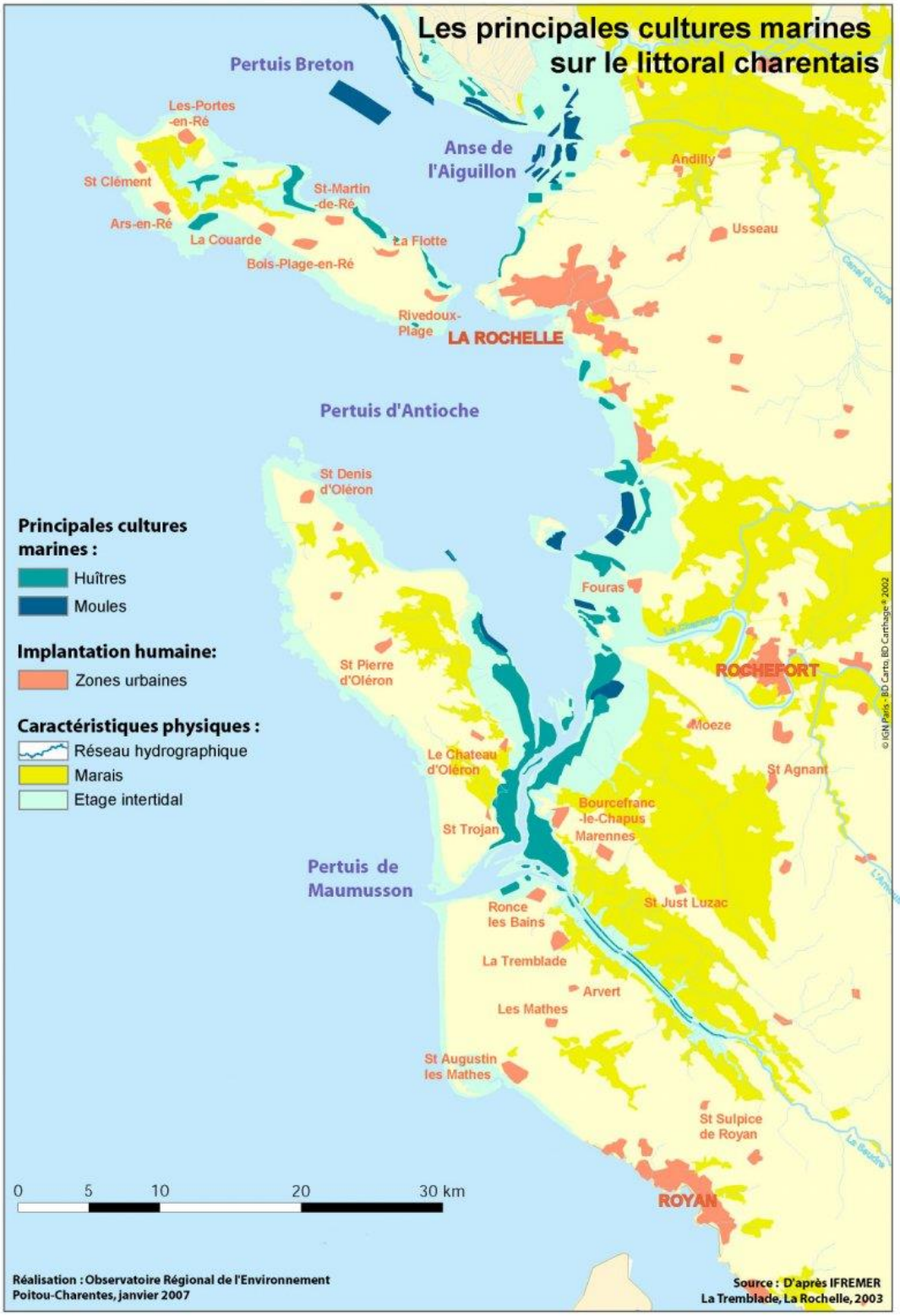

Figure 6 : Main marine cultures in the Pertuis charentais (legend : oyster, mussel, urban area, hydrografic network, swamp, tide zone) – (©ORE 2007)

The coastal waters are indeed subjected to increasing pollution. Pollution related inputs of pollutants located on the coastal border activities (discharges from sewage treatment plants, industries) or more related upstream inputs of pollutants from rivers (industrial and agricultural waste). Also pollution related contributions of maritime origin such as those of merchant traffic, fishing or pleasure (degassing, engine oil, paintings, discards consumer waste ...) and as those of any wrecks or accidents (black tide losses drums containing hazardous substances ...).

These human activities affect the physical, chemical and biological characteristics of marine ecosystems and the quality of coastal waters is of concern locally. Poor quality water is then, for example, a disruptive factor in tourist activities and shellfish.

3. MOHID MODEL

This chapter describes the numerical model used to study this thesis' subject.

3.1 Overview

MOHID is a three-dimensional water modelling system, developed at the Marine and Environmental Technology Research Centre (MARETEC) at Instituto Superior Técnico (IST) which belongs to Technical University of Lisbon in Portugal. The model has been applied in Portugal and worldwide such as to the Sado Estuary (Cancino and Neves, 1998; Martins *et al.*, 2001), to the Aveiro lagoon in Portugal (Vaz *et al.*, 2007), to the Ria de Vigo in Spain (Taboada *et al.*, 1998), to the Western European Margin (Coelho *et al.*, 1999), and to Brazilian reservoirs (Deus *et al.*, 2013) among others.

3.2 Hydrodynamic

The Hydrodynamic Module is the core of the MOHID Water modelling system. This is a three-dimensional hydrodynamic model which solves the Navier-Stokes equations, considering the Boussinesq and hydrostatic approximations. The equations are numerically solved by using the finite volumes approximation concept with a generic vertical discretization, which allows for the simultaneous implementation of various types of vertical coordinates. The equations solved in the model are:

Eq. 1 $$\frac{\partial u}{\partial x}+\frac{\partial v}{\partial y}+\frac{\partial w}{\partial z}=0$$

Eq. 2 $$\frac{\partial u}{\partial t}+\frac{u\partial u}{\partial x}+\frac{v\partial u}{\partial y}+\frac{w\partial u}{\partial z}-fv=-\frac{1}{\rho r}\frac{\partial \rho}{\partial x}+\frac{\partial}{\partial x}\left(A_h\frac{\partial u}{\partial x}\right)+\frac{\partial}{\partial y}\left(A_h\frac{\partial u}{\partial y}\right)+\frac{\partial}{\partial z}\left(A_h\frac{\partial u}{\partial z}\right)$$

Eq. 3 $$\frac{\partial v}{\partial t}+\frac{u\partial v}{\partial x}+\frac{v\partial v}{\partial y}+\frac{w\partial v}{\partial z}+fu=-\frac{1}{\rho r}\frac{\partial \rho}{\partial y}+\frac{\partial}{\partial x}\left(A_h\frac{\partial v}{\partial x}\right)+\frac{\partial}{\partial y}\left(A_h\frac{\partial v}{\partial y}\right)+\frac{\partial}{\partial z}\left(A_h\frac{\partial v}{\partial z}\right)$$

Eq. 4 $$\frac{\partial \rho}{\partial z}+\rho g=0$$

u, v and z are the components of the velocity in the x, y and z directions respectively, f is the Coriolis parameter, A_h is the coefficient of turbulent viscosity along the horizontal direction and A_v is the coefficient of turbulent viscosity along the vertical direction, p is the pressure, ρ_r is the reference density and ρ is the water density calculated on the basis the UNESCO equation of state as a function of the temperature and salinity.

3.3 Transport

Transport phenomena in the water column for a given property (P), can be described by the 3D advection-diffusion differential equation:

Eq. 5 $$\frac{dP}{dt} = \frac{\partial P}{\partial t} + u_j \frac{\partial P}{\partial x_j} = \frac{\partial}{\partial x_j}\left(k_\Theta \frac{\partial P}{x_j}\right) + (Sources - Sinks)$$

P is the concentration ($M.L^{-3}$), j is the index for the correspondent Cartesian axis (x1, x2, x3) or (x,y,z), KΘ is the turbulent mass diffusion coefficient (horizontal/vertical). Sources and sinks related to reaction processes taken place inside the assumed control volume, which undertakes local production and destruction terms.

Particulate properties transport is governed by a 3D advection-diffusion equation where the vertical advection includes the particle settling velocity.

Eq. 6 $$u_z = u_{z'} + w_s$$

Where **uz** is the overall vertical velocity of the particulate property, **uz**' is the vertical current velocity, and **ws** is the property's settling velocity. This methodology enables to compute particulate properties transport, like particulate contaminants or particulate organic matter, likewise and dependent of cohesive sediments.

3.4 Boundary Conditions

The interpretation of transport phenomena through a numerical model requires that appropriate boundary conditions are provided. These boundary conditions can be provided at the surface and bottom of the domain and on the lateral boundaries, and can be closed, open or mobile. Imposed values, inwards-outwards fluxes, decaying laws can be imposed depending in the type of boundary. In the water column, any flux between land and water, such as a river or an effluent, is computed as a discharge. Discharges can contain hydrodynamic properties (e.g. momentum), or water properties (e.g. temperature, salinity, suspended particulate matter, pollutant loading, nutrients, phytoplankton).

The open boundary can correspond, for example, to the oceanic boundary. Tide is imposed at the open boundary, where water level is normally imposed after being computed through tidal harmonic components. For an open boundary, a property can be relaxated from each dataset/property boundary condition within a number of cells from the boundary into the domain. Relaxation coefficients values increase progressively from boundary to domain interior, providing a larger weight for the model defined solution in the interior and a smaller weight for this solution at the boundary. This scheme is based on Martinsen and Engedahl (1987).

Open boundary conditions is a "science" within hydrodynamic and transport modelling. An extensive overview on how this type of boundaries is handled in MOHID Water can be found in Leitão (2003).

3.5 Lagrangean Tracers

The contaminants in the water column can be simulated through lagrangian tracers approach (Leitão, 1996) instead of a eulerian approach:

Eq. 7 $$\frac{dx_i}{dt} = u_i(x_i, t)$$

Where u stands for the mean velocity and x for the particle position. The velocity at any point of space is calculated using a linear interpolation between the points of the hydrodynamic model grid. Turbulent transport is responsible for dispersion. The effect of eddies over particles depends on the ratio between eddies and particle size. Eddies bigger than the particles make them move at random. Eddies smaller than the particles cause entrainment of matter into the particle, increasing its volume and mass according to the environment concentration. The random movement is calculated following the procedure of Allen (1982). The random displacement is calculated using the mixing length and the standard deviation of the turbulent velocity component, as given by the turbulence closure of the hydrodynamic model. Particles retain that velocity during the necessary time to perform the random movement, which is dependent on the local turbulent mixing length (Leitão, 1996).

3.6 Oil spills

The prediction and simulation of the trajectory and weathering of oil spills are essential to the development of pollution response and contingency plans, as well as to the evaluation of environmental impact assessments.

The oil weathering module (OWM) of the MOHID system uses variables from the hydrodynamics and the Lagrangian transport module and calculates oil density, viscosity, and the weathering processes. Processes such as oil spreading, evaporation, dispersion, sedimentation, dissolution, emulsification, oil beaching and removal techniques are available in the model (Fernandes, 2001, 2008, 2012).

Next sub-chapters detail the theoretical background for the algorithms behind evolution of processes and properties used.

3.6.1 Density and viscosity

Oil density is calculated as follows:

Eq. 8 $$\rho_e = F_{wv} \cdot \rho_w + \rho_{oil}(1 - F_{wv})(1 + c_{DE}F_e)[1 - c_{DT}(T - T_0)]$$ (NOAA, 1994)

where ρ_e is the density of the emulsion at temperature T, F_{wv} is the volume water fraction of the emulsion, ρ_{oil} is the density of fresh oil at reference temperature T_0 , ρ_w is the water density, c_{DE} e c_{DT}

are empirically fitted constants with values of c_{DE} =0.18 and c_{DT} = 8x10^{-4}, as suggested by NOAA (1994). The oil initial density is its API density.

Viscosity is changed by three major processes: temperature, evaporation and emulsification. The influence of temperature can be calculated by Andrade's correlation:

Eq. 9 $$\boldsymbol{\mu = \mu_0 e^{c_t\left(1/T - 1/T_0\right)}}$$

Where μ is the oil viscosity at temperature T, μ_0 is the initial oil viscosity at reference temperature T0 and c_T is an empirical constant controlling the viscosity variation with temperature. A value of 5000 K is recommended by NOAA (1994). Viscosity modification due to emulsification is defined by Mooney's equation (1951):

Eq. 10 $$\boldsymbol{\mu = \mu_0 e^{\left[\frac{c_v F_{wv}}{(1 - c_M F_{wv})}\right]}}$$

Where F_{wv} is the volumetric water fraction of the oil water emulsion, c_V is an adimensional empirical constant controlling the effect of emulsion with a value of 2.5 recommended by Mackay et al., (1980). c_M is the Mooney's constant with a value of 0.65.

The effect of evaporation on viscosity is calculated by the following equation:

Eq. 11 $$\boldsymbol{\mu = \mu_0 e^{(c_E F_{em})}}$$ (Mackay et al., 1980)

F_{em} is the mass fraction of evaporated oil, and the adimensional empirical constant c_E varies with oil type, between 1 and 10, with higher values for more viscous products.

The model assumes c_E = 10 when fresh oils at 15ºC have a cinematic viscosity greater than 38 *cSt*. In case of less viscous oils, c_E is estimated by a second degree polynomial regression:

Eq. 12 $$\boldsymbol{c_E = -0.0059.V_{cin15}^2 + 0.4461.V_{cin15} + 1.413}$$

where V_{cin15} is the oil cinematic viscosity at 15ºC. The three previous equations can be joined in the single viscosity equation:

Eq. 13 $$\boldsymbol{\mu = \mu_0 e^{\left[(c_E F_{em}) + \frac{c_v F_{wv}}{(1 - c_M F_{wv}} + c_t\left(1/T - 1/T_0\right)\right]}}$$

3.6.2 Spreading

Spreading is the horizontal expansion of an oil slick due to mechanical forces, such as gravity, inertia, viscous and interfacial tension. It is an important process in the early stages of oil slick transformation and is affected by the weathering processes, which tend to change the mass and physicochemical properties of the slick. In free-surface conditions the oil slick area also has a strong influence on the weathering processes, such as evaporation and dissolution, and because of this, slick area and thickness are key variables in oil weathering and transport models.

In case of an instantaneous spill, the initial slick area is determined by an equation deduced from Fay's solutions (Fay, 1969). Because the initial phase of the spreading (gravity-inertial phase) is too short, the initial area is calculated when that phase ends, and the gravity-viscous phase starts:

Eq. 14 $$\boldsymbol{A_0 = \pi \frac{k_2^4}{k_1^2} \left(\frac{\Delta g V_\rho^5}{v_w} \right)^{\frac{1}{6}}}$$

Where A_0 is the initial area of the spill, $\Delta = \frac{\rho_w - \rho_0}{\rho_w}$ is the water density, ρ_0 is the oil density, g the gravity acceleration, V_0 the volume of spilled oil, v_w the water kinematic viscosity and k_1 = 0.57 and k_2 = 0.725 (as recommended by Flores et al, 1998). The average oil thickness for each computational cell is estimated by dividing the sum of the volume of particles that have their center of mass in the cell, by the cell area.

To simulate the oil spreading, a random velocity is added to the particles movement. The effect of this velocity reproduces the spreading effect, since it works as a diffusive term that reduces the thickness of the slick in time. The random velocity is calculated from the diffusion coefficient estimated from the Fay (1969) equation for the gravity- viscous phase.

Eq. 15 $$\boldsymbol{k = \frac{\pi k_2}{16} \left(\frac{\Delta g V^2}{\sqrt{v_w}} \right)^{1/3} \frac{1}{\sqrt{t}}}$$

The evolution in time of k (spreading diffusion coefficient) can be calculated in the following way.

Eq. 16 $$\boldsymbol{a(t) = \frac{\pi k_2}{16}\left(\frac{\Delta(t) g V(t)^2}{\sqrt{v_w}}\right)^{1/3}}$$

Eq. 17 $$\boldsymbol{k(t) = \frac{a(t)}{\sqrt{t}}}$$

Eq. 18 $$\boldsymbol{k(t+\Delta t) = \frac{a(t+\Delta t)}{\sqrt{\left(\frac{a(t)}{k(t)}\right)^2 + \Delta t}}}$$

If average oil thickness becomes too thin – less than a value between 0.1 and 0.01 mm, depending on product viscosity – oil spreading is stopped, according to Reed (1989) see Table **3** below.

API	**Thickness limit [mm]**
<17.5	0.1
>17.5 and <45	0.157 – 0.0033 * API
>45	0.01

Table 3 : Thickness limit depending on product viscosity

3.6.3 Evaporation

The oil evaporation process is estimated using the analytical method of Stiver & Mackay (1984), also known as the evaporative exposure method. The variation of volume fraction of evaporated oil (Fe) is given by:

Eq. 19 $$\boldsymbol{\frac{dF_e}{dt} = \frac{K_e A_s}{V_0} exp\left(A - \frac{B}{T}(T_0 + T_G F_e)\right)}$$

Where T is oil temperature, A_s is the oil slick area, V_0 is the initial oil volume, A and B are empirical constants, T_0 is the initial boiling point and T_G is the distillation curve gradient and K_e is the mass transfer coefficient, determined by the formulation proposed by Buchanan & Hurford (1988):

Eq. 20 $$\boldsymbol{K_e = 2.5 \times 10^{-3} W^{0.78}}$$

Where W is the wind speed in mh^{-1}.

All these parameters depend on oil type. In this model, they are estimated, and T_0 e T_G is obtained from API density, according to version 1.1 of ADIOS model (NOAA, 1994) A= 6.3, B = 10.3 and:

Eq. 21 $$\boldsymbol{T_0 = 532.98 - 3.1295 \times API}$$

Eq. 22 $$\boldsymbol{T_G = 985.62 - 13.597 \times API}$$

3.6.4 Emulsification

For the emulsification process the Mackay et al., (1980) equation is used:

Eq. 23 $$\boldsymbol{\frac{dF_{wv}}{dt} = K_w(1+W)^2\left(1 - \frac{F_{wv}}{F_{wv}^{final}}\right)}$$

Where F_{wv} is the water volume fraction incorporated into emulsion; F_{wv}^{final} is the final volumetric fraction of water incorporated in emulsion, K_w is an empirical constant, introduced by the user. Usually this constant assumes values between 1. 10^{-6} and 2.10^{-6}. MOHID default value is 1.10^{-6}, which is also used in the ADIOS model (NOAA, 1994).

Another less known formulation, but taking into account some oil properties, is Rasmussen's equation (1985):

Eq. 24 $$\boldsymbol{\frac{dF_{wv}}{dt} = R_1 - R_2}$$

being:

- R1 Water intake rate (s-1), given by:

Eq. 25 $$R_1 = \frac{K_1}{\mu_0}(1+W)^2\left(F_{wv}^{final} - F_{wv}\right)$$

- R2 Water output rate (s-1), given by:

Eq. 26 $$R_2 = \frac{K_2}{Asph \cdot Wax \cdot \mu_0} F_{wv}$$

Asph is Asphaltenes content in oil (%) Wax is paraffin content (%), and K1 and K2 are constants determined experimentally by Rasmussen (1985): K1 = K2 5x10-7 kg m-3 = 1.2 x10-7 kg.m-1.s-2.

The algorithm of the formation of emulsions Oil-in-water emulsification using a constant, which means the percentage of oil which evaporates before starting the emulsification process. However, there are plenty of petroleum products for which the information concerning the start of this process is unknown.

Although the update and review on formulations for oil spreading and weathering processes in MOHID is still a work-in-progress, at the moment of the edition of this study, a new additional method has been included for the simulation of emulsification process. Emulsification is responsible for the incorporation of water droplets in oil, changing substantially the oil viscosity and therefore its behaviour at sea. In fact, after evaporation, emulsification can be considered the most important transformation process (Fingas, 2008). Emulsions had been studied extensively in the laboratory and field, thus many facets of their formation are now known, and the basics of water-in-oil emulsification are finally understood and well-established (Fingas and Fieldhouse, 2006; Sjöblom et al., 2003). The new method adopted in MOHID was proposed and detailed in Fingas, 2011, and already implemented in (Berry et al., 2012). The approach is based on the determination of stability class from extensive empirical data obtained in previous studies, and then related to an emulsion state (stable emulsion, meso-stable emulsion, entrained water and unstable mixture). The proposed model has the oil starting viscosity, its asphaltene and resin content and its density as the most mathematically relevant factors when determining stability class. This formulation is considered to be very much more accurate than the old methods (Fingas, 2011). (Fernandes, 2013)

3.6.5 Dispersion / Movement of Entrained Oil

Although a major number of oil spills take place at the surface, after the accidents the oil can be pushed down into the water column by the energy of breaking waves. Since its implementation, MOHID is able to compute the entrainment rate using Mackay, 1980 approach, or the classic method from Delvigne and Sweeney, 1988.

If the oil penetrates the water column after a surface spill, this means that oil will be subject to a vertical velocity, depending on the density differences and oil droplets diameter. The correct modelling of these processes forces the implementation of a three-dimensional modelling approach. More details about modelling process implemented in MOHID can be found in Fernandes et al., 2013.

By default, OSS doesn't simulate 3D vertical movement of oil particles. It simply quantifies the amount of oil dispersed in the water column using the formulation proposed by Mackay et al., (1980):

Eq. 27 $$\frac{dm_d}{dt} = 0.11 m_{oil} \frac{(1+W)^2}{1+50\mu^{1/2}h\sigma} \qquad (kg.h^{-1})$$

where moil is the oil mass that remains on the surface, μ is the oil dynamic viscosity (cP), h is the slick thickness (cm), W is the wind velocity ($m.s^{-1}$) and σ is oil-water interfacial tension ($dyne.cm^{-1}$). This equation represents a simplified algorithm for vertical dispersion as a function of the square of the wind velocity. The turbulent energy of the process is not considered.

In case of considering OSS advanced options with a 3D vertical movement, the first process to model is the entrainment of an oil tracer in the water column, which will be based on a random procedure. The probability of a tracer being entrained in the water column due to breaking waves is obtained from the instantaneous model "entrainment deficit" - difference between the theoretical fraction of dispersed oil estimated by one of the dispersion formulas previously implemented in MOHID (in case of OSS, it's Mackay's formulation previously mentioned), and the global mass fraction of entrained oil particles. Thus, the probability of a tracer entraining the water column is greater when the entrainment deficit is greater, i.e., when the difference between the global dispersion fractions obtained by the theoretical equations and the mass fraction of oil droplets in the water column is greater.

Once a particle is on the water column, the second process to compute is the specific depth position. The particle's depth is randomly determined between surface and the intrusion depth $D_i = 1.5H_b$. (*Di* is the intrusion depth, and *Hb* is the breaking wave height) (Tkalich and Chan, 2002).

The next step is to decide the droplet diameter associated to the particle. Ideally, each surface particle entrained in the water column should then generate new entrained particles with different diameters following a droplet size distribution (Delvigne and Sweeney, 1988). For computational reasons, the surface particle, once in the water column, has only one diameter. Different methods can be used for the determination of droplet diameter; OSS uses a single typical median diameter (0.05 mm), as proposed by Delvigne and Sweeney, 1988.

The last step is the computation of the droplet buoyancy. The rising velocity will be based on the assumption that oil particles can be represented as spheres of given diameter and density. Thus, buoyancy velocity w_s will depend on density differences, droplet diameter d and water kinematic viscosity *v*, as well as critical diameter d_{crit} (Soares dos Santos and Daniel, 2000).

Eq. 28 $$\boldsymbol{d_{crit}} = \boldsymbol{\alpha} \frac{\boldsymbol{v}^{2/3}}{|\boldsymbol{g'}|^{1/3}}$$

where g' is the reduced gravity (buoyancy)

Eq. 29 $$\boldsymbol{g'} = \boldsymbol{g}\left(\mathbf{1} - \frac{\boldsymbol{\rho_P}}{\boldsymbol{\rho}}\right)$$

If the particle's diameter is greater than *dcrit* then

Eq. 30 $$\boldsymbol{w_s} = \frac{\boldsymbol{g'}}{|\boldsymbol{g'}|}\sqrt{\boldsymbol{\beta d}|\boldsymbol{g'}|}$$

Else

Eq. 31 $$\boldsymbol{w_s = \frac{g'}{|g'|}\left(\frac{d^2|g'|}{18v}\right)}$$

The values for α and β defined by default are 9.52 and 8/3, respectively, as proposed by (Soares dos Santos and Daniel, 2000).

The droplet buoyant velocity is then integrated with the vertical advection and diffusion components (the advected vertical velocity – from the hydrodynamic solution – and the vertical turbulent diffusion velocity component). This means that in waters with higher turbulence, the buoyant velocity becomes less important.

3.6.6 Dissolution

The dissolution rate (gh^{-1}) is the rate in which the soluble fraction of the oil breaks into small particles mixing with water forming homogeneous moisture between them. This rate is estimated by the Cohen et al., (1980) equation:

Eq. 32 $$\boldsymbol{\frac{dDiss}{dt} = K.f_s.A_s.S}$$

Where K is the dissolution mass transfer coefficient ($0.01 m.h^{-1}$), fs is the surface fraction covered by oil (considered equal to oil content in emulsion water + oil); As is the oil slick area (m^2) and S is the oil solubility in water calculated as:

Eq. 33 $$\boldsymbol{S = S_0 e^{\alpha t}}$$ Huang & Monastero (1982)

where S_0 is the solubility of the "fresh" oil (30 $g.m^3$); α is a decay constant (0.1); t is the time after spill (h).

3.6.7 Sedimentation

Although oil sedimentation process is relatively complicated and difficult to estimate, a formulation developed by Science Applications International (Payne et al., 1987) is used in MOHID:

Eq. 34 $$\boldsymbol{\frac{dm_{sed}}{dt} = 1.3\sqrt{\frac{E}{V_w}}K_a.C_{oil}.z_i.A_s}$$

This equation gives the mass of sedimented oil per time unit ($kg.s^{-1}$), where: Vw is the water dynamic viscosity ($kg.m^{-1}.s^{-1}$); Ka is the stick parameter with value $m^3.kg^{-1}$; z_i is the intrusion depth of oil droplets in the water column due to breaking waves, given by Delvigne & Sweeney (1988):

Eq. 35 $$z_i = 1.5.H_0$$

C_{sed} is the sediment concentration in water column (kg.m^{-3}), C_{oil} is the oil droplet concentration in water column (kg.m^{-3}). This concentration can be determined from dispersion rate proposed by Delvigne & Sweeney (1988) (explained in dispersion section), integrating this rate for wave period and intrusion depth of oil droplets:

Eq. 36 $$\frac{dC_{oil}}{dt} = \frac{\frac{dm_d}{dt}}{z_i}$$

E is the rate of dissipated energy from water surface (J.m^{-3}.s^{-1}):

Eq. 37 $$E = \frac{D_{ba}}{z_i.T_w}$$

Where D_{ba} is the wave dissipation energy per unit of surface area, which can be calculated by:

Eq. 38 $$D_{ba} = 0.0034\rho_w g H_{rms}^2$$

In previous equation, H_{rms} is:

Eq. 39 $$H_{rms} = \frac{1}{\sqrt{2}} H_0$$

where H_0 is wave height.

3.7 Mohid Studio

MOHID Studio is a graphical user interface for the MOHID Water Modelling System. MOHID Studio enables to edit data files, create and launch simulations and analyze model results. Map data can be displayed through an integrated GIS system and time series data can be displayed in an integrated graph visualization engine. A set of tools enables the user to create and preprocess MOHID data files. MOHID Studio also offers the possibility to convert data among a set of common formats and MOHID internal formats. All features of MOHID Studio are described along the user guide (Braunschweig *et al.*, 2012).

4. MODEL IMPLEMENTATION

This chapter describes the 2D model used to simulate the hydrodynamics of the domain area.

This domain spans from latitudes 44.03N to 47.5N and longitudes 0.16W to 3.94W, and includes tidal, wind forcing and river discharges. The domain span was chosen in order to include the Gironde River.

Data were obtained from different sources as show in **Table 4**.

	Bathymetry		**River discharge**	**Open Boundary**	**Meteorology**	
Data source	SHOM (HistoLitt)	SHOM (MNT)	Banque hydrologique de France	Myocean (NEMO model)	Météo France (AROME model)	Météo France (ALADIN model)
Temporal Resolution	N/A		24 h	24 h	3 h	
Spatial resolution	50 m	1 km	N/A	3 km	2.5 km	12 km

Table 4 : Data for model implementation

The model was implemented by using downscaling. The idea of downscaling consists of simulating hydrodynamics on a local scale, based on information provided by larger-scale models. The geographic area covered by a model is called a domain. A domain included inside the domain of another model is named as nested domain, or subdomain. A domain can have one or more subdomains. The boundary conditions are then provided from a domain to its subdomains. Models with larger domains are called "father" models, and provide boundary conditions to their nested models, known as "son" models. Son models are used to represent estuaries, harbors, and lagoons at a spatial resolution higher than this of the father model.

4.1 Model domains

The model used at La Rochelle includes 4 domains (Figure 7):

- Domain 0
- Domain 1
- Domain 2
- Domain 3

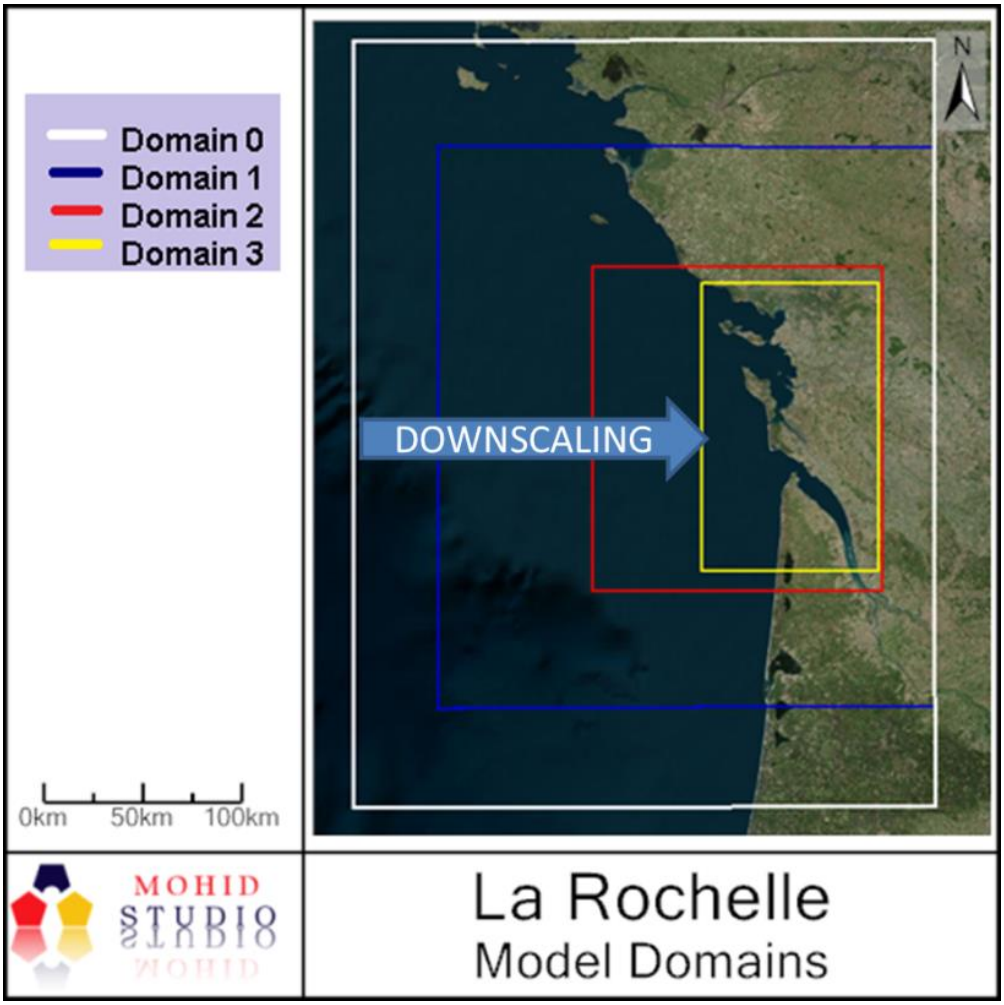

Figure 7 : La Rochelle model domains

For each model domain, a bathymetry was obtained by using MOHID Studio tools for digital terrain creation. The geographic extent and the resolution of the grids used to represent each domain are described in **Table 5**.

Name	Data source	Step	Cells	Min Depth	Max Depth	Min Lon	Max Lon	min Lat	max Lat
Domain 0	SHOM (1km)	7x12 km	52x34	0	4200	-3.9	-0.16	44.03	47.5
Domain 1	SHOM (1km)	7x12 km	38x29	0	3779	-3.3	-0.16	44.5	47.0
Domain 2	SHOM (1km) + (25 m)	2.5 km	66x85	-2.4	130	-2.3	-0.5	45.03	46.5
Domain 3	SHOM (1km) + (25 m) EMODNET (500m)	500 m	295x260	-7	70	-1.6	-0.5	45.12	46.4

Table 5 : La Rochelle Model grid

The bathymetry was compiled by Isabella Ascione (MARETEC) who applied integration and smoothing routines, using different data sources.

The interpolation procedure required the definition of grid points considered land or sea. To do this, a land mask was used. This mask consists of a polygon shapefile representing the land. All the grid points falling outside of the polygon were considered sea. The shapefile used to build the land mask is GSHHG Version 2.2.2 January 1, 2013 (Wessel and Smith, 1996). All the bathymetries were created with the same land mask. The bathymetry of Domain 0 was obtained by interpolating SHOM bathymetric data (available at a resolution of 1 km) over a grid with 52x34 cells and a resolution of 7x12km. The bathymetry of Domain 1 was obtained by interpolating SHOM bathymetric data (available at a resolution of 1 km) over a grid with 38x29 cells and a resolution of 7x12km. The bathymetry of Domain 2 was obtained by interpolating SHOM bathymetric data over a grid with 66x85 cells and a fixed resolution of 2.5 km. Finally, the bathymetry of Domain 3 was obtained by interpolating SHOM bathymetric data over a grid with 295x260 cells and a fixed resolution of 500 m. For Domains 2-3, SHOM bathymetric data with a variable high resolution (about 25 m) were used. Data gaps were filled with EMODNET 500 m resolution bathymetric data, available at http://www.emodnet.eu/. Model bathymetries are described in **Table 5** and Figure **8**.

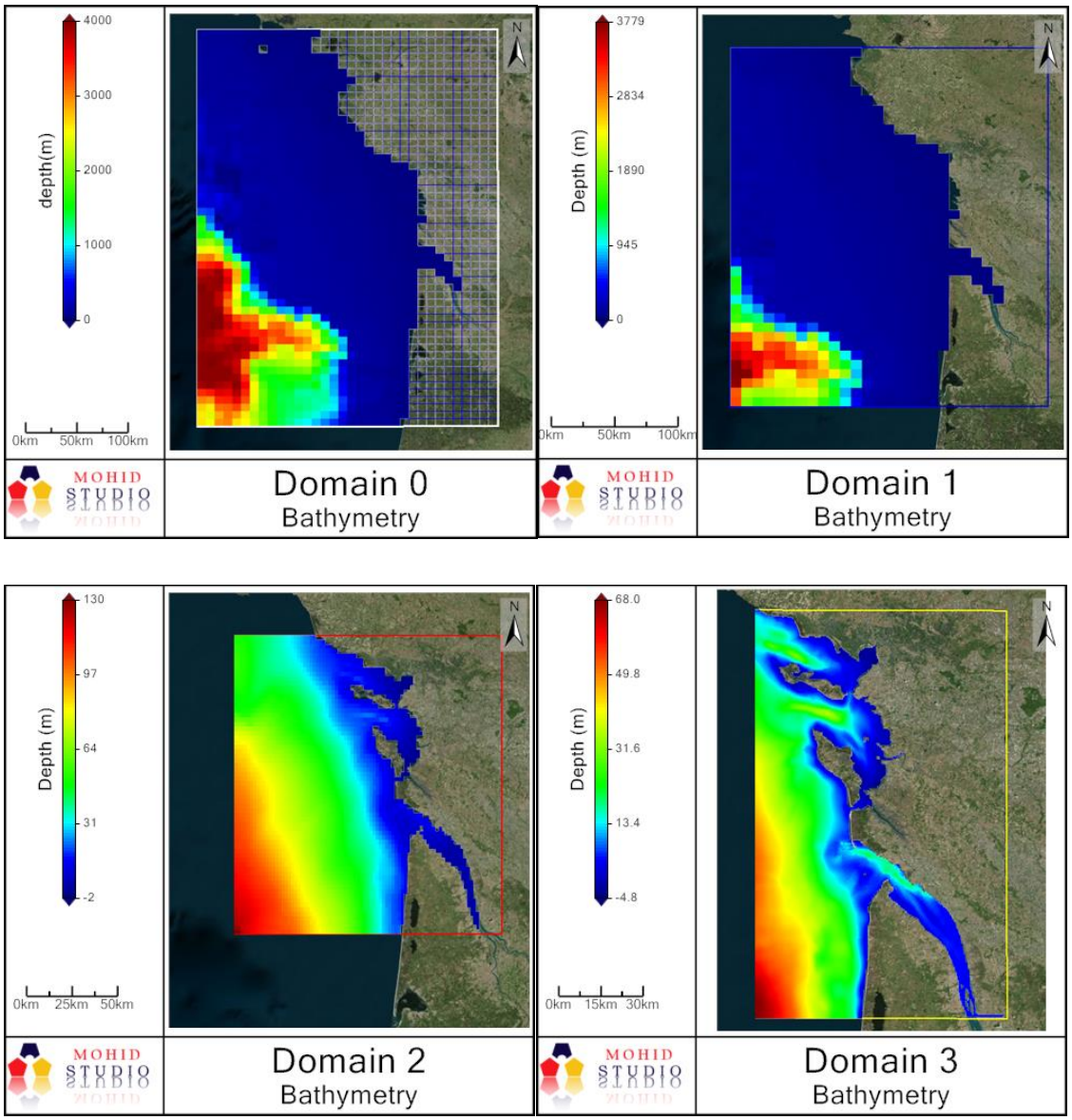

Figure 8 : La Rochelle model bathymetries.

4.2 Vertical grid

Domain 0 has a 2D geometry consisting of one sigma layer extending between the surface and the maximum model depth. For Domains 1-3 a vertical grid was used, consisting of 7 sigma layers (between the surface and -8.68 m) overlapped to 43 Cartesian layers (between -8.68 m and 458 m), for a total of 50 vertical layers. The geometry of Domain 1 includes 50 vertical layers. Domains 2-3 include only 33 vertical layers, because their maximum depth is shallower than Domain 1.

4.3 Time span and spin up run

The time period on the test simulation was selected to coincide with available *in situ* data. In order to validate the model using available data, a preliminary simulation of 6 months has been carried out from January 1st 2012 to July 1st 2012. It includes a spin up run for 2 weeks and then runs 6 months at a time, all with a timestep indicated in table 6**.**

Name	Timestep
Domain 0	180 s
Domain 1	90 s
Domain 2	30 s
Domain 3	15 s

Table 6 : Timestep

4.4 Tidal Forcing

Tidal boundary conditions were obtained from the FES 2004 (Finite Element Solution) tide model (Lyard *et al.*, 2006), based on a hydrodynamic model which assimilates tide gauges and altimeter data (Topex/ Poseidon and ERS-2). The FES 2004 model comprises global coverage of tidal components at resolution of 1/8º. Tide gauges were defined around the open boundary of Domain 0 (**Figure 9**), and tidal components were extracted at the defined gauges.

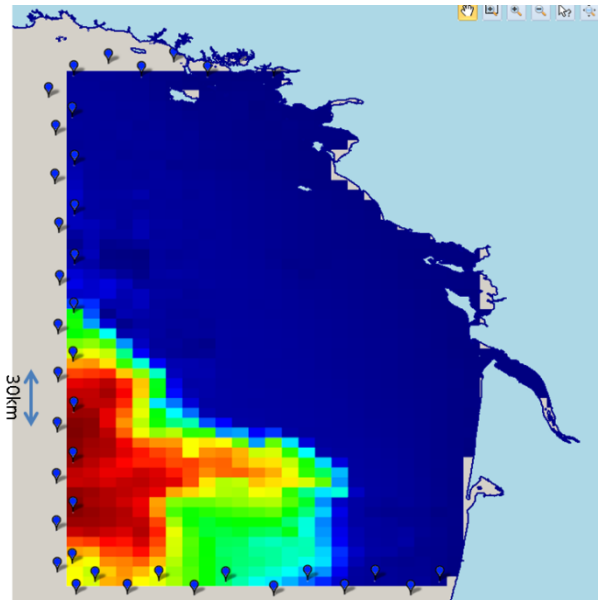

Figure 9 : Tidal gauges defined around the open boundary of Domain 0.

The tide was forced in the boundary of the domain using the FES2004 global solution (Lyard et al , 2006).

The resulting input file for the model has 168 tidal gauges dispersed around the boundaries of the domain, inputting 11 harmonic components to the model (M2, S2, K2, N2, K1, O1, P1, Q1, Ssa, Mm, Mf). The boundary is also defined as an open boundary with tidal gauges.

4.5 Open boundary conditions

Open boundary conditions were considered from Mercator-Ocean GLOBAL_ANALYSIS_FORECAST_PHYS_001_002 (available at MYOCEAN website) for North Atlantic region at a spatial resolution of 18x13 km. The vertical resolution of the database includes 43 vertical layers between 0-6000m. The database contains the average daily distribution of the following parameters:

- Temperature
- Salinity
- Velocity
- Water level

The open boundary conditions for Domain 1 were defined by interpolating Mercator-Ocean solution over the grid of Domain 1 (**Figure 10**).

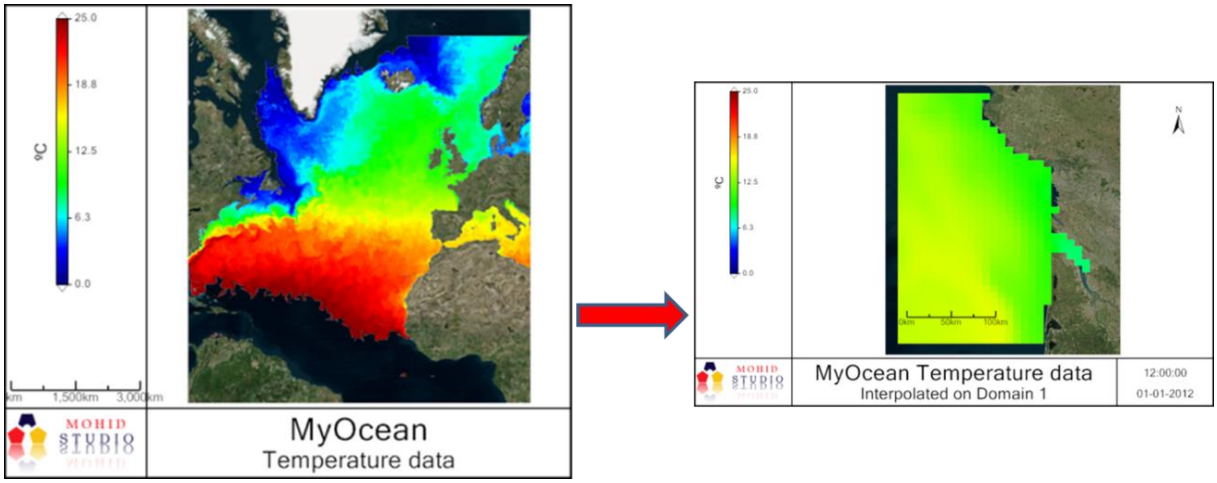

Figure 10 : Example of open boundary conditions for Domain 1.

4.6 Freshwater discharges

Freshwater discharge data for rivers Dordogne, Garonne, and Charente were provided by EIGSI La Rochelle at a temporal resolution of 1 day, over the period 01/01/2012 – 31/12/2012 (**Figure 11**).

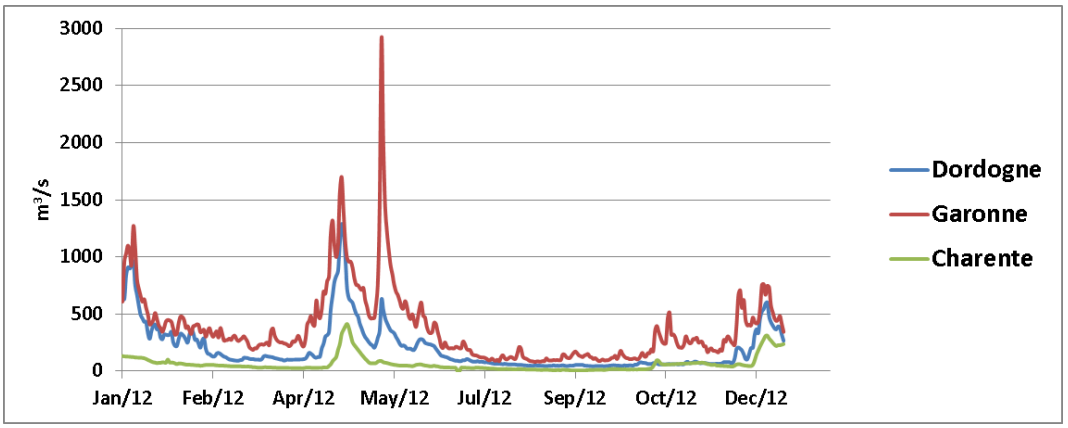

Figure 11 : Freshwater discharge data imposed at the river boundary.

Freshwater discharges were imposed for Charente, Garonne and Dordogne rivers in Domain 3. The freshwater discharges were imposed at the upstream boundary of rivers. For Garonne and Dordogne rivers, the sum of the freshwater inflows was considered. The location of the points where freshwater discharges were imposed in the model is described in **Figure 12**.

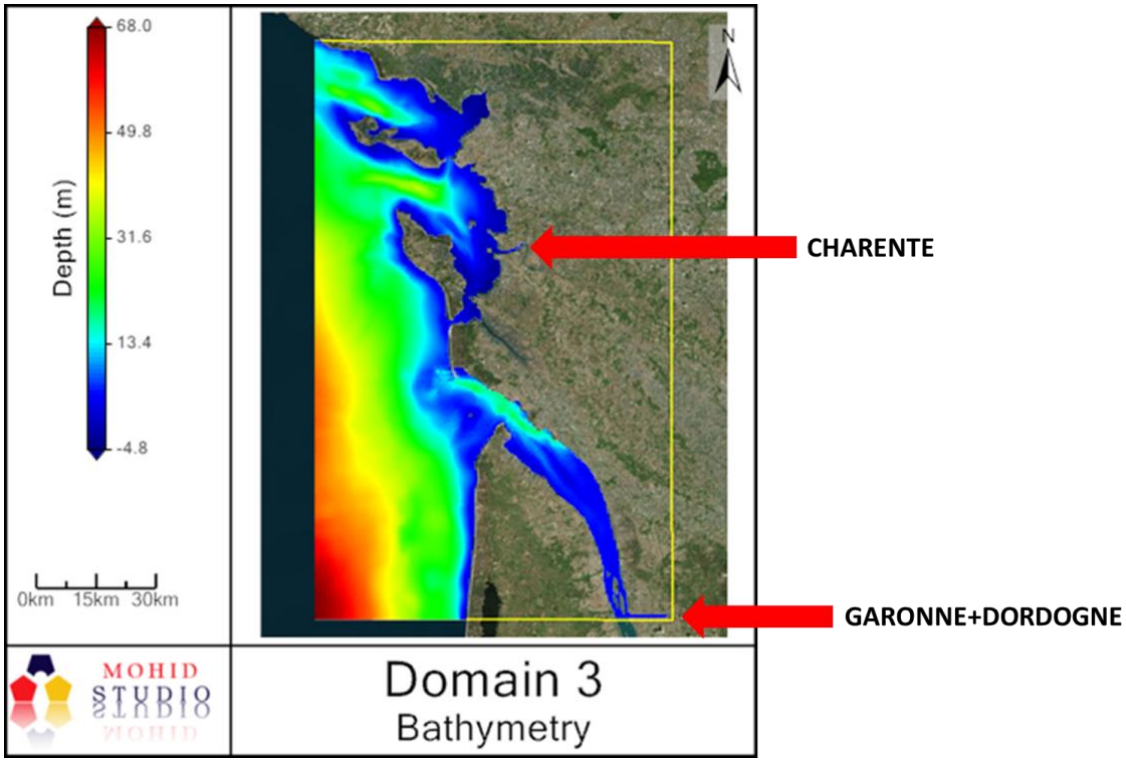

Figure 12 : Location of freshwater discharges in the model.

4.7 Atmospheric forcing

Atmospheric data from MeteoFrance were provided by EIGSI La Rochelle, and include the following parameters:

- Atmospheric pressure
- Wind velocity
- Solar radiation
- Air temperature
- Relative humidity
- Downward long wave radiation
- Cloud cover

These parameters were provided at a resolution of 2.5 km and at 3 hour frequency for the period 01/01/2012-01-07/2012. The area covered by atmospheric data is shown in Figure 13. The atmospheric data were interpolated over the grids of Domains 2-3, and saved as HDF5 file format to be used in MOHID. Atmospheric forcing was not considered in domains 1 because the available data did not cover their whole area.

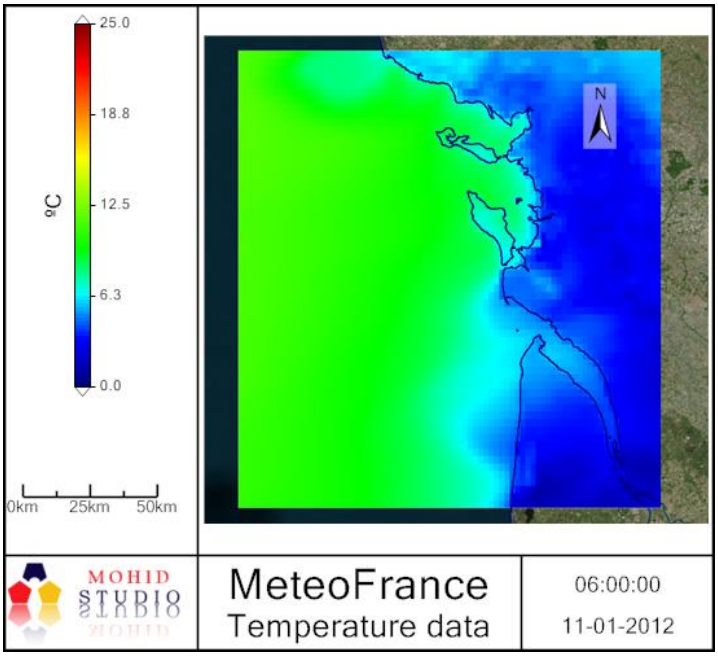

Figure 13 : Air temperature data from MeteoFrance, used to force the hydrodynamic model.

5. MODEL VALIDATION

The hydrodynamic model will be validated by comparing simulated results with observed data available for the period 01/01/2012 – 01/07-2012. Presently, measured data available for model validation include water levels, temperature and salinity.

5.1 Water level and Tidal Harmonic Analysis

Water level data from SHOM were provided by EIGSI La Rochelle at seven gauges in the area. Four of these locations fall in the model domain and will be used to validate water level. The list of the water level gauges is provided in

Table 7. Additionally, the map with gauges location is provided in **Figure 14**.

Name	**Latitude (CGS WGS84)**	**Longitude (CGS WGS84)**	**Time period**
Bordeaux	44.86	-0.5528	01/01/2012-01/01/2013
Ile d'Aix	46.007357	-1.174341	05/01/2012-02/12/2012
La Rochelle La Pallice	46.1585	-1.22064	01/01/2012-01/01/2013
Les Sables D'Olonne	46.4973	-1.7935	01/01/2012-01/01/2013
Pointe de Grave Port Bloc	45.568	-1.0615	01/01/2012-01/01/2013
Rochefort	45.946	-0.953	01/01/2012-01/01/2013
Royan	45.6205	-1.0278	01/01/2012-01/01/2013

Table 7 : Water level gauges used in the hydrodynamic model validation

Figure 14 : Water level gauge location.

The harmonic analysis comparison is an important part of model validation, as it can say much about the hydrodynamical precision of the model.

For the comparison of the model results with measured sea levels, an analysis is made with data from several tidal gauges from around the domain (**Figure 14**). The field data was retrieved from SHOM.

We can notice that 3 points have been excluded from this analysis as they were not accurate in the model (Bordeaux, Rochefort and Les Sables D'Olonne) because of the bathymetry resolution.

XTIDE harmonic component database (XTIDE, 2004), using the interface from T_TIDE (Pawlowicz, 2002). This database is one of the world's references in harmonic component as many national hydrography authorities use it for official recording (for e.g. RIKZ in the Netherlands).

5.1.1 Timeseries analysis

In order to compare the model's result with the field data, which has only tidal data, one has to remove the non-tidal interactions from the model's timeseries to be able to compare solely the tide. This procedure is done by performing a harmonic analysis on the model's timeseries, and then reconstruct it based on the resulting harmonic components. This was computed with the T_Tide package (Pawlowicz 2002; Foreman, 1977) using MatLab. The analysis can be made by comparing the timeseries (statistical analysis) and by comparing the harmonic components (harmonic analysis).

The tidal simulation of the coastal gauges is reasonably accurate, but in the case of the Royan tidal gauges, although the timing of the tide is accurate, the simulated water level is underestimated. The following figures show these differences.

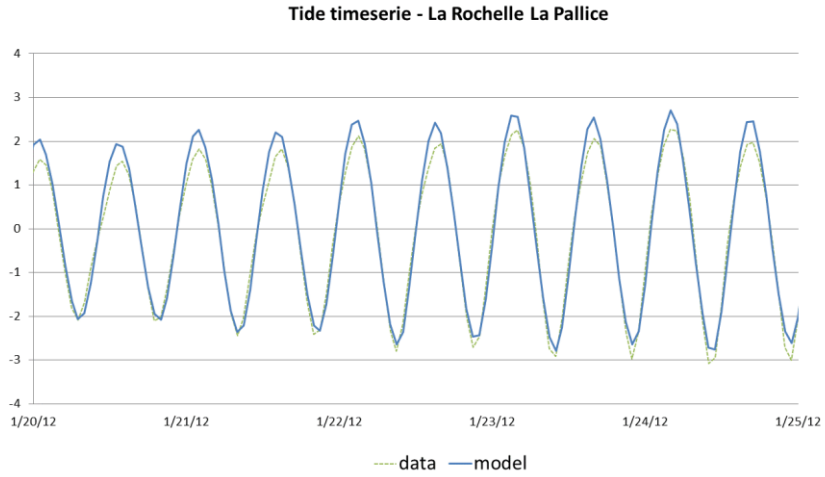

Figure 15 : La Rochelle tidal gauges timeseries (in m)

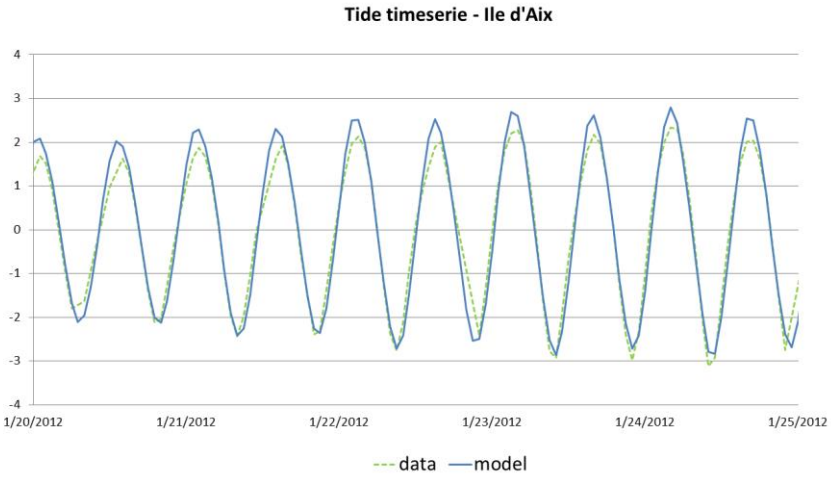

Figure 16 : Ile d'Aix tidal gauges timeseries (in m)

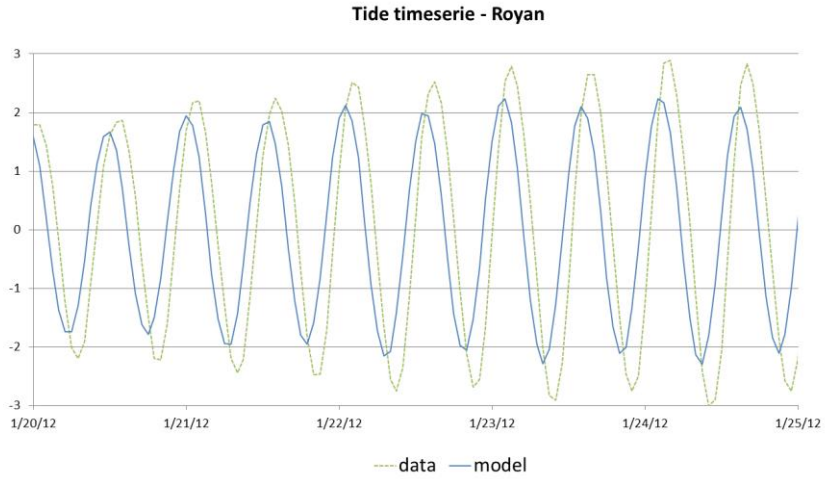

Figure 17 : Royan tidal gauges timeseries (in m)

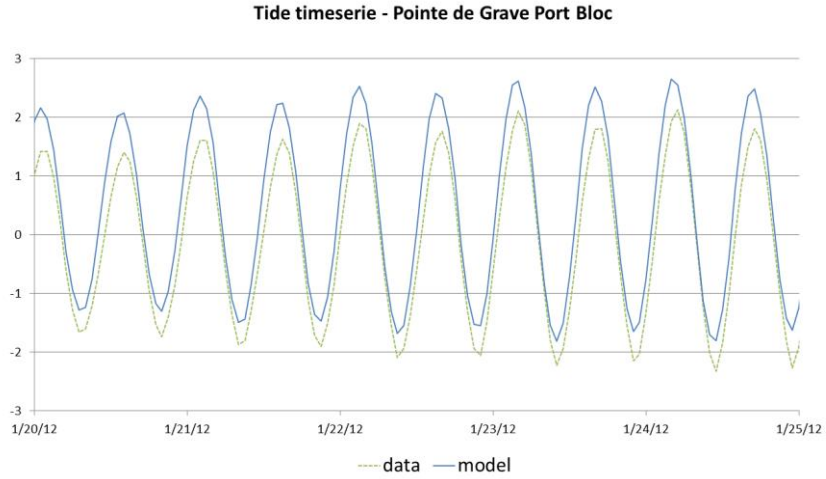

Figure 18 : Port Bloc tidal gauges timeseries (in m)

From the resulting two timeseries, a statistic analysis was made using several descriptors. The descriptors are based on Chambel-Leitao (2007) from Evans (2003):

- Correlation coefficient: also known as the Pearson product-moment correlation coefficient;
- RMSE: Root Mean Square Root.

The following figure (**Figure 19**) shows the resuts of the descriptors, for all 4 tidal gauges analysed (map from **Figure 14**). The model generally agrees with the observations. It presents a good correlation coefficient (>80%), indicating that there is a linear correspondence between the two timeseries.

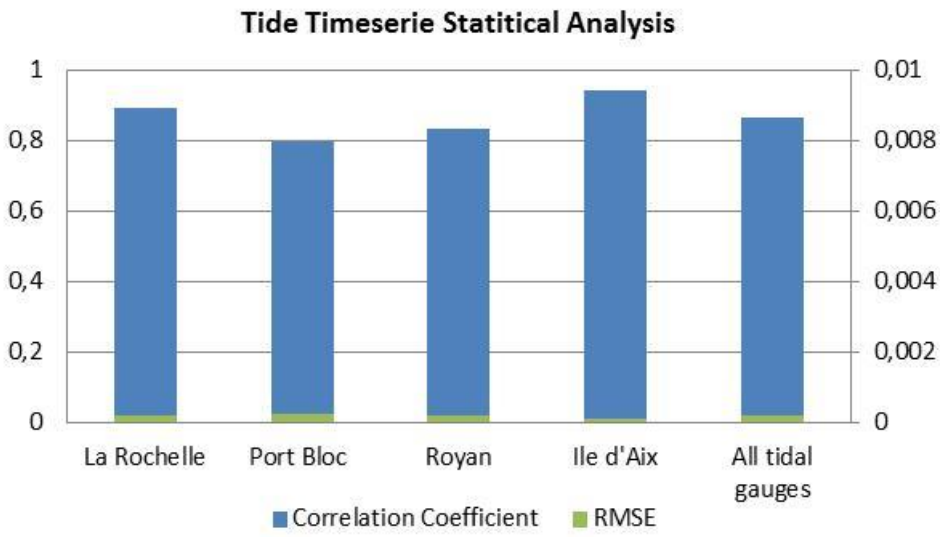

Figure 19 : Model vs field data timeseries statistical analysis
(left scale : Correlation Coefficient admimensional , right scale : RMSE in m)

5.1.2 Harmonic components analysis

For the selected gauges, a comparison between the model's harmonic components and the field data is done. **Figure 20**, **Figure 21**, **Figure 22** and **Figure 23**, show the 8 main harmonic components, based on the model's amplitude.

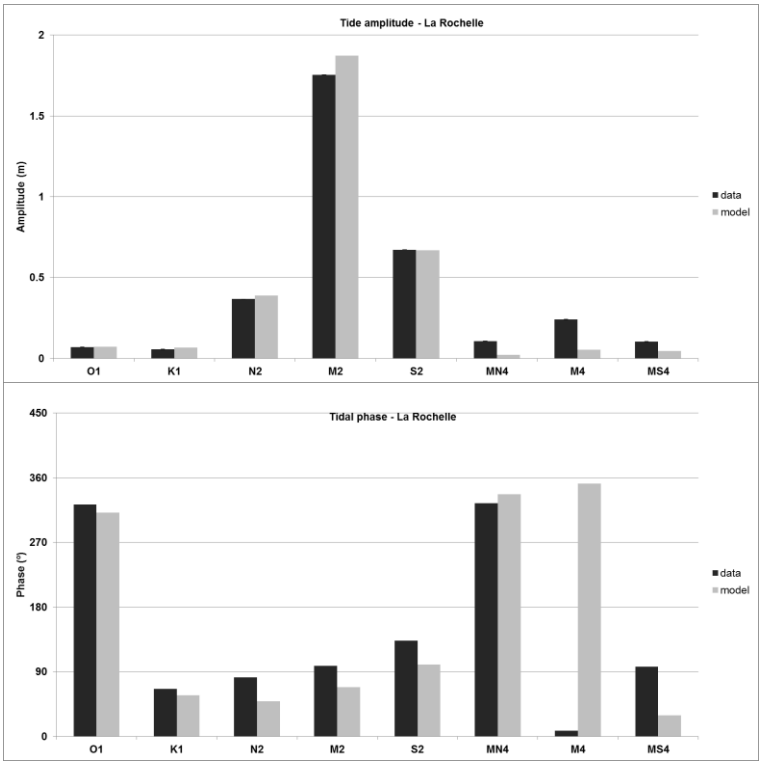

Figure 20 : La Rochelle tidal gauge harmonic analysis

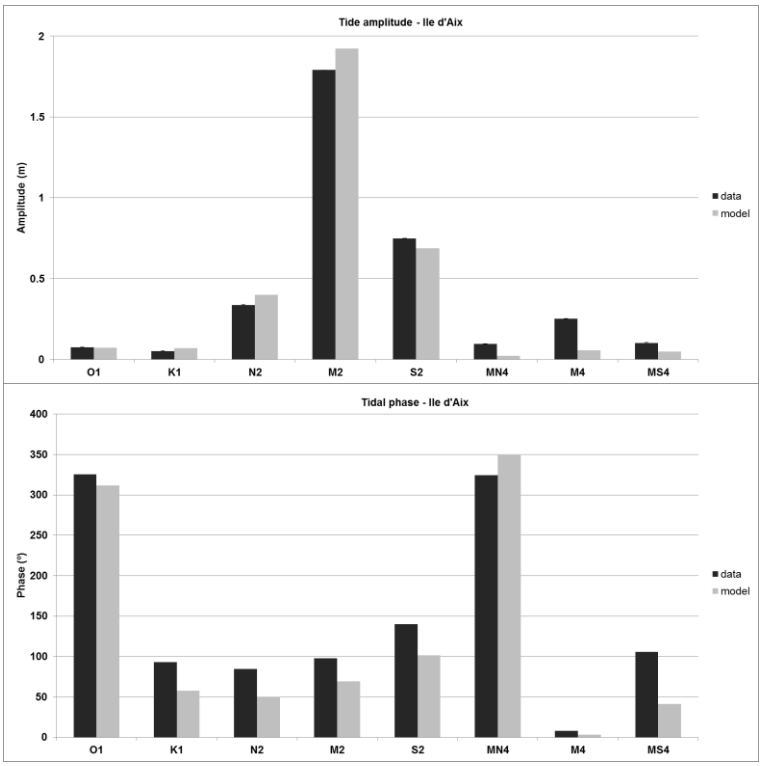

Figure 21 : Ile d'Aix tidal gauge harmonic analysis

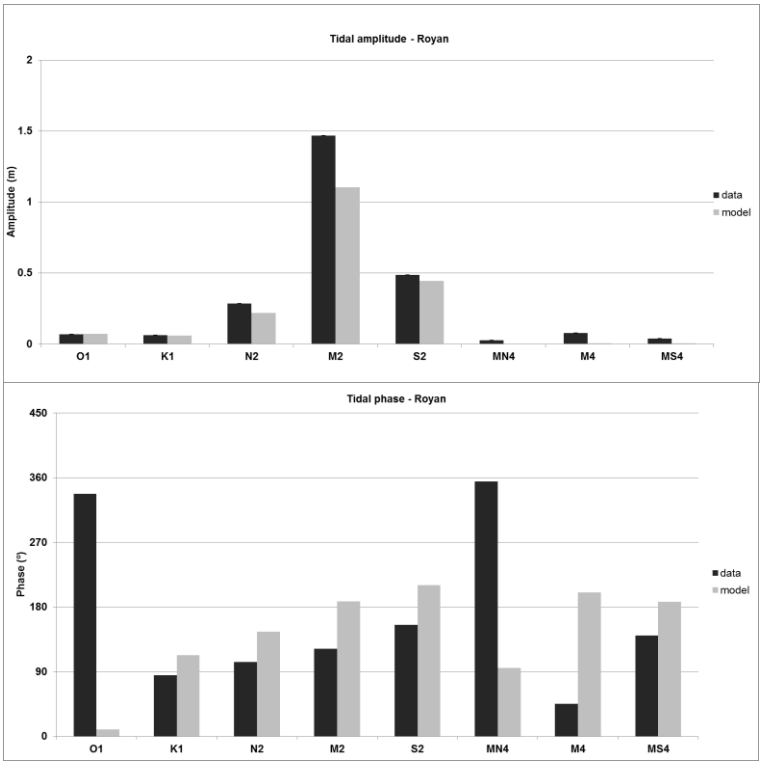

Figure 22 : Royan tidal gauge harmonic analysis

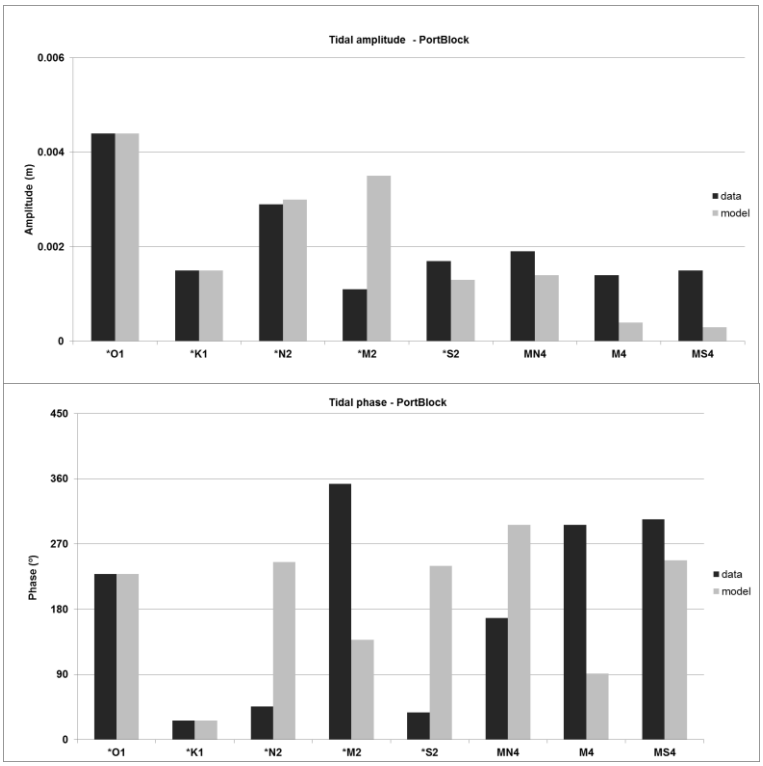

Figure 23 : Port Bloc tidal gauge harmonic analysis

From the results it is possible to conclude that we retrieve harmonic components characteristic for a semi-diurnal tide as expected from the context analysis (M2, S2, N2). We notice that there are some phase differences on the tidal gauges near Gironde coasts (Royan and Port Bloc essentially), which could be explained by a lower bathymetry accuracy in this local (**Figure 23**).

5.2 Temperature and salinity data

Temperature and salinity data were provided by EIGSI La Rochelle. The data include Medatlas CTD vertical profiles between 15 and 40m depth, for the period April 25 to June 5th, 2012. The vertical profiles were collected during the Pelgas Cruise, described in **Figure 24**.

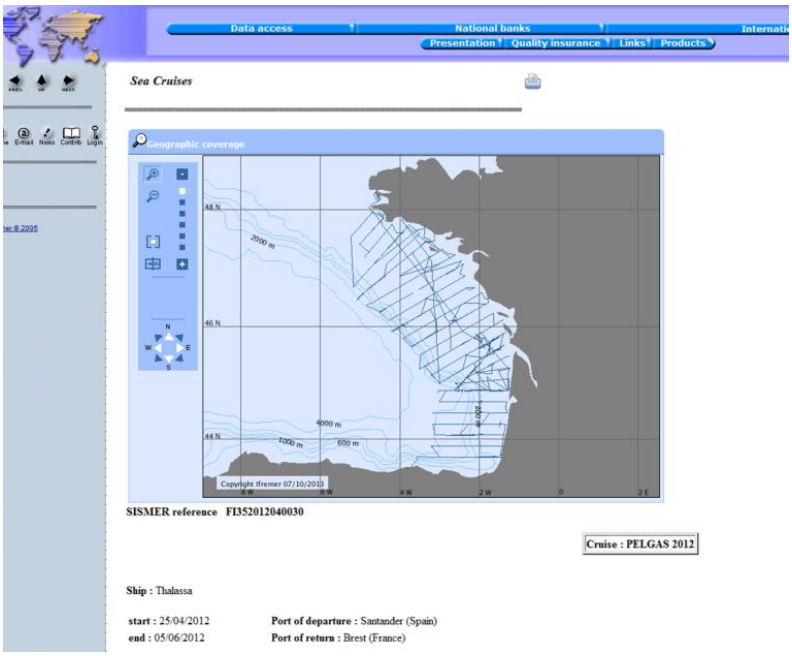

Figure 24 : Pelgas Cruise track.

5.2.1 Water level validation

Simulated water levels were compared with measured data provided by the french navy, giving good agreement.

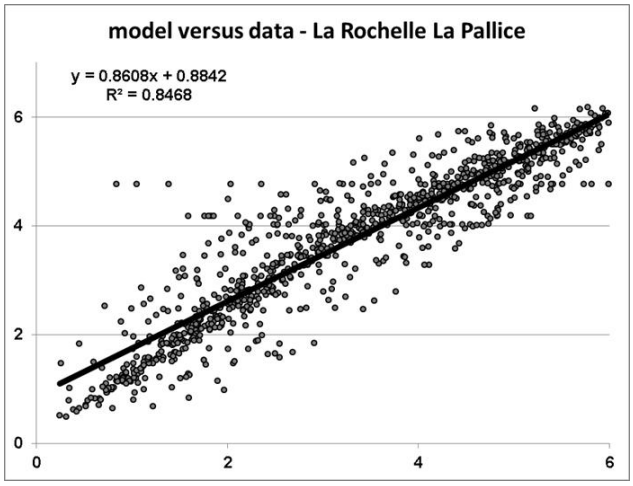

Figure 25 : Water level validation La Rochelle

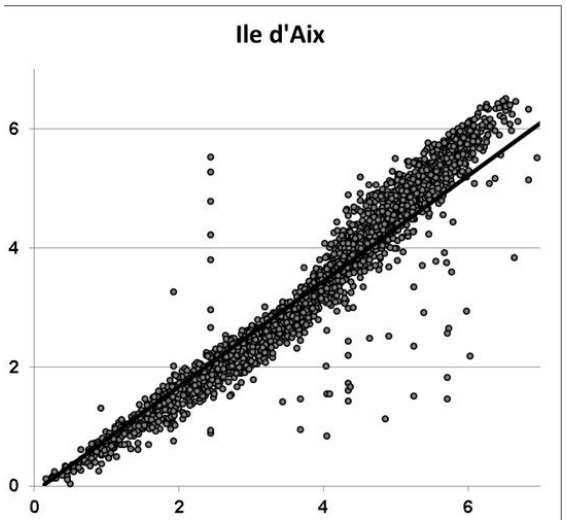

Figure 26 : Water level validation Ile d'Aix

5.2.2 Vertical profiles

Simulated salinity was compared with CTD vertical profiles available for the month of may-june 2012, collected by Pelgas Cruises, and provided by Ifremer.

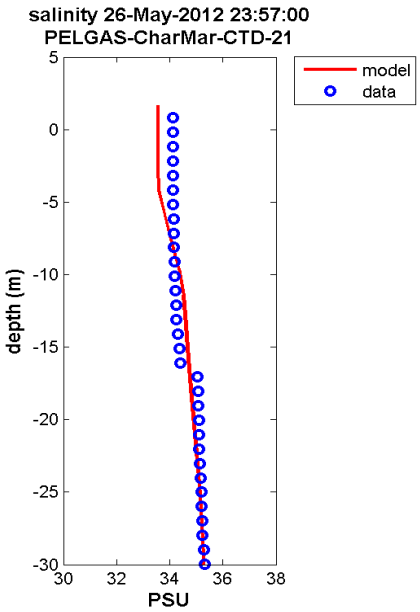

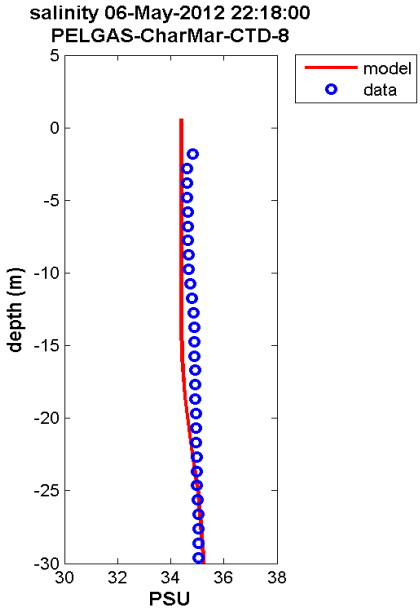

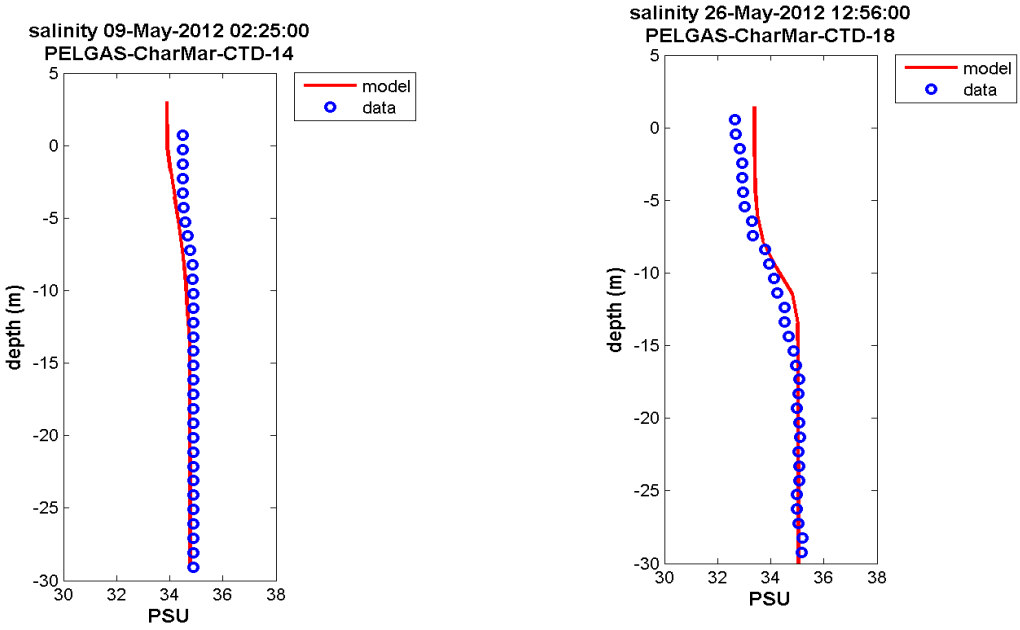

Figure 27 : Examples of comparison between simulated and measured vertical profiles

This picture shows examples of comparison between simulated and measured vertical profiles in the study area, showing a good agreement.

5.2.3 Sea Surface Temperature

A wider outlook of the whole domain can be obtained if the sea surface temperatures from the model are compared from satellite data field.

Comparison was done with satellite Sea Surface Temperature (SST) data using Odyssea Sea Surface Temperature Analysis data[1] (Group for High Resolution Sea Surface Temperature (GHRSST) Level 4 sea surface temperature analysis produced daily on an operational basis at Ifremer/CERSAT (France) using optimal interpolation (OI) on a regional 0.02 degree grid. It provides a daily cloud-free field of foundation sea surface temperature at approximately 2 km resolution (0.02 degree)).

[1] It is generated by merging microwave and infrared satellite sea surface temperature observations including those from the Advanced Very High Resolution Radiometer (AVHRR), the Advanced Along Track Scanning Radiometer (AATSR), the Spinning Enhanced Visible and Infrared Imager (SEVIRI), the Advanced Microwave Scanning Radiometer-EOS (AMSRE), the Tropical Rainfall Measuring Mission Microwave Imager (TMI) and the Geostationary Operational Environmental Satellite (GOES) Imager. The satellite SST observations are intercalibrated using the AATSR sensor as a reference (previously re-calibrated using all available in situ data). The development of the global real-time sea surface temperature at Ifremer/CERSAT is supported by European Commission initially in the frame of MERSEA project.
Product ID : MEDSPIRATION-MED-SST-OBS
Mersea Products & Services –
http://www.mersea.eu.org/html/information/catalog/products/catalog-partner.html

Simulated sea surface temperature (SST) were compared to satellite data (Figure 28 : Comparison of simulated and observed SST.

R: correlation coefficient; R2: determination coefficient; RMSE: Root mean square error; z Fisher: Fisher transformation; a, b: linear regression coefficients; Sm: simulated mean value; Om: Observed mean value; N: sample size.Figure **28Erro! A origem da referência não foi encontrada.**).

A comparison tool developed in Universidade dos Açores provides visual and statistical descriptors as :

- Correlation coefficient: also known as the Pearson product-moment correlation coefficient;
- RMSE: Root Mean Square Root.

The following **Table 8** shows the results of the descriptors, for two different duration 60 days (01-02-2012 to 31-03-2012) and 150 days (01-02-2012 to 30-06-2012).

Period	Domain	Correlation	RMSE	Bias (ºC)
60 days (01-02-2012 to 31-03-2012)	2	0.8	1.36	0.33
60 days (01-02-2012 to 31-03-2012)	3	0.6	1.68	-0.05
150 days (01-02-2012 to 30-06-2012)	2	0.5	1.15	0.48
150 days (01-02-2012 to 30-06-2012)	3	0.45	1.37	0.54

Table 8 : Statistical results of SST comparison

The model generally agrees with the observations for the first period (01-02-2012 to 31-03-2012). It presents a good correlation coefficient respectively 80% for domain 2, 60% for domain 3, indicating that there is a good correspondence between the two dataset. For the whole period (01-02-2012 to 30-06-2012), results fall down to 50% and 45% respectively.

Comparison with satellite images shows good agreement between model results and satellite images in the offshore area. The differences with satellite Sea Surface Temperature data appears to be localized closes to the coast (Gironde river and pertuis area), an example is presented in **Figure 28**.

Close to the coast, the model tends to underestimate temperature. The temperature imposed at the river boundary was based on the analysis of historical data for the years 1978-2005. Following this, one of the reasons of the error can be lack of information in the model about actual temperature of the waters discharged by the rivers. Indeed the results are worse for Domain 3 as this is the domain where freshwater inputs are imposed. Another source of error can be due to the approximations done in the model to calculate heat fluxes at the interface water-air (Ascione, 2014).

In order to validate the hypothesis of error due to lack of information about actual temperature of the waters discharged by the rivers, one can compare salinity between field data and simulation for booth domain. The advantage of this approach is to remove uncertainty with field data as salinity is null for rivers water discharges. We expect better results for Domain 3 that have higher resolution. Because of lack of time, it was not possible to do this research in this study.

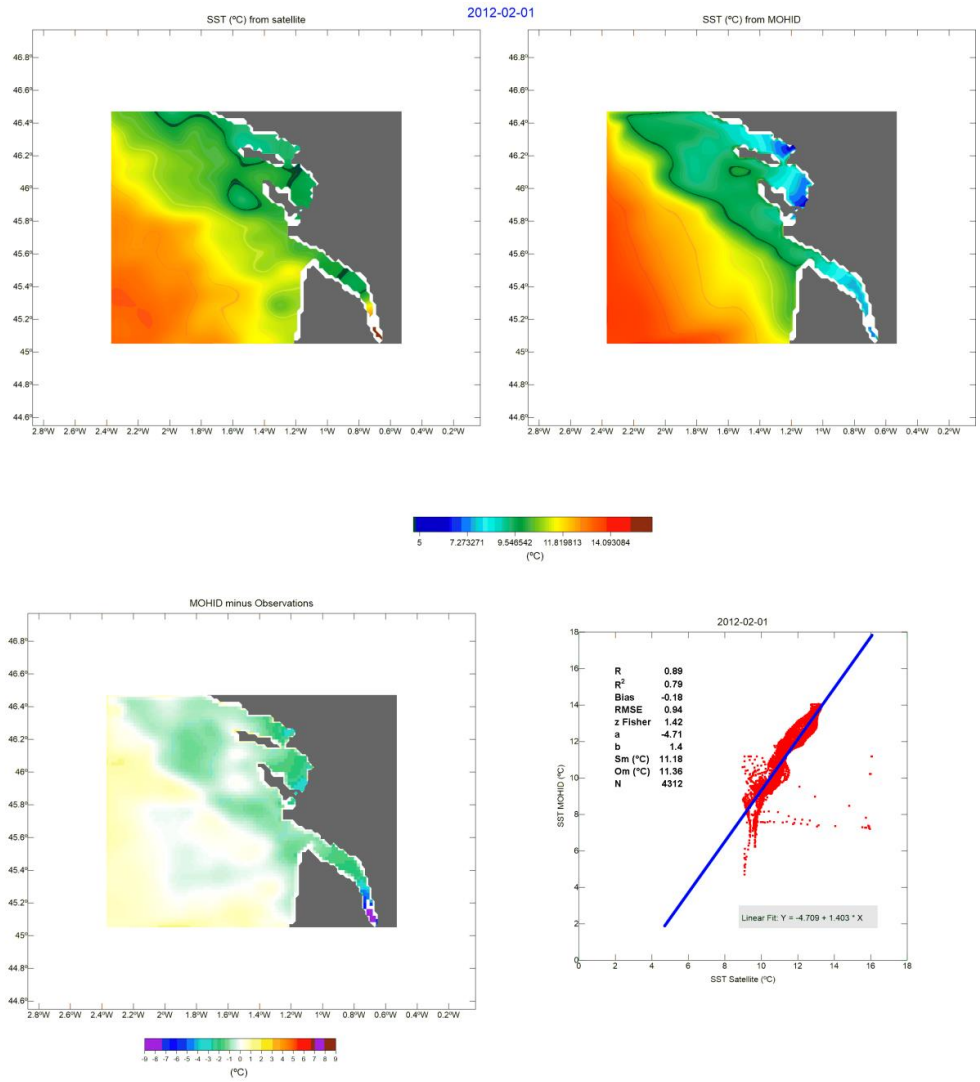

Figure 28 : Comparison of simulated and observed SST.

R: correlation coefficient; R2: determination coefficient; RMSE: Root mean square error; z Fisher: Fisher transformation; a, b: linear regression coefficients; Sm: simulated mean value; Om: Observed mean value; N: sample size.

6. OIL SPILL SIMULATION

This chapter describes the oil spill submodel, which is a 0D submodel coupled with solution imposed from the hydrodynamical model described previously.

In this submodel we use a lagrangean module that simulates the oil spill evolution in the two domains area, domain 2 and 3.

The objective here is to determine existence of spatial pattern, identify areas of shoreline affected by oil spills, and analyze the weathering processes affecting oil spills evolution.

6.1 Model Setup

The structure of the project implemented in MOHID Studio is described in Figure **29**. Each model domain is represented by the symbol with the domain name. Each model domain contains one folder with input data (named as General data) for bathymetry, boundary conditions, and initial conditions. Each model simulation ( ) is defined by the user over the desired time span.

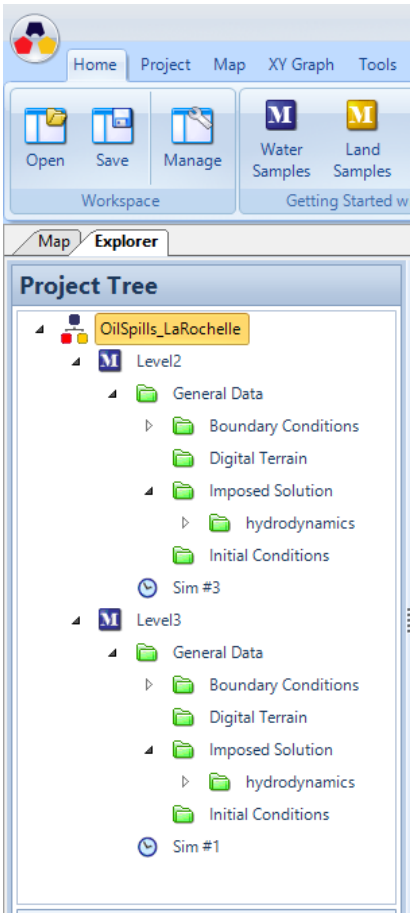

Figure 29 : Project structure

6.1.1 Grid and Bathymetry

To study the oil spill evolution on the domain, we use the same grid as the father model (domain 2 and domain 3).

6.1.2 Time span

The time span for oil spill simulation has been chose to 3 days.

6.1.3 Model coupling / Imposed hydrodynamic solution

The oil model is coupled to the hydrodynamical model in such a way that there is a flow of information (namely the hydrodynamical features: water level and velocities) to the sub model. This was done to have realistic hydrodynamical solution for the submodel without having to perform the entire run.

6.1.4 Meteorology

The meteorology dataset is the same as used in the hydrodynamical model.

6.1.5 Initial and boundary conditions

The initial condition is the property dataset field at the model start-up time.

6.1.6 Oil spill location

To choose the oil spill location, we analyze major maritime traffic road in the area. Historical information were obtained from MarineTrafic website showing all vessel positions recorded during last semester 2013, as show in Figure **30**.

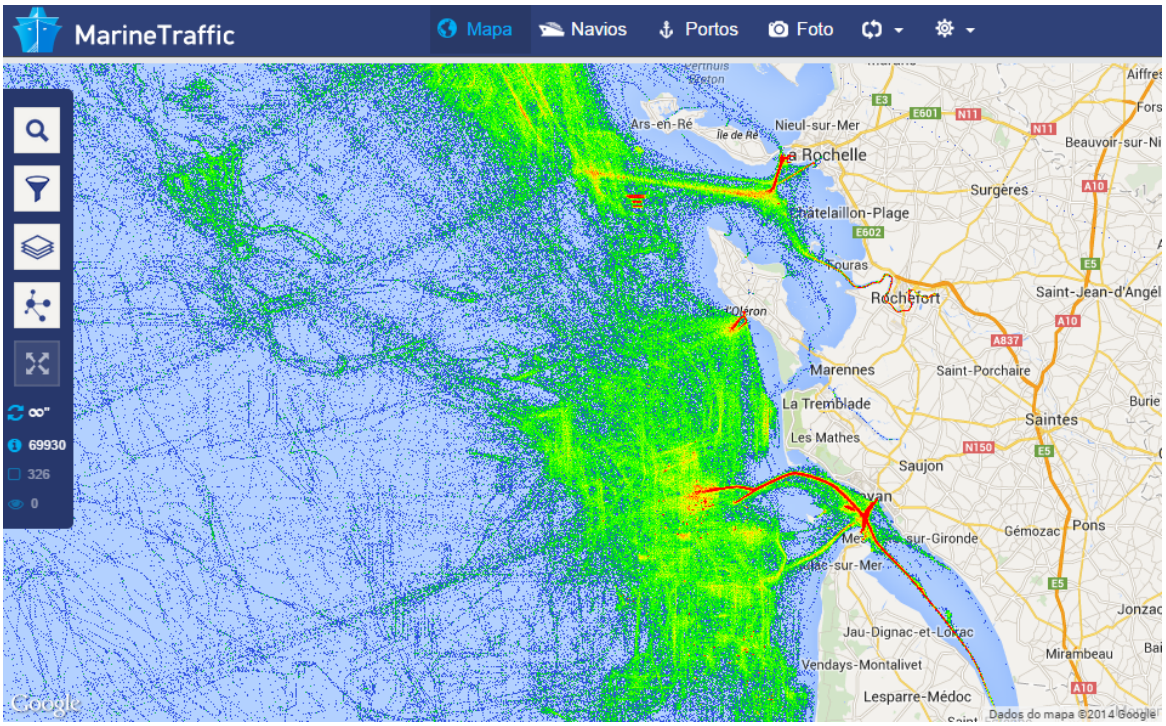

Figure 30 : Density map of all vessel positions (MarineTraffic, 2013)

Three locations origins were chosen to simulate oil spills. One origin is located near La Rochelle La Palice harbor where vessels are stationing before going to oil wharf terminal. Another one is located at the entry of Gironde estuary near Royan where we can see a crossing between local road (passenger ferry) and vessel traffic. The last origin is inside the estuary.

The list of the origin location is provided in **Table 9**. Additionally, the map with gauges location is provided in

Name	**Latitude (CGS WGS84)**	**Longitude (CGS WGS84)**
La Rochelle	-1.25	46.13
Royan	-1.05	45.6
Gironde	-0.9	45.6

Table 9 : Oil spill origin used in the oil spill simulation

Figure 31 : Oil spill location

6.1.7 Oil type

We think of oil as being a single substance, but there actually are many different kinds of oil. Oil types differ from each other in their viscosity, volatility, and toxicity. Viscosity refers to an oil's resistance to flow. Volatility refers to how quickly the oil evaporates into the air. Toxicity refers to how toxic, or poisonous, the oil is to either people or other organisms.

Generally we can group oil into four basic types in function of API[2] :

- Class 1 – Very light oils - (Jet Fuels, Gasoline): API (15ºC) > 45.0 ;
- Class 2 – Light oils - (Diesel, No. 2 Fuel Oil, Light Crudes): 45.0 > API (15ºC) >35 ;
- Class 3 – Medium oils - (Most Crude Oils): 35 > API (15ºC)> 17.5 ;
- Class 4 – Heavy oils - (Heavy Crude Oils, No. 6 Fuel Oil, Bunker C): API(15ºC) < 17.5.

We gathered characteristics from ADIOS (Automated Data Inquiry for Oil Spills), a database of more than a thousand different crude oils and refined products developed by NOAA (National Oceanic and Atmospheric Administration).

---

[2] API Gravity is used by the petroleum industry rather than density. It is determined by the following equation; API at 60°F = 141.5/oil density -131.5. The API scale provides a greater distinction between the different kinds of oils.
NOAA, 1994. ADIOStm (Automated Data Inquiry for Oil Spills) user's manual. Seattle: Hazardous Materials Response and Assessment Division, NOAA. Prepared for the U.S. Coast Guard Research and Development Centre, Groton, CT.

Two representative kind of oil have been chosen for oil spill simulation. Their characteristics are provided in **Table 10** below.

Oil name	**Carpinteria**	**West Delta**
Group	Medium oil (Group 3)	Very light oil (Group 1)
API	22.9	50.2
Pourpoint (ºC)	-21	-27
Viscosity at 15ºC (cP)	164	1
Aromatic (% weight)	30	7
Saturates (% weight)	44	92
Resins (% weight)	17	1
Asphaltene (% weight)	9	-
Maximum water content of the emulsion (%)	72	-

Table 10 : Oil characteristics for spill simulation

6.1.8 Oil spill quantity

Information from ITOPF («International Tanker Owners Pollution Federation»): http://www.itopf.org, gives a more accurate idea of accidental pollution by oil from ships. The database contains over 25 years from 1970 to 1995, about 10,000 accidents. This represents a cumulative discharge of 5 Mt of oil at sea (0.2 Mt / year), which corresponds to the release of a ton of oil to 10,000 tons transported. The majority of accidents (83%) represent small spills (less than 7 tons). For major accidents (spills greater than 700 tons), the annual number of accidents decreased from an average of 24 accidents / year during the 70s, 9 accidents / year in the 80s.

6.1.9 Oil simulation parameter

To construct scenarios of oil spill we have to choose different parameter for all process involved in oil related process as described in previous chapter.

The Figure **32** shows the weathering processes affecting oil spills.

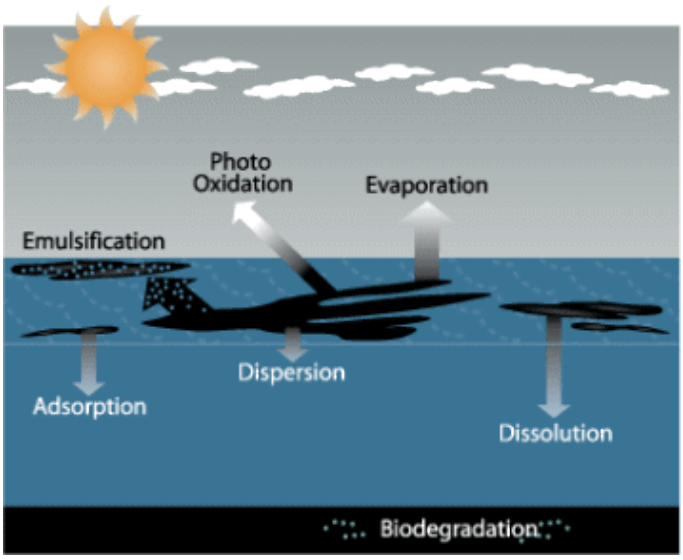

Figure 32 : Weathering processes affecting oil spills

Parameters used to configure the oil related processes in MOHID are given in **Table 11**.

Name	Tracers	Emission	Spreading	Evaporation	Dispersion	Emulsification	Beaching	Dissolution Sedimentation
Active 0 / inactive 1 (Method)	1000	Accident Instantaneous	1 (Fay)	1 (Evaporative Exposure)	1 (Delvigne)	1 (Fingas)	1	0

Table 11 : Description of parameters used in the MOHID system to configure the oil related processes

For this simulation where we are interested mainly on direction taken by oil spill we deactivated the two processes Dissolution and Sedimentation.

6.2 Model Results and Discussion

This chapter describes the results obtained with oil simulation.

6.2.1 Spatial analysis

The following images depict a synoptic view over the domain area at surface depth (0-5 m). An instant in the winter (February 2012) and the summer (june 2012) was selected for this purpose.
The different simulations show no difference between the two oil types in term of trajectory. Results are only different in term of oil spill thickness. The thickness of oil spill for the very light oil (West Delta) is inferior to medium oil (Carpinteria). The oil spill for very light oil tends to disappear during the second days of spill.

One example is presented in **Figure 33**. The medium oil (Carpinteria) shows a thickness of 3 cm, at the same time the very light oil (West Delta) already shows a thickness inferior to 0.5 cm.

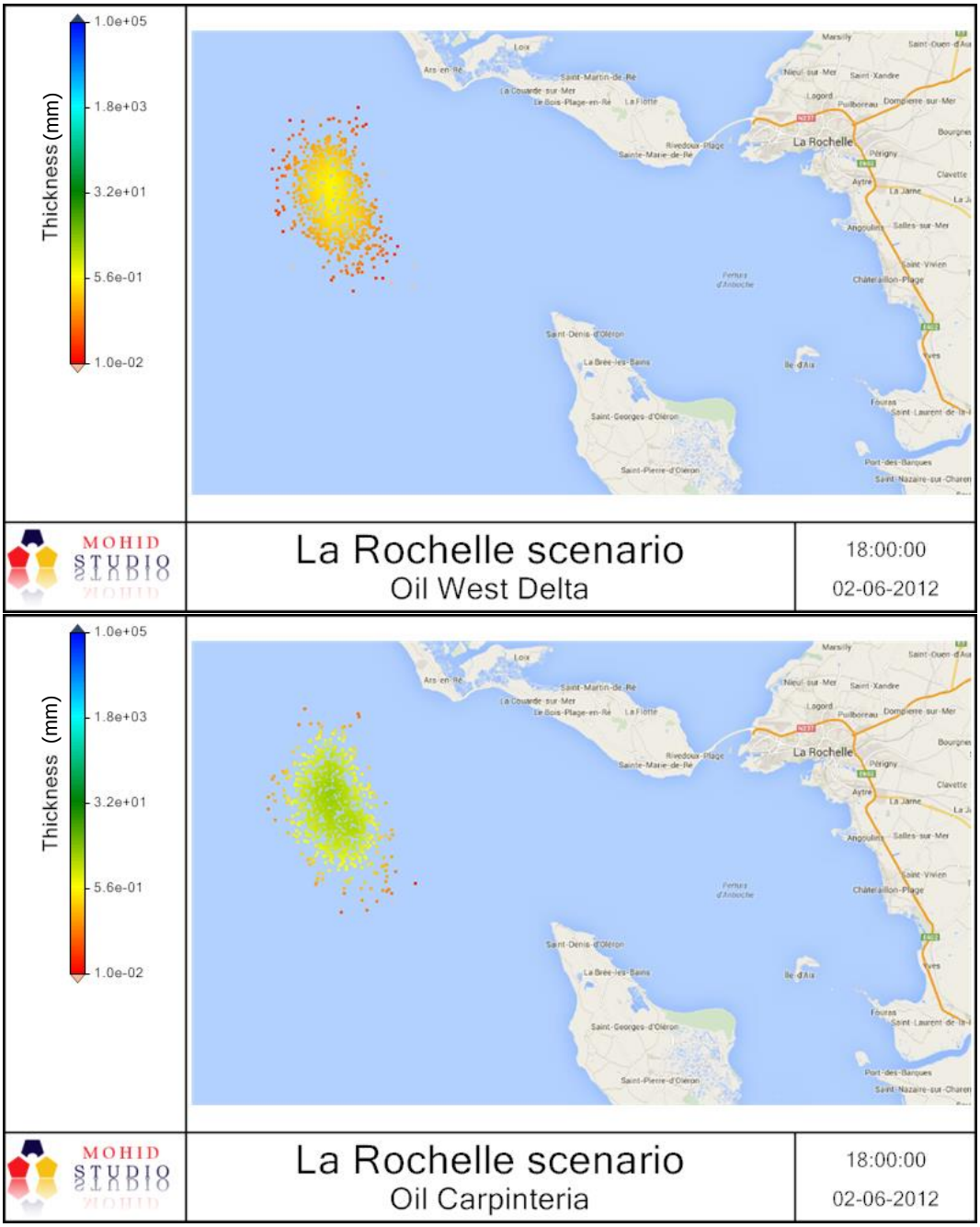

Figure 33 : Oil spill simulation showing booth type of oil

6.2.1.1 Winter scenario

The first scenario has been run for three days (01-02-2012 to 04-02-2012) for the three origins in domain 2 and 3. All scenarios are giving the same shape of plume behavior where the oil plume is quickly push off to ocean in direction South – West and exit the domain in 2 days for domain 2 and less of 2 days for domain 3. We will present here the case of La Rochelle origin.

We compare the lagrangean tracers course with hydrodynamic velocity and wind stress to determine which of them is responsible of the plume movement. Figure **34** and Figure **35** present the same location at 3 hours of interval (16 hrs and 19 hrs) for the day 01-02-2012.

Figure **34** below is coupling the oil spill tracer with the hydrodynamic velocity which represents the current at the surface. The hydrodynamic parameter seems to have no influence on the oil spill movement.

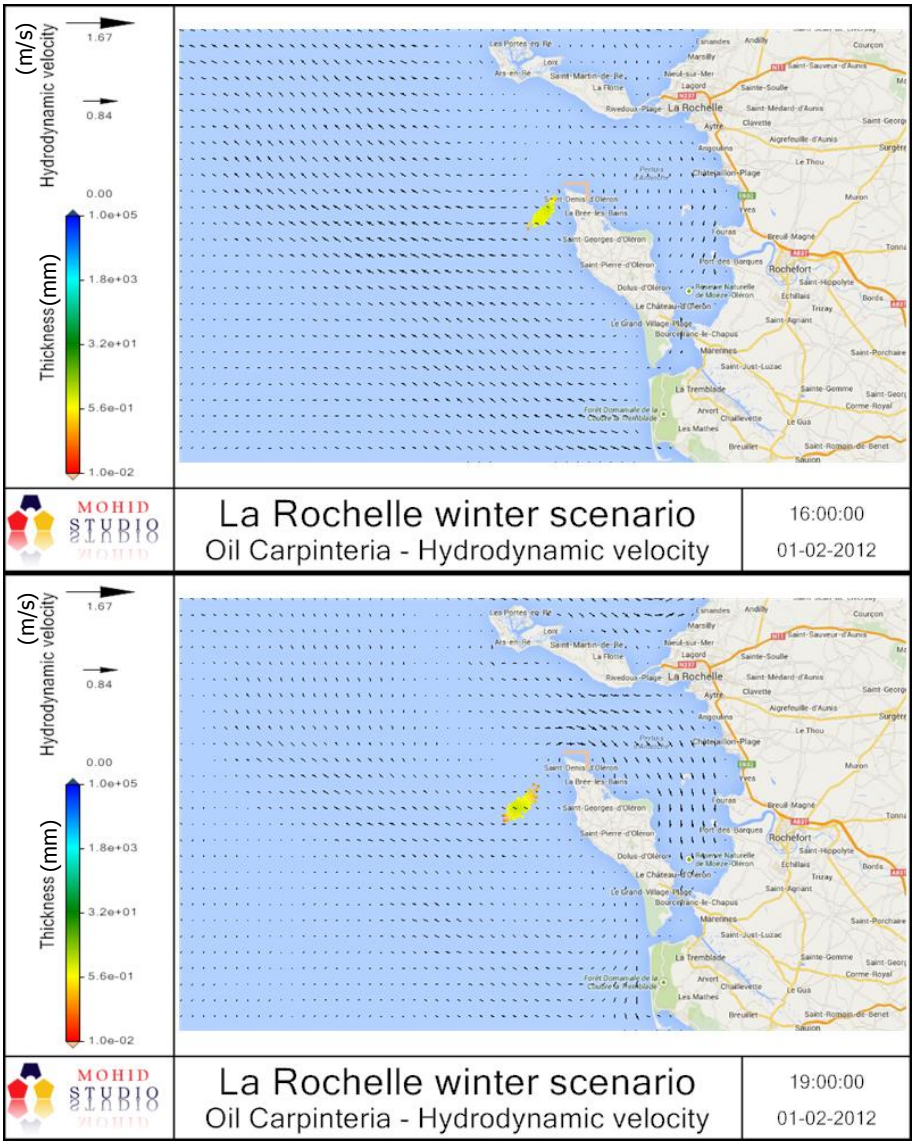

Figure 34 : Oil spill simulation for La Rochelle in winter scenario showing hydrodynamic velocity

Figure 35 is coupling the oil spill tracer with the wind stress which represents the wind at the surface. We can notice that the tracers are exactly following the wind stress direction South-West.

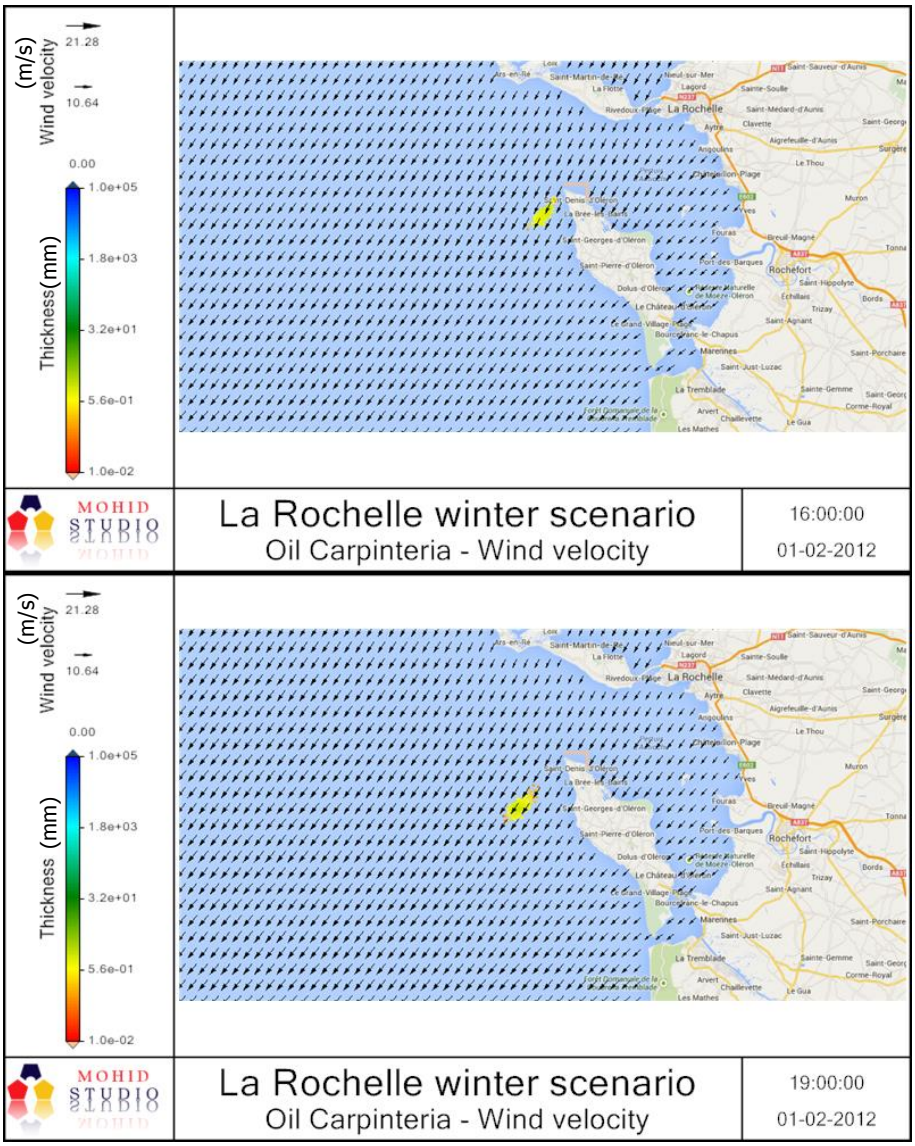

Figure 35 : Oil spill simulation for La Rochelle in winter scenario showing wind stress

The winter scenario presents a typical wind driven movement of the plume. This meteorological scenario is typical for this season as we seen in previous chapter, with light winds coming mostly from the continent (NE to SE) for a cumulative frequency inferior a 48% of the time.

6.2.1.2 Summer scenario

The second scenario has been run for three days (01-06-2012 to 04-06-2012) for the three origins in domain 2 and 3. The different scenarios are giving the same kind of results where the plume seems to oscillate around the origin and finally beach to the coastal area. We will present here the case of La Rochelle origin.

We compare the lagrangean tracers course with hydrodynamic velocity and wind stress to determine which of them is responsible of the plume movement. Figure **36** and Figure **37** present the same location at 2 hours of interval (8 hrs and 10 hrs) for the day 01-06-2012.

Figure **36** is coupling the oil spill tracer with the hydrodynamic velocity which represents the current at the surface. We can notice that the tracers are following the hydrodynamic velocity. Oil plume is transported following the tide movement.

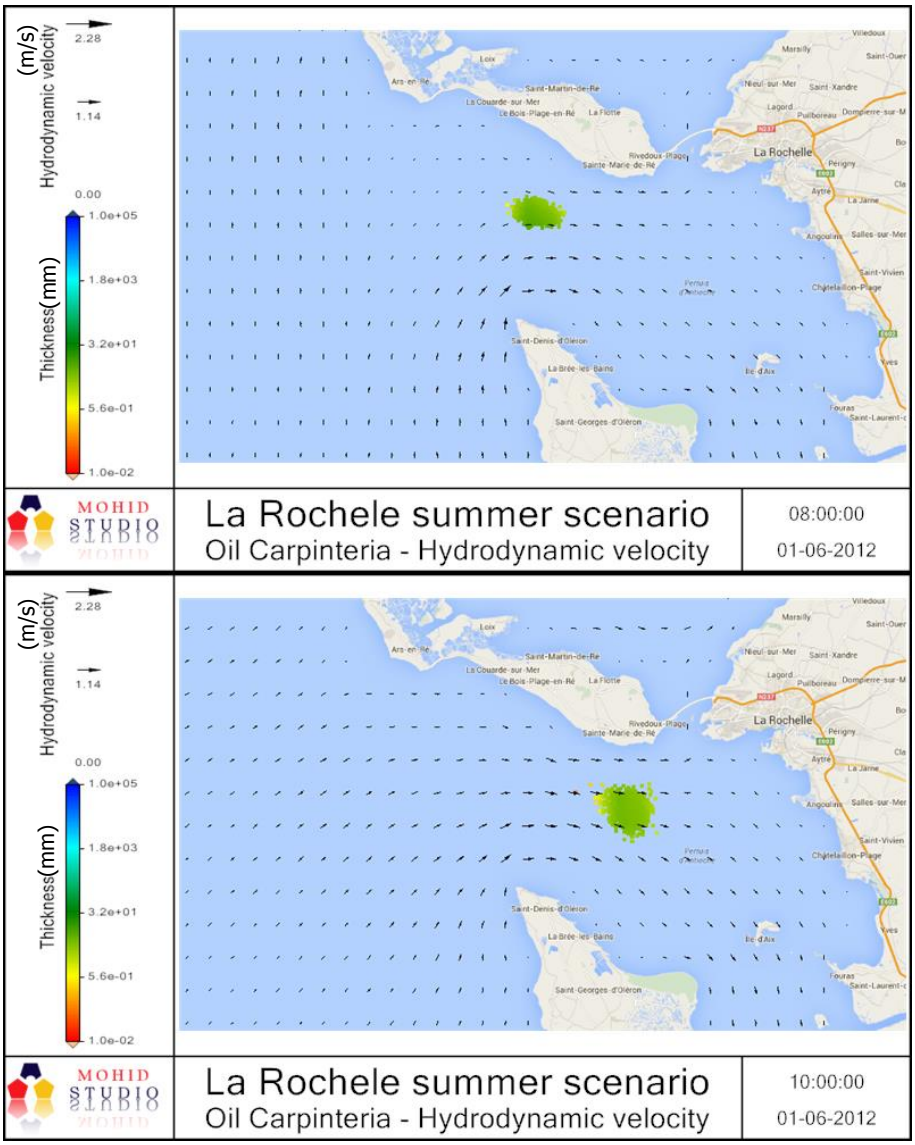

Figure 36 : Oil spill simulation for La Rochelle in summer scenario showing hydrodynamic velocity

Figure **37** is coupling the oil spill tracer with the wind stress which represents the wind at the surface.

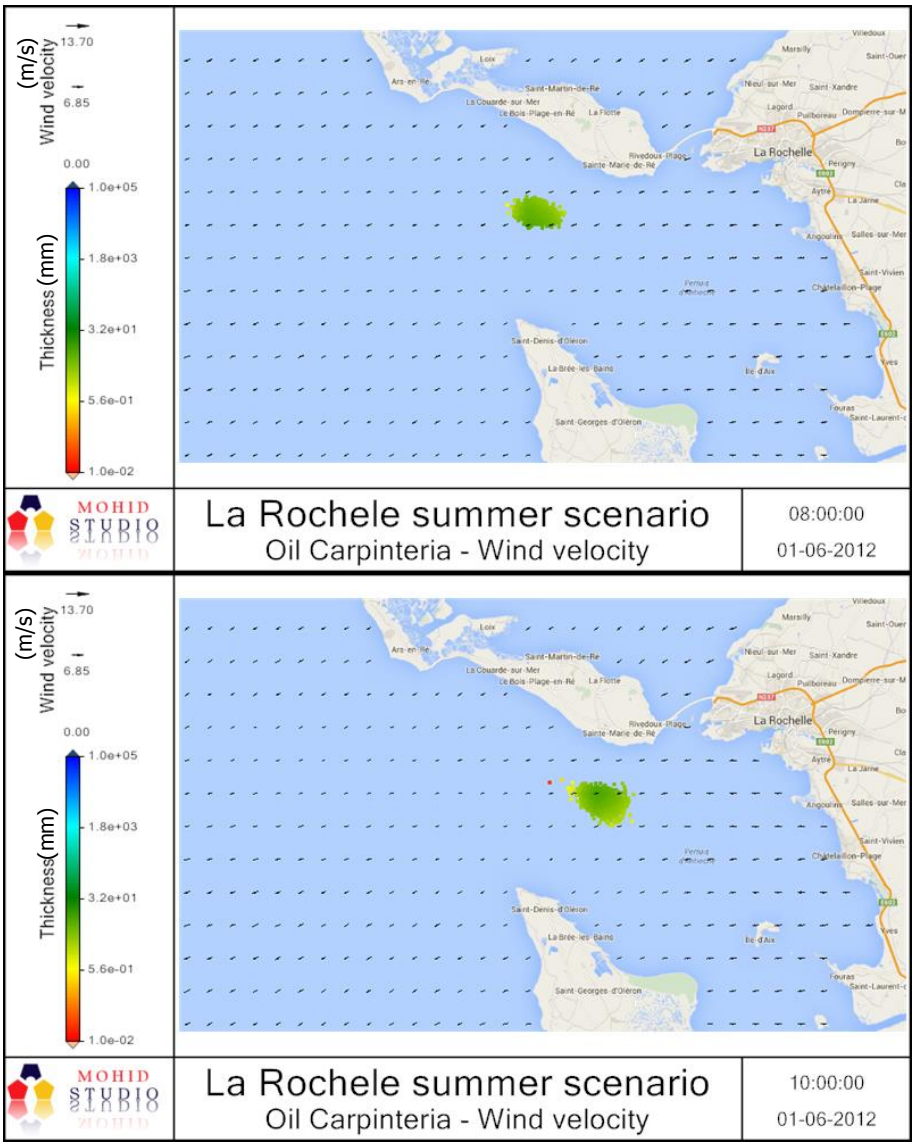

Figure 37 : Oil spill simulation for La Rochelle in summer scenario showing wind stress

We are in a scenario with almost absence of wind stress. This meteorological scenario is typical for this season as we seen in previous chapter where weak winds are present near 60% of the time, mainly to West North East (NW 15% of the time Chassiron, N 14% of the time and W 13.5% of the time in La Rochelle). The summer scenario presents a typical hydrodynamic driven movement of the spill.

We can notice the effect of wind stress in the third day where there is a cumulative effect of wind Figure **38** and tide Figure **39** pushing the plume toward the coastal area despite the hydrodynamic velocity field being null or in opposite direction.

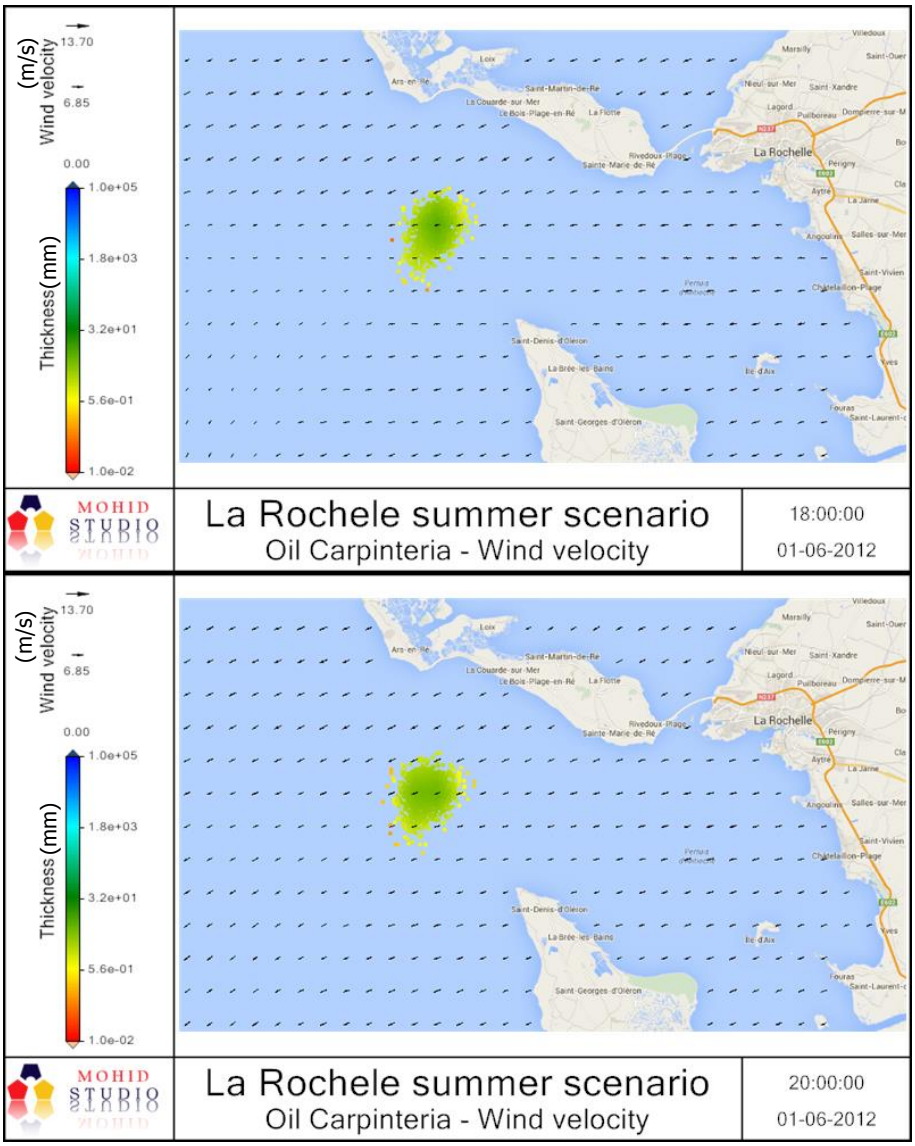

Figure 38 : Third day of oil spill simulation for La Rochelle in summer scenario showing wind stress

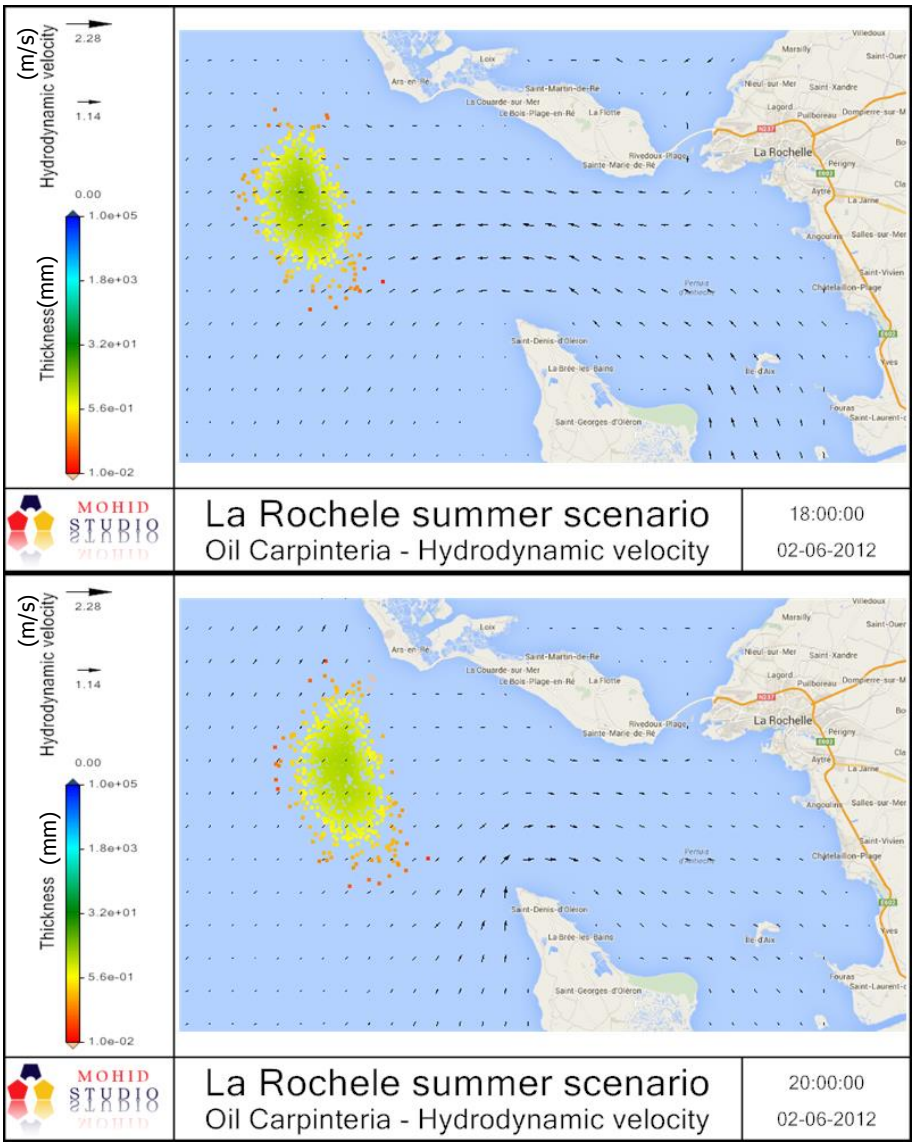

Figure 39 : Third day of oil spill simulation for La Rochelle in summer scenario showing hydrodynamic velocity

6.2.2 Areas of shoreline affected by oil spills

We found previously scenarios where the shoreline is affected by oil spills. While activating the beaching parameter in our model we can determine areas affected by this spill.

Winter scenario

We will present here the results for the tree origins selected in **Figure 31** in the winter scenarios running for five days (01-02-2012 to 06-02-2012). **Figure 43**, **Figure 44** and **Figure 45** show results for the end of simulation for respective origins.

Figure 40 : Beaching results of oil spill simulation for La Rochelle in winter scenario

We can see here a limited coastal area of approximately 3 km in the north of Ile d'Oléron impacted by the oil spill.

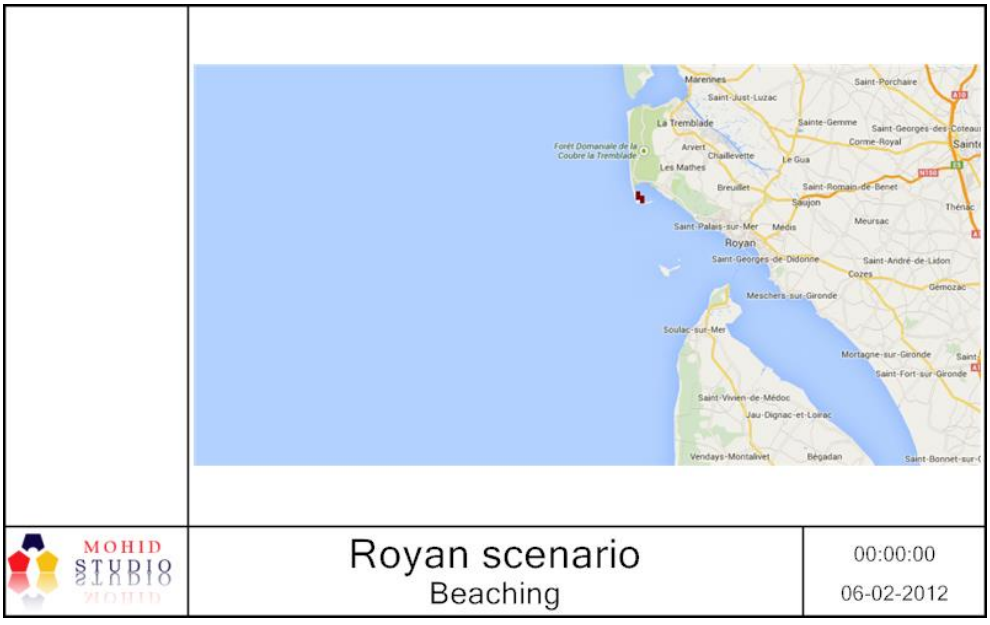

Figure 41 : Beaching results of oil spill simulation for Royan in winter scenario

We can see here a limited coastal area of approximately 2 km in the north of Gironde estuary impacted by the oil spill.

Figure 42 : Beaching results of oil spill simulation for Gironde in winter scenario

We can see here a limited coastal area of approximately 7 km in the south of Gironde estuary impacted by the oil spill.

Summer scenario

We will present here the results for the tree origins in the summer scenario running five days (01-06-2012 to 06-06-2012). **Figure 43**, **Figure 44** and **Figure 45** show results for fourth and fifth days of simulation for respective origins.

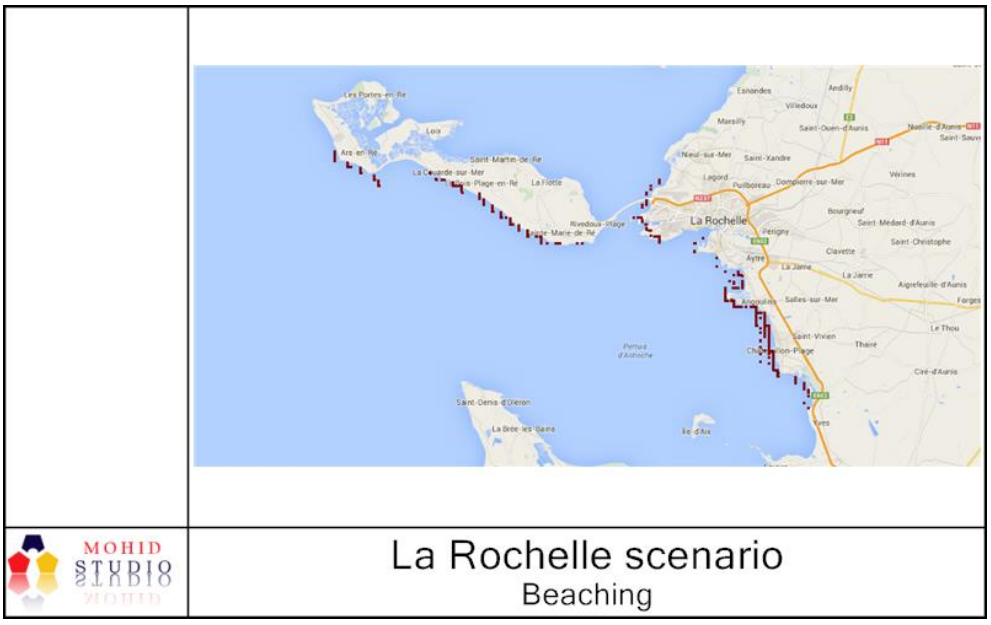

Figure 43 : Beaching results of oil spill simulation for La Rochelle in summer scenario

We can see here a coastal area of approximately 50 km impacted by the oil spill. The coastal area on south of La Rochelle is first impacted. The Ile de Ré island is also impacted by the spill. Finally currents move oil spill to north spreading impact to Pertuis Breton coastal area.

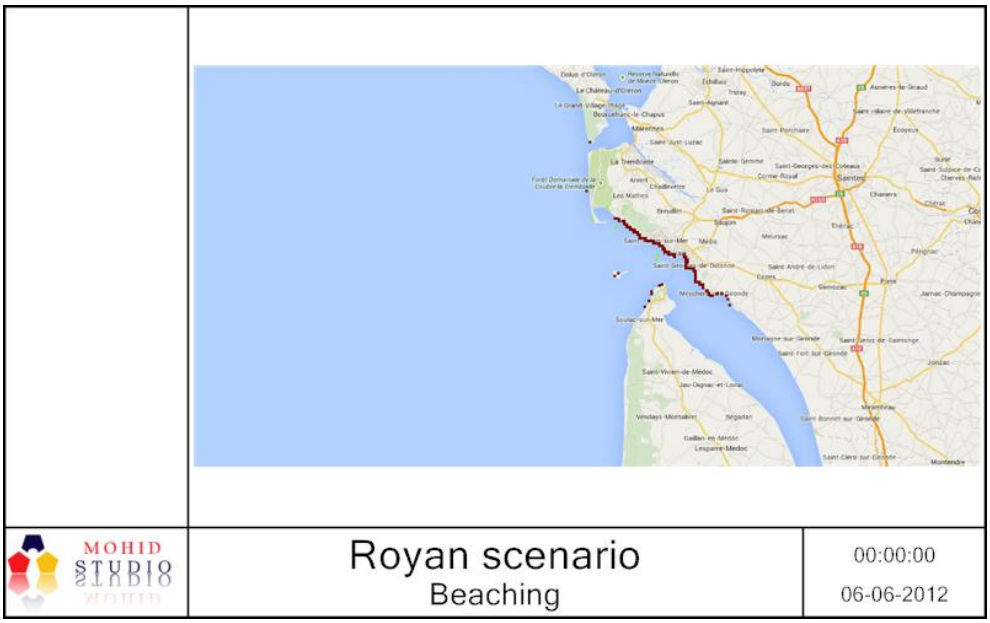

Figure 44 : Beaching results of oil spill simulation for Royan in summer scenario

We can see here a coastal area of approximately 30 km impacted by the oil spill. A small coastal area on south of origin is firstly impacted by the spill. Spill move after to north impacting coastal area from Royan to Pertuis de Maumusson and also south of Ile d'Óleron Island.

Figure 45 : Beaching results of oil spill simulation for Gironde in summer scenario

Results are similar to Royan scenario. We can see here a coastal area of approximately 30 km impacted by the oil spill. Difference is here that some oil will enter in Gironde estuary impacting north and south of Gironde estuary.

Areas most subject to the impact of spills found here correspond to areas very sensitive as we have seen in the first chapter, booth for tourist and shellfish activities. Oil spill will affect the physical, chemical and biological characteristics of marine ecosystems and the quality of coastal waters.

6.2.3 Oil arrival time

Another way to study trajectory and evolution of spill can be represented by the oil arrival time.

The following figures show this parameter for the different origins scenario.

Figure 46, Figure **47** and Figure **48** correspond to winter scenario. Figure **49**, Figure **50** and Figure **51** correspond to summer scenario.

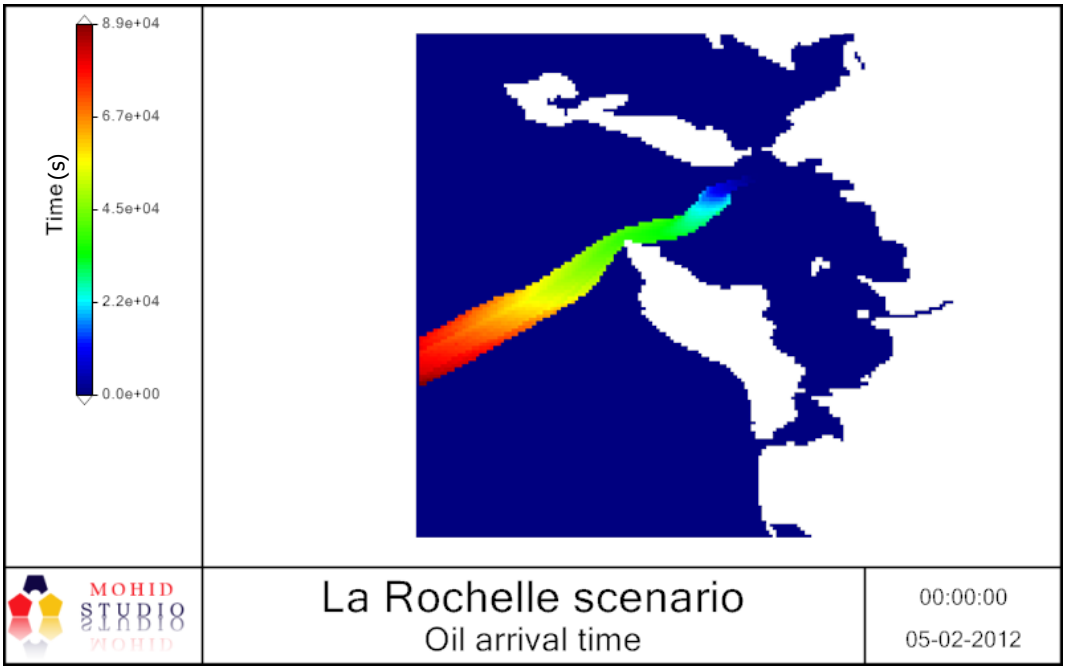

Figure 46 : Oil arrival time (second) for La Rochelle in winter scenario

We retrieve in **Figure 46** the trajectory toward south west in winter scenario induced by wind stress as seen previously. The spill reaches north Oléron Island in only 12h and exit the domain in 24h.

The scenario appears favorable for coastal area as oil spill spread toward the Atlantic Ocean. It is important to note here that we do not know where the oil spill will propagate when it exist the domain and can be push to any coastal area.

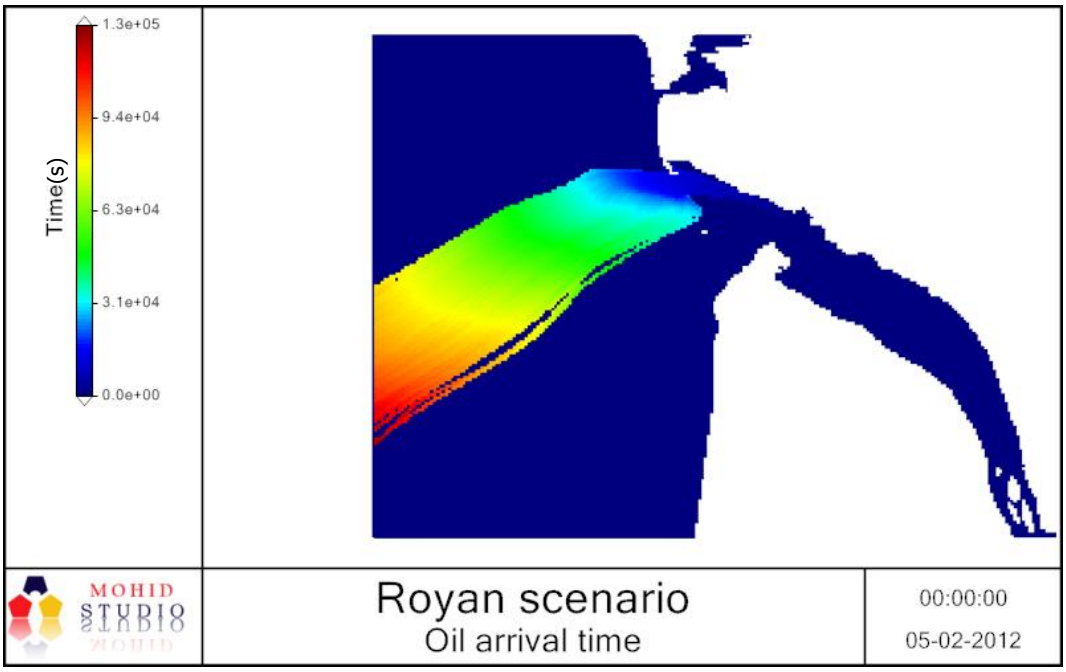

Figure 47 : Oil arrival time (second) for Royan in winter scenario

The result for Royan scenario is similar to La Rochelle where the spill spread out of domain in 24 hours.

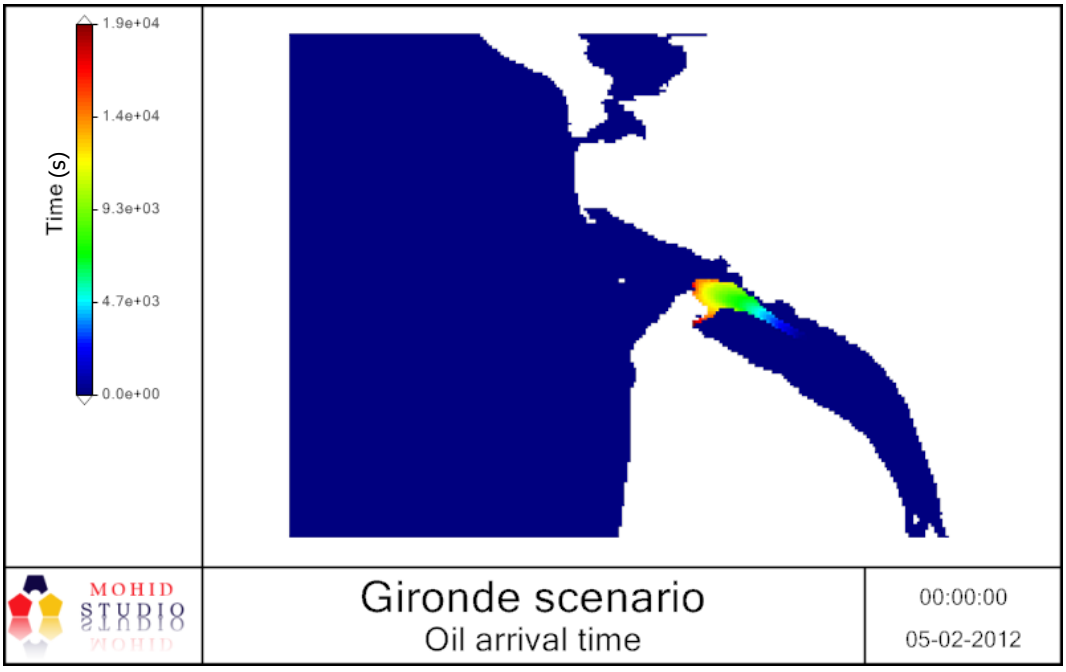

Figure 48 : Oil arrival time (second) for Gironde in winter scenario

For Gironde origin scenario the spill encounters in its path the south coast of Gironde Estuary after 4h.

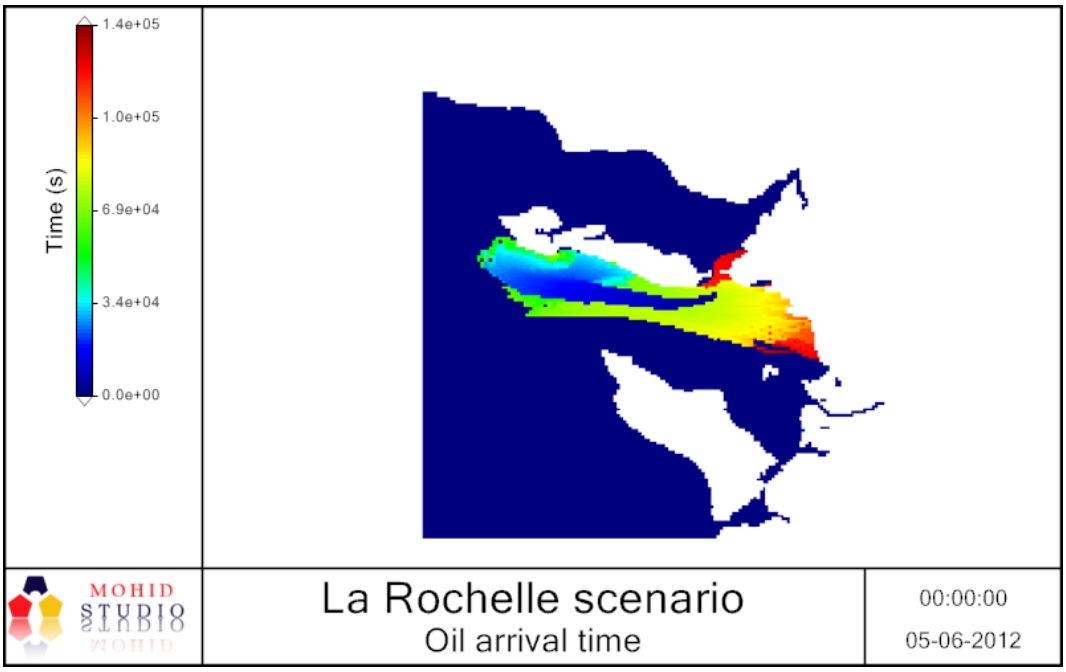

Figure 49 : Oil arrival time (second) for La Rochelle in summer scenario

We retrieve in Figure **50** the oscillating trajectory identified for summer scenario as seen previously. The spill oscillates from origin following tide current and reaches finally La Rochelle coast after 2 days.

The information of oil boom movement and position in function of time can be very helpful to determine where to place oil barrier for spill response.

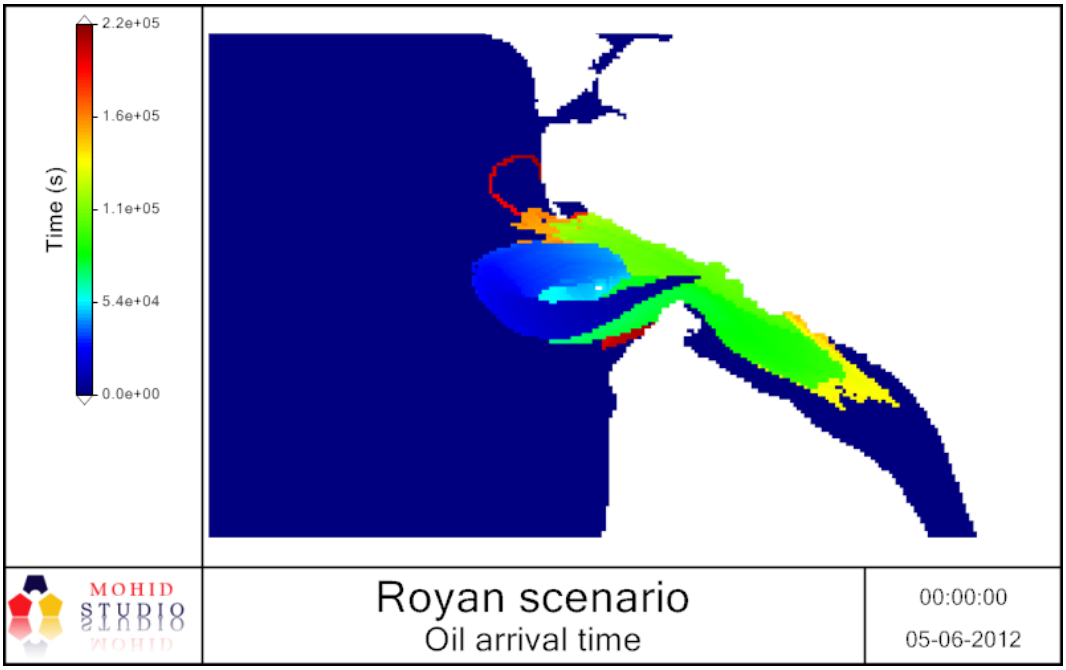

Figure 50 : Oil arrival time (second) for Royan in summer scenario

The result for Royan scenario is similar to La Rochelle. Oil spill will reach north Gironde estuary coast after 30 hours and remains 2.5 days to ends.

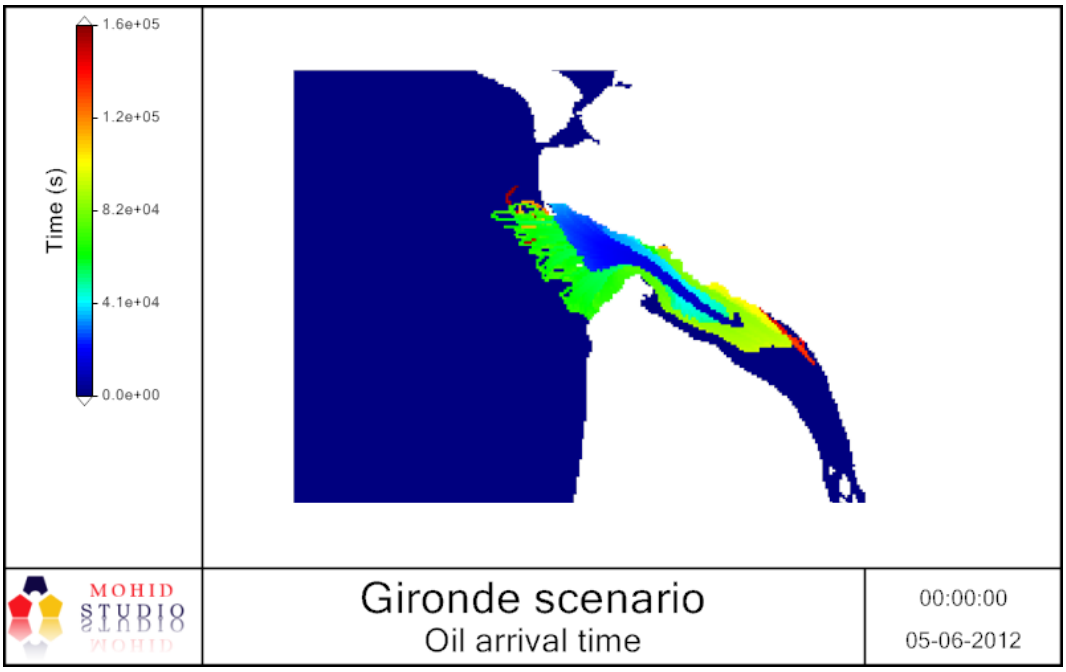

Figure 51 : Oil arrival time (second) for Gironde in summer scenario

The result for Royan scenario is similar to La Rochelle. Oil spill will reach north and south Gironde estuary coast after 20 hours and remains less than 2 days to ends.

6.2.4 Oil weathering process - Detailed analysis (Timeseries)

The behavior of oil depends closely on the type of product spilled. We should also consider the spill origin (coastal, estuary, offshore), weather and sea conditions (waves, currents, wind, sunshine).
Oil is subject to the effects of the environment resulting to its dispersion in the marine environment and at the same time changing its physical and chemical characteristics, the so-called "aging" of oil. The behavior of oil spill is the result of a set of interactions between the spill and the external environment.
A phase of short-term evolution occurs in the first days after the spill marked by the following process:

- spread of the spill,
- evaporation of light fractions,
- dissolution of the most soluble compounds,
- emulsification of the product as a result of agitation,
- sedimentation by attaching the product to the suspended solids.

It is during this phase of evolution that many major phenomena are observed: the movement of oil spills on the surface of the water under the effect of winds and currents, potential coastal pollution,

the dispersion of oil in the body of water, contamination of the seabed, the immediate ecological effects kills and heavy contamination of marine species (shellfish, fish).

Crude oils are complex and variable mixtures of hydrocarbons. Therefore their consistence may range from a volatile liquid to that of a viscous semi-solid. Refined products represent different distillation fractions of crude oils in the order of their increasing density: gasoline, kerosene, fuel oils, lubricating oils, residual fuel oils, bitumen. A petroleum product is characterized by its chemical composition and physical properties.

The following figures show the weathering processes affecting oil spills for two selected representative's kind of oil: a medium oil (Carpinteria) and a very light oil (West Delta).

6.2.4.1 Area

The area for the very light oil is almost the double than for the medium oil (50 km^2). Results agree with the expected as the light oil viscosity is much lower than the medium oil (respectively 1 and 164 cP at 15ºC). And viscosity is a measure of a fluid's resistance to flow and spread. Figure **52** shows the evolution of the plume area for the first day of spill.

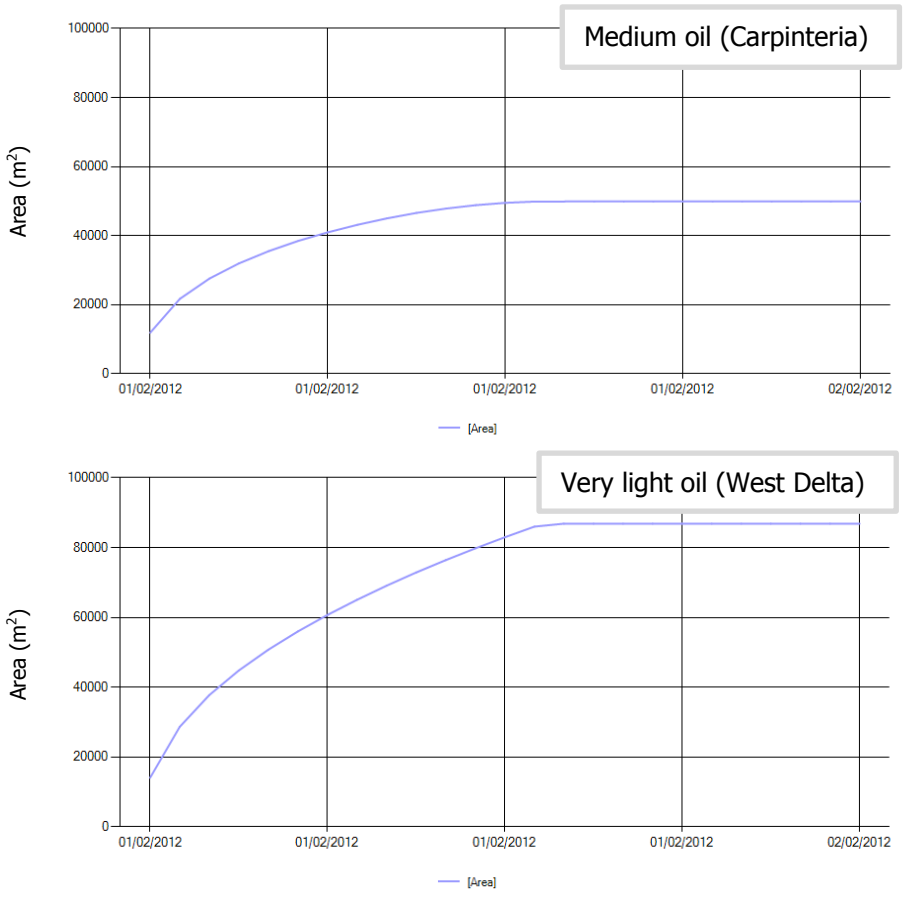

Figure 52 : Area of oil spill in m^2

6.2.4.2 Mass fraction evaporated and dispersed

The mass fraction evaporated and dispersed represented in Figure **53** correspond to a percentage of mass loss from this two oil process weathering. The medium oil (Carpinteria) is not dispersed and evaporated about 20% of this mass at the end of the first day of spill. The very light oil (West Delta) is dispersed about 40% of mass and evaporated about 60%.

The dispersion corresponds to the distribution of spilled oil into the upper layers of the water column by natural wave action. The presence of Asphaltenes[3] (9% of weight) in the medium oil can explained the absence of dispersion due to the fact that oils containing them more than 0.5% of weight tends to form emulsions. The viscosity explained also these phenomena.

The evaporation is the process whereby any substance is converted from a liquid state to become part of the surrounding atmosphere in the form of a vapor. The value is explained by the higher volatility of the light oil.

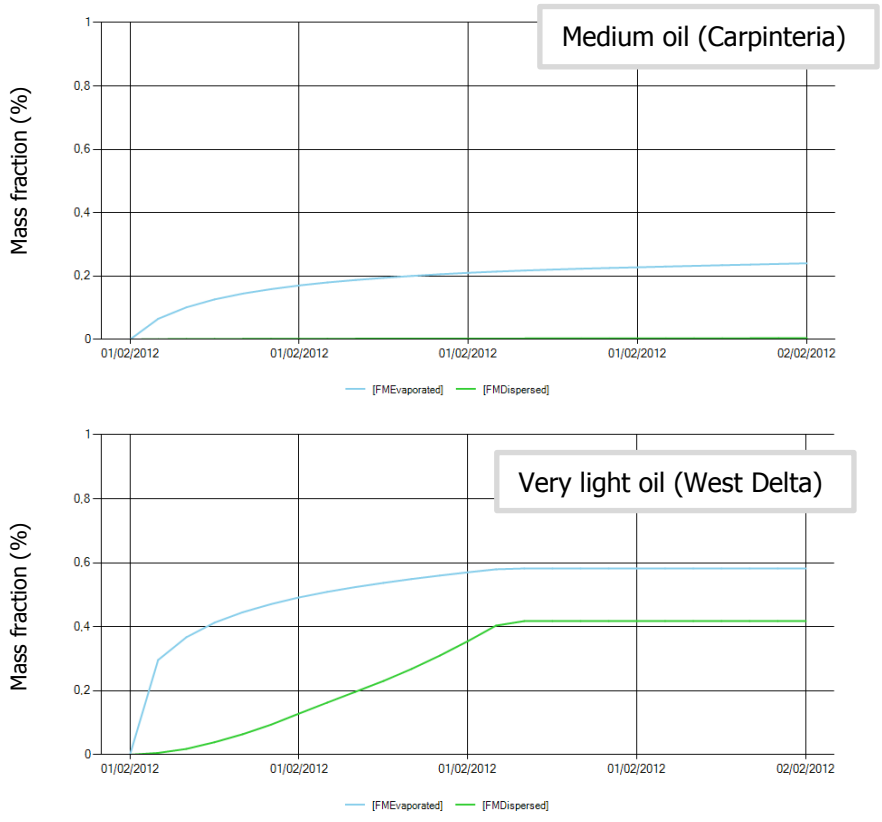

Figure 53 : Mass fraction evaporated and dispersed in %

[3] Defined as pentane insoluble hydrocarbons consisting of large aromatic molecules that can carry alkyl and alicyclic substitutions with heteroatoms and trace metals.
Elizabeth A. Harvey 10/21/98 "Crude Oil Characterization Spill Sheets".

6.2.4.3 Thickness

The thickness of the oil plume represented in Figure **54** agree with the results obtained previously with the very light oil (West Delta) tending to expend plume area and also evaporating and dispersing more, resulting in a fine layer in the middle of the first day. Contrarily to the medium oil (Carpinteria) staying with a stable layer of almost 2 cm corresponding to an emulsion evaporating slowly.

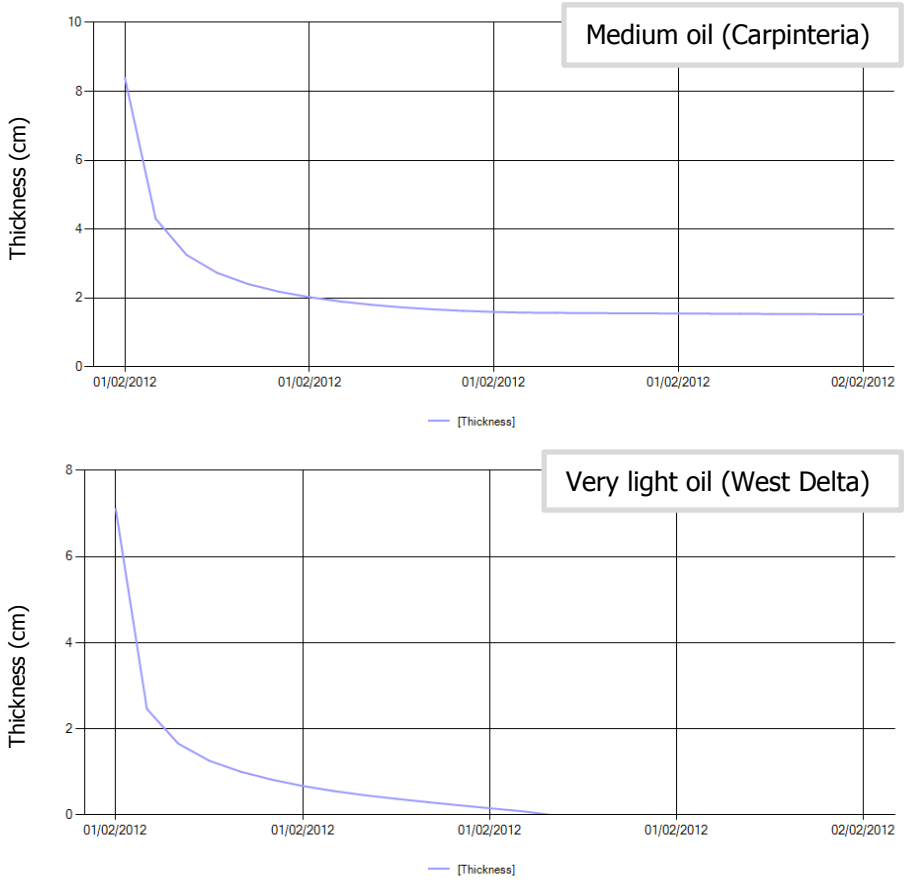

Figure 54 : Thickness of oil spill in centimeter

6.2.4.4 Volume of oil evaporated and dispersed

Figure **55** resumes the oil weathering processes previously explained with the evolution in term of total volumes, evaporated and dispersed. We notice here that for medium oil almost 80% will persist as floating oil. Contrary to light oil that is either evaporated or naturally dispersed into the water column in time frames of a couple of hours.

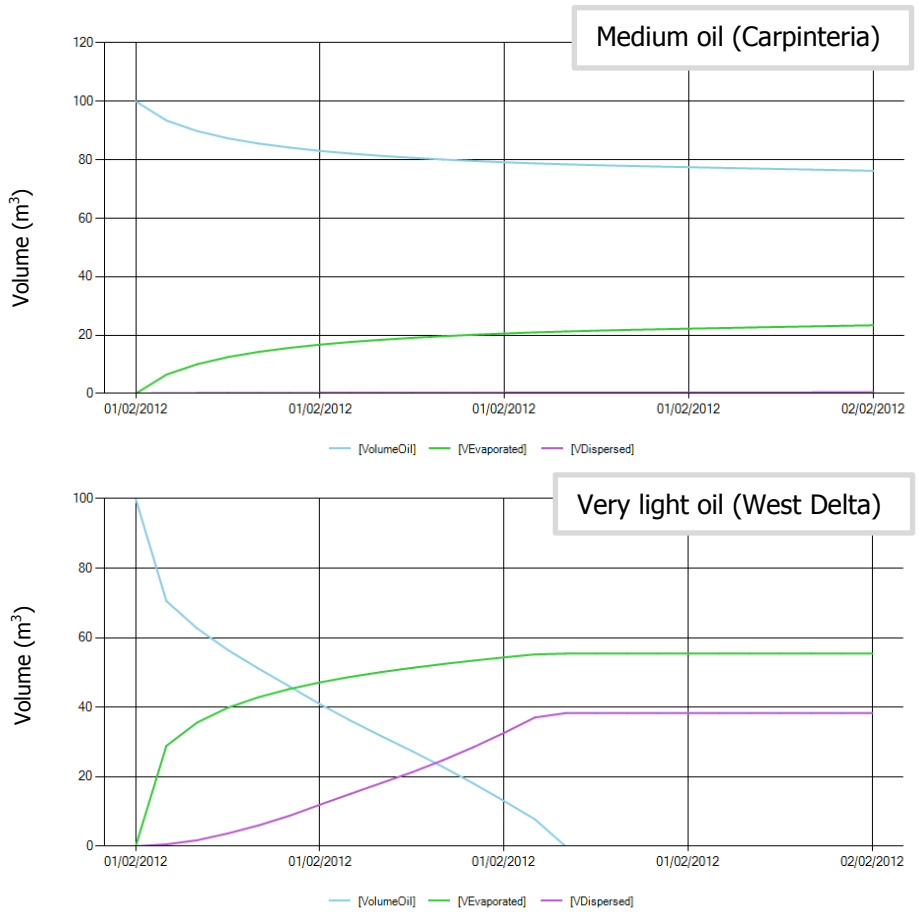

Figure 55 : Volume of oil total, evaporated and dispersed in m^3

6.2.4.5 Water content

This parameter is characteristic of the emulsification process whereby one liquid is dispersed into another liquid in the form of small droplets. Emulsification is responsible for the incorporation of water droplets in oil, changing substantially the oil viscosity and therefore its behaviour at sea. In fact, after evaporation, emulsification can be considered the most important transformation process (Fingas, 2008). **Figure 56** demonstrates that the water content of oil is increased for the medium oil (Carpinteria) up to 60%. Water content remains null for the very light oil.

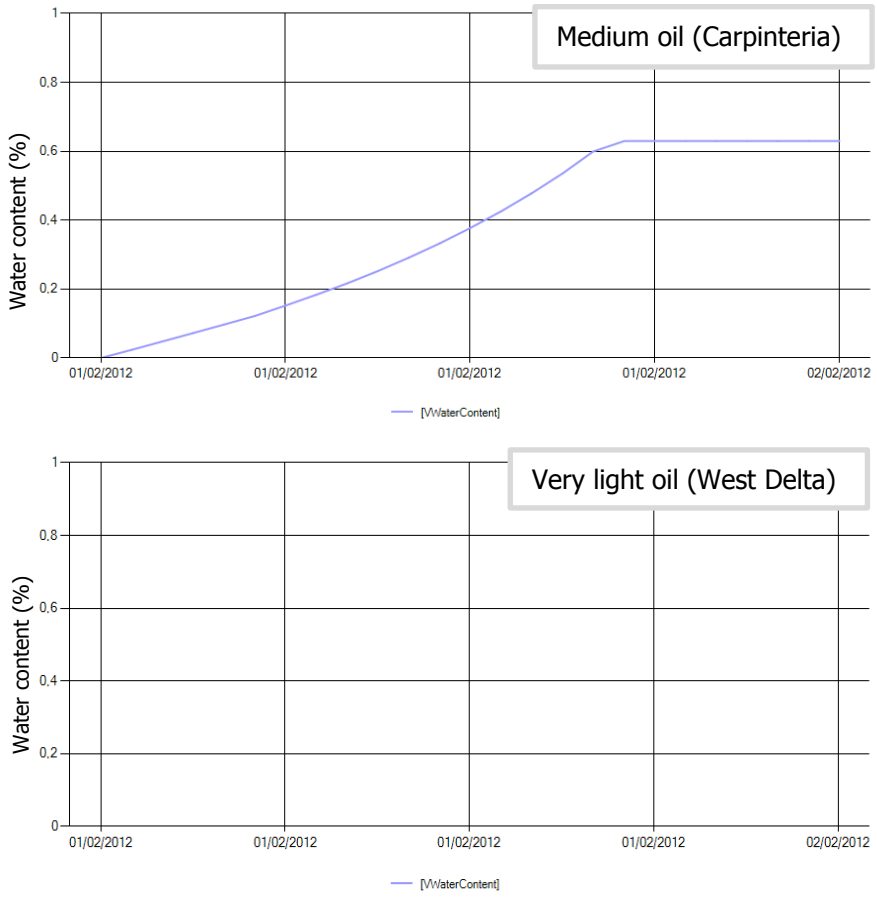

Figure 56 : Water content in oil plume in %

6.2.4.6 Synthesis

If we compare the analysis made in terms of behavior and impact for the two oil type, light oil and medium oil, it shows that we are dealing with two completely different events (

Table 12).

The light oil is dispersed in all environmental compartments (air, surface water, sediment and water column) and acted by physical and toxic effects on all biological communities.

This effect is especially significant for the sensitive area of La Rochelle where we have the immediate ecological effects kills and heavy contamination of marine species (shellfish, fish).

Medium fuel oil behaved more like a stain on the surface of the water essentially physical effects occurred mainly on seabirds.

Medium oil will emulsify quickly when spilled, creating a stable mousse that presents a more persistent cleanup and removal challenge. Even in high winds, usually over 80% of a Medium Oil spill will persist as floating or beached oil for some days or longer (Marchand, 2002).

According to literature, aromatic hydrocarbons are the main cause of the ecotoxicological impact of oil pollution on aquatic ecosystems. Asphaltenes and resins are heterocyclic molecules (N, S, O) with a high molecular weight. Also in this fraction are found metals such as nickel and vanadium. Effects on aquatic fauna and flora are poorly known and the evaluation of such polymers escapes almost completely chemical analysis (Marchand, 2002).

Group	**I**	**III**
Oil type	Light oil (West Delta)	Medium oil (Carpinteria)
Behavior and effects	Low persistence Short-term toxicity	Medium / high Persistence Toxic effect and smothering Effects
Spill response	None	Contain, recover, dispersing
Viscosity at 15ºC (cP)	1	164
Aromatic (% weight)	7	30
Saturates (% weight)	92	44
Resins (% weight)	1	17
Asphaltene (% weight)	-	9
Maximum water content of the emulsion (%)	-	72

Table 12 : Evolution of accidentally spilled oil and ecological consequences

After the short-term evolution, a long-term evolution can takes place over weeks, months or even years phase. This second phase of development is associated with the decontamination phase of the marine environment as a result of the energy levels of contaminated sites: solar (photo-oxidation), mechanical energy of the environment (natural dispersion), biological energy (biodegradation in vivo metabolism). Decontamination speeds are very different depending on polluted sites (sea water, coastline, sediment).

During this long-term development phase, the ecological effects result mainly by consecutive imbalances immediate effects: loss of species occurrence of opportunistic species, competition, back to the original balance. The monitoring carried out to assess the recovery of balances of origin is generally well correlated with the process of environmental decontamination (Marchand, 2002).

7. CONCLUSIONS

The hydrodynamic model has been validated for water level and Tidal harmonic analysis demonstrating good coherence comparing with field data. Temperature and salinity have also been validated for the hydrodynamic model using comparison with CTD vertical profiles and satellite data.

The model was applied using a nested configuration which enabled to transfer boundary conditions from the large scale to the local scale. A lagrangian model was coupled to the hydrodynamic model.

We have seen that oil spill modelling is a complex process depending on many parameters, meteorological, hydrodynamical and also oil weathering processes.

In term of plume trajectory, two main scenarios stand out. A winter scenario, where the oil spill is pushed off the coast due to wind stress. A summer scenario, where the oil spill follow tide current and tends to beach in coastal area. Wind appears to be the most important factor driving the oil spill trajectory. Nevertheless the scenario can become totally opposite in function of wind force and direction. Wind will be a major parameter to take into account for oil boom barrier location.

In term of oil weathering process, the types of oil spilled will completely transform the scenario in term of evolution of the spill, ecological consequences and emergency spill response. The various types of oil differ in how they weather (chemically or physically change when exposed to the elements). Most crude oil blends will emulsify quickly when spilled, creating a stable mousse that presents a more persistent cleanup and removal challenge. Even in high winds, usually over 80% of a Medium Oil spill will persist as floating or beached oil for some days or longer. On the other hand, over 90% of the Light Oil in a spill in the marine environment is either evaporated or naturally dispersed into the water column in time frames of a couple of hours to a couple of days.

Some process of oil weathering have been excluded for this analysis like dissolution and sedimentation, it can be interesting to study this process.

We can ameliorate this study by integrating different climatological scenarios for currents and weather of the last 10 years in La Rochelle, and also different kind of oil.

Future works to develop are the simulation of the oil barrier impact on the plume for different scenarios.

8. BIBLIOGRAPHIC REFERENCES

Ascione I., Fernandes R., Franz G., Campuzano F., Machado F., Campbell R., Muttin F., Neves R. Water fluxes and renewal rates at Pertuis d'Antioche/Marennes-Oléron Bay, France. Draft

Ascione I., Garcia A. C. and Neves R., 2012. Residence time of water in the Mondego estuary (Portugal). Estuarine, Coastal and Shelf Science 106: 13-22.

Ascione I., Fernandes R., Franz G., Pinto L., 2014. Hydrodynamic model Implementation at La Rochelle. ISDAMP.

Bacher C., 1989. Modélisation des écosystèmes conchylicoles : bassin de Marennes-Oléron – IFREMER.

Balseiro C.F., Carracedo P., Gómez B., Leitão P.C., Montero P., Naranjo L., Penabad E.& Pérez-Muñuzuri V. (2003). Tracking the Prestige Oil Spill. An operational Experience in Simulation at MeteoGalicia. Weather, 58: 452-458.

Bartolomeu L. B., Hydrodynamical and Ecological Modelling of the North Sea. Trabalho de Final de Curso (Graduation Thesis), Instituto Superior Técnico, Portugal, 2007.

Barusseau J.P., 1973. Evolution du plateau continental rochelais (Golfe de Gascogne) au cours du pleistocene terminal et de l'holocene: les processus actuels de la sedimentation. Thesis, University of Bordeaux, France.

Bertin X., Fortunato A., Oliveira A., 2009. Simulating morphodynamics with unstructured grids: description and validation of a modeling system for coastal applications. Ocean Modelling 28 (1–3), 75–87.

Bertin X., Castelle B., Chaumillon E., Butel R. and Quique R, 2008. Estimation and inter-annual variability of the longshore transport at a high-energy dissipative beach: the St Trojan beach, SW Oléron Island, France. Continental Shelf Research 28, 1316-1332.

Bertin X., Chaumillon E., Sottolichio A., Pedreros R., Tidal inlet response to sediment infilling of the associated bay and possible implications of human activities: the Marennes-Oleron Bay and the Maumusson Inlet, France, Continental Shelf Research 25 (2005) 1115–1131.

Bertin X., 2005. Morphodynamique séculaire, architecture interne et modélisation d'un système baie/embouchure tidale: le Pertuis de Maumusson et la baie de Marennes-Oléron. Thèse de Doctorat, Université de La Rochelle.

Bennett A.F., 2002. Inverse modeling of the ocean and atmosphere. Book.

Braunschweig F., Fernandes L. and Lourenço F. (2012). MOHID Studio User Guide. Lisbon.

Campuzano F. J., Fernandes R., Leitão P. C., Viegas C., de Pablo H., Neves R., 2012, Implementing local operational models based on an offline downscaling technique: The Tagus estuary case. 2.as Jornadas de Engenharia Hidrográfica. 105-108.

Cancino L. and Neves R. (1998). Hydrodynamic and sediment suspension modelling in estuarine systems. Part I: description of the numerical models. Journal of Marine Systems 22: 105-116.

Chaumillon E., Proust J.N., Menier D., Weber N., 2008. Incised-valley morphologies and sedimentary-Vlls within the inner shelf of the Bay of Biscay (France): a synthesis. Journal of Marine Systems 72, 383–396

Chaumillon E., Weber N., 2006. Spatial variability of modern incised valleys on the French Atlantic coast: comparison between the Charente and the Lay-Sèvre incised valleys. In R. Dalrymple, D. Leckie, R. Tillman, (Eds.), Incised valleys in time and space, vol. 85 (spec. pub.). Society of Economic Paleontologists and Mineralogists, Tulsa, 57–85.

Creocan, 2005. Etude des conditions naturelles en vue de l'extension du port des minimes. Ville de La Rochelle.

Delvigne G.A.L. and Sweeney C.E., "Natural Dispersion of Oil", Oil & Chem. Pollut. 4: 281–310, 1988.

Fay J. A., 1969. The spread of oil slicks on a calm sea. Oil on the Sea, Plenum Press, New York. pp. 53-63.

Fernandes R., Neves R., Viegas C., Leitão, P. 2013. Integration of an Oil and Inert Spill Model in a Framework for Risk Management of Spills at Sea – A Case Study for the Atlantic Area. Proceedings of the 36th AMOP Technical Seminar on Environmental Contamination and Response. 326-353.

Fernandes R., Modelação de Derrames de Hidrocarbonetos. Trabalho de Final de Curso (Graduation Thesis), Instituto Superior Técnico, Portugal, 2001 (In Portuguese).

Fernandes R., 2012. Improving maritime safety and Atlantic Regions coastal pollution response through technology transfer, training and innovation. Technical Report on HNS model implementation & Selection of HNS. ARCOPOLplus.

Fingas M., Models for Water-in-Oil Emulsion Formation. Oil Spill Science and Technology, Chapt. 10, Gulf Professional Publishing, UK, 2011.

Fingas M., A Review of Knowledge on Water-in-Oil Emulsions, in International Oil Spill Conference, pp. 1269-1274, Savannah, Georgia, 2008.

Fingas M. and Fieldhouse B., A Review of the Knowledge on Water-in-Oil Emulsions, Proceedings of the 29th Arctic Marine Oilspill Program Technical Seminar, Vancouver, British Columbia, Canada, Environment Canada, Ottawa, Ontario, Canada, pp.1-56, 2006.

Fingas M., 2004. Modeling evaporation using models that are not boundary-layer regulated. Journal of Hazardous Materials 107 (2004) 27–36.

Gouriou T., 2012. Evolution des composants du niveau marin à partir d'observations de marégraphie effectuées depuis la fin du 18eme siècle en Charente-Maritime. Thèse de doctorat, Université de la Rochelle.

Gonzalez J.L., Jouanneau J.M., Dominik J., Boutier B., 1991. Particulate Cd and Hg Wuxes to the sediment in the Marennes-Oléron Bay : origin and evolution. Environmental Technology 12, 209–216.

Instituto Superior Técnico, (2013), MOHID Water Modelling System, http://www.mohid.com/

ITOPF (« International Tanker Owners Pollution Federation »): http://www.itopf.org

Le Moine O., 2009. Impacts des différents fleuves côtiers. LER-PC Ifremer.

Le Moine O., Soletchnik P., Stanisiere, J.-Y., 2009 Caractérisation hydrologique des pertuis charentais, IFREMER.

Mackay D., Buistt I.A., Mascarenhas R. and Paterson S.. Oil Spill Processes and Models, Environment Canada Manuscript Report No. EE-8, Ottawa, Ontario, 1980.

Mackay D. and McAuliffe C. D. 1988. Fate of hydrocarbons discharge at sea. Oil and Chemical Pollution, 5, 1-20.

Macur O., 1999. Etude des courants de marée dans les Pertuis Charentais. SHOM n°564 EPSHOM/CH/GG/NP.

Marchand M., Les pollutions marines accidentelles. Au-delà du pétrole brut, les produits chimiques et autres déversements en mer. 2002

Mateus M., Riflet G., Chambel P., Fernandes L., Fernandes R., Juliano M., Campuzano F., de Pablo H. and Neves R. (2012). An operational model for the West Iberian coast: products and services. Ocean Science 8(4): 713-732.

Mateus M., Fernandes R., 2008. Modelling pollution : Oil spills and faecal contamination. R. Neves, J. Baretta & M. Mateus (eds.), IST Press. 89-96

Modéran J., Bouvais P., David V., Le Noc S., Simon-Bouhet B., Niquil N., Miramand P. and Fichet, D., 2010. Zooplankton community structure in a highly turbid environment (Charente estuary, France): Spatio-temporal patterns and environmental control. Estuarine, Coastal and Shelf Science, 88: 219–232.

Neves R., "The MOHID Concept", in Ocean Modelling for Coastal Management - Case Studies with MOHID, M. Mateus and R. Neves (eds.), IST Press, 2013.

Nicolle A., Karpytchev M.,2007 "Evidence for spatially variable friction from tidal amplification and asymmetry in the Pertuis Breton (France)", Continental Shelf Research 27 (2007) 2346–2356.

Nicolle A., 2006. Modélisation des marées et des surcotes dans les Pertuis Charentais. Thèse de Doctorat, Université de La Rochelle.

NOAA, 2000. ADIOStm (Automated Data Inquiry for Oil Spills) version 2.0. Seattle: Hazardous Materials Response and Assessment Division, NOAA. Prepared for the U.S. Coast Guard Research and Development Centre, Groton, CT. Observatoires du littoral, 2000.

NOAA, 1994. ADIOStm (Automated Data Inquiry for Oil Spills) user's manual. Seattle: Hazardous Materials Response and Assessment Division, NOAA. Prepared for the U.S. Coast Guard Research and Development Centre, Groton, CT.

http://www.observatoire-environnement.org/tbe/Liens-avec-des-enjeux-economiques,1905.html

Pawlowicz R., Beardsley B., Lentz S., Classical tidal harmonic analysis including error estimates in MATLAB using T_TIDE, Computers and Geosciences 28 (2002), 929-937

Poirier C., 2010, Enregistrements sédimentaires des changements environnementaux séculaires à millénaires par la micro- et la macrofaune benthiques littorales. Thèse de doctorat, Université de La Rochelle.

Poirier C., Sauriau P.-G., Chaumillon E., Bertin X., 2010. Influence of hydro-sedimentary factors on mollusc death assemblages in a temperate mixed tide-and-wave dominated coastal environment: Implications for the fossil record. Continental Shelf Research, October 2010, Volume 30, Issue 17, Pages 1876-1890.

Schillinger, S., 2000. Genèse et architecture d'une flèche sableuse: le Banc du Bucheron, ıle de Ré, France. Thesis, Univ. La Rochelle, France, 228pp.

Stiver W., Mackay, D., 1984. Evaporation rate of spills of hydrocarbons and petroleum mixtures. Environmental Science and Technology 18 (11), 834-840.

Strady E., Kervella S., Blanc G., Robert S., Stanisiere J.Y., Coynel A., Schafer, J., 2011, Spatial and temporal variations in trace metal concentrations in surface sediments of the Marennes Oleron Bay .Relation to hydrodynamic forcing, Continental Shelf Research 31(2011)997–1007.

Stanisiere J.-Y., Maurer, D., Dumas, F., 2007, Etude comparative des composantes hydrodynamiques de deux systèmes côtiers mésotidaux, les Bassins d'Arcachon et de Marennes-Oléron. 2007, IFREMER.

Stanisière J.Y., Dumas F., Plus M., Maurer D., Robert S., 2006. Caractérisation des composantes hydrodynamiques d'un système côtier semi-fermé : le bassin de Marennes-Oléron. Rapport technique., LER-PC Ifremer.

Tesson M., 1973. Aspects dynamiques de la sédimentation dans la baie de Marennes-Oléron (France). Thèse de Doctorat, Université Bordeaux 1.

Weber N., Chaumillon E., Tesson M., 2004. Enregistrement de la dernière remontée du niveau marin dans l'architecture d'une vallée incisée: le Pertuis Breton (Charente-Maritime). Compte Rendu Géoscience 336, 1273–1282.

Weber N., 2003. Morphologie, architecture des dépôts, évolution séculaire et millénaire du littoral charentais. Thèse de Doctorat, Université de La Rochelle.

Weber N., Chaumillon E., Tesson M., and Garland T., 2002, Architecture and morphology of the outer segment of a mixed tide and wave dominated incised-valley, revealed by pseudo 3D seismic reflection profiling: The paleo-Charente River, France: submitted to Marine Geology.

9. ANNEXES

Annex 1 – MOHID Oil Module Keywords

Description of the keywords used in the MOHID system to configure the following oil related processes: spreading, evaporation, dispersion, dissolution, sedimentation, chemical dispersion and mechanical clean up.

OUTPUT				
Keyword	**Type**	**Default**	**Units**	**Description**
OIL_TIMESERIE	Character	No default	-	Name of the output time series file
DT_OUTPUT_TIME	Character	No default	-	Time between output results
OIL GENERIC PROPERTIES				
Keyword	**Type**	**Default**	**Units**	**Description**
OILTYPE	Character	Crude	-	Oil type. Can be: Crude or Refined
API	Real	No default	-	American Petroleum Institute (API) Gravity
POURPOINT	Real	No default	ºC	Pour Point
TEMPVISCREF	Real	No default	ºC	Temperature of Reference Viscosity
VISCREF	Real	No default	cP	Reference Dynamic Viscosity
VISCCINREF	Real	No default	cP	Reference Cinematic Viscosity
OIL SPREADINGS				
Keyword	**Type**	**Default**	**Units**	**Description**
OIL_SPREADING	logical	1	-	Oil Spreading Process: 0 – false, 1- true
SPREADINGMETHOD	Character	No default	-	Method for Spreading: Fay/ThicknessGradient
USERCOEFVELMANCHA	Real	10	-	Empirical Thickness Gradient (typical values 5-30) Spreading Vel. Coef.
OIL DISPERION				
Keyword	**Type**	**Default**	**Units**	**Description**
OIL_ DISPERSION	logical	0	-	Oil dispersion process: 0 –false, 1- true
DISPERSIONMETHOD	Character	Delvigne	-	Method for dispersion: Delvigne/Mackay
OWINTERFACIALTENSION	Real	No default	Dyne/cm	Oil-Water Interfacial Tension (needed if DISPERSIONMETHOD = Mackay)

OIL DISPERSION (3D) (keywords from Lagrangian_1.dat)				
Keyword	**Type**	**Default**	**Units**	**Description**
METHOD_BW_DROPLETS_DIAMETER	Integer	1	-	method to obtain oil droplets diameter: 1-UserDefined_; 2-Computed_Half_D50_; 3-Computed_Classes_Random
DROPLETS_D50	Real	$50e^{-6}$	-	Median droplet diameter
METHOD_FLOAT_VEL	Integer	1	-	method to compute rising velocity of submerged droplets: 1-SoaresDosSantos_; 2-PADM_; 3-Zheng_
OIL DISSOLUTION				
Keyword	**Type**	**Default**	**Units**	**Description**
OIL_DISSOLUTION	logical	0	-	Oil dissolution process: 0 – false, 1- true
OIL SEDIMENTATION				
Keyword	**Type**	**Default**	**Units**	**Description**
OIL_SEDIMENTATION	logical	0	-	Oil sedimentation process: 0 – false, 1-true
OIL EVAPORATION				
Keyword	**Type**	**Default**	**Units**	**Description**
OIL_EVAPORATION	logical	0	-	Oil Evaporation Process: 0 – false, 1-true
EVAPORATIONMETHOD	Character	EvaporativeExposure		Method for Evaporation: EvaporativeExposure / Fingas
Evaporation Method = Fingas keywords				
FINGAS_EVAP_EQTYPE	Character	No default	-	Evaporation Equation Type: Logarithmic / SquareRoot
FINGAS_EVAP_EMP_DATA	Integer	0	-	Knowledge of Empirical Data for Evaporation
FINGAS_EVAP_CONST1	Real	No default	-	Empirical Constant only necessary If Fingas_Evap_Emp_Data=1
FINGAS_EVAP_CONST2	Real	No default	-	Empirical Constant only necessary If Fingas_Evap_Emp_Data=1
PERC_MASSDIST180	Real	No default	%	%(Weight) of Oil Evaporated until 180ºC only necessary If Fingas_Evap_Emp_Data=0
OIL EMULSIFICATION				
Keyword	**Type**	**Default**	**Units**	**Description**
OIL_ EMULSIFICATION	logical	0	-	Oil emulsification process: 0 – false, 1- true
EMULSIFICATIONMETHOD	Character	Rasmussen	-	Methods for Emulsification: Mackay / Rasmussen / Fingas
CEMULS	Real	0	%	Emulsification constant (%

				of evaporated oil before emulsification begins)
MAXVWATERCONTENT	Real	null_real	%	Maximum Volume Water Content (only needed when EMULSIFICATIONMETHOD = Mackay or Rasmussen)
ASPHALTENECONTENT	Real	-	%	Asphaltene Content (only needed when EMULSIFICATIONMETHOD = Fingas or Rasmussen)
WAXCONTENT	Real	-	%	Wax Content (only needed when EMULSIFICATIONMETHOD = Rasmussen)
EMULSPARAMETER	Real	1.6E-6	-	Water Uptake parameter (typical values 1E-6 to 2E-6)
Emulsification Method = Fingas keywords				
RESINCONTENT	Real (%)	No default	-	Resine Content
SATURATECONTENT	Real (%)	No default	-	Saturate Content
OIL CHEMICAL DISPERSION				
Keyword	**Type**	**Default**	**Units**	**Description**
OIL_CHEM_DISPERSION	logical	0	-	Chemical Dispersants Application: 0 – false, 1- true
P_AREA_SPRAYED	Real	No default	%	% of Spill Area sprayed with dispersant
EFFICIENCY	Real	No default	%	% of Area sprayed effectively dispersed
START_CHEM_DISPERSION	YYYY MM DD HH MM SS	Start (see model_x.dat)	-	Starting Time of Dispersant Application
END_CHEM_DISPERSION	YYYY MM DD HH MM SS	End (see model_x.dat)	-	Ending Time of Dispersant Application
OIL MECHANICAL CLEANUP				
Keyword	**Type**	**Default**	**Units**	**Description**
OIL_MEC_CLEANUP	logical	0	-	Mechanical Cleanup Operation: 0 – false, 1- true
RECOVERY_ DATAFORM	Character	No default	%	Data units of emulsion recovered: Rate [l/h] / Amount [l]
RECOVERY	Real	No default	[l/h] or [l]	rate or volume of Emulsion Recovered
START_MEC_CLEANUP	YYYY MM DD HH MM SS	Start (see model_x.dat)	-	Starting Time of Mechanical Cleanup Operation
END_MEC_CLEANUP	YYYY MM DD	End (see	-	Ending Time of Mechanical

Annex 2 - Oil classes group and MOHID parameters

The ADIOS data base defined the follow oil classes group:

- Class 1 – Very light oils - (Jet Fuels, Gasoline); API(15ºC)>45.0
- Class 2 – Light oils - (Diesel, No. 2 Fuel Oil, Light Crudes); 45.0>API(15ºC)>35
- Class 3 – Medium oils - (Most Crude Oils); 35 >API(15ºC)> 17.5
- Class 4 – Heavy oils - (Heavy Crude Oils, No. 6 Fuel Oil, Bunker C);API(15ºC)< 17.5

Processes connect in the MOHID oil model for each of the oil classes listed above (1 – connected, 0 – not connected).

Name	ID	Beaching	Spreading	Evaporation	Dispersion	Emulsification	Dissolution	Sedimentation
Inert	0	0	1	0	0	0	0	0
Very Light Oils (Jet Fuels, Gasoline)	1	1	1	1	1	1	1	1
Light Oils (Diesel, No. 2 Fuel Oil, Light Crudes)	2	1	1	1	1	1	1	1
Medium Oils (Most Crude Oils)	3	1	1	1	1	1	1	1
Heavy Oils (Heavy Crude Oils, No. 6 Fuel Oil, Bunker C)	4	1	1	1	1	1	1	1

Parameters assumed in the MOHID oil model for each of the oil classes listed above. The viscosity values were estimated based in the function presented in Figure 1. The maximum water content and the Oil-Water Interfacial Tension values were assumed equal to the values assumed in the model Oil Map (ASA, 2009).

Name	API	Product Type	Viscosity	Visc. Temp. ref.	Max. water content	Oil water tension
Inert	30	Crude	39	15	0	26
Very Light Oils (Jet Fuels, Gasoline)	50	Crude	2	15	0	26
Light Oils (Diesel, No. 2 Fuel Oil, Light Crudes)	40	Crude	8	15	30	26
Medium Oils (Most Crude Oils)	30	Crude	39	15	70	20
Heavy Oils (Heavy Crude Oils, No. 6 Fuel Oil, Bunker C)	13	Crude	3603	15	80	20

Annex 3 – Scenario La Rochelle February 2012 (Wind stress)

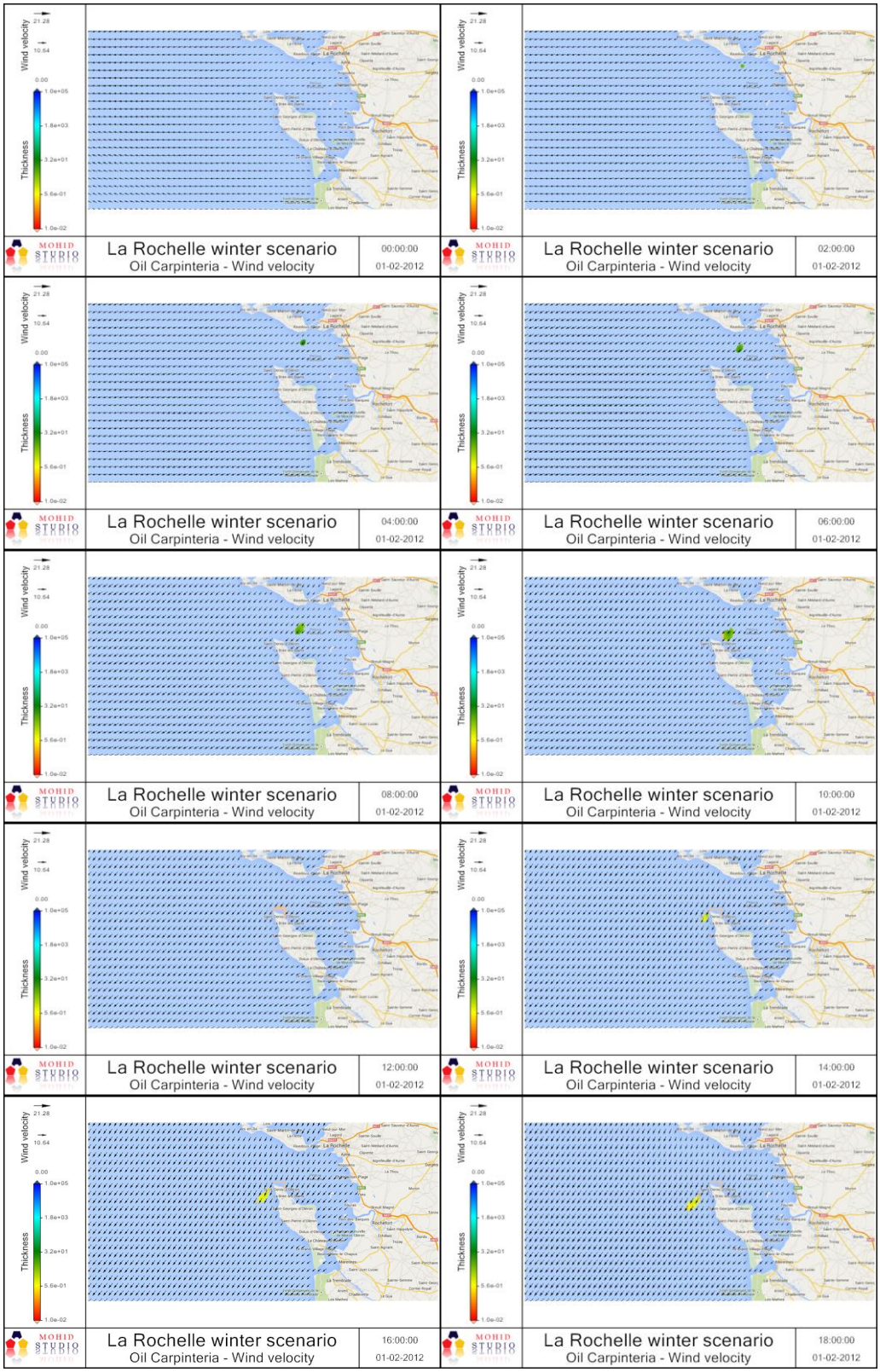

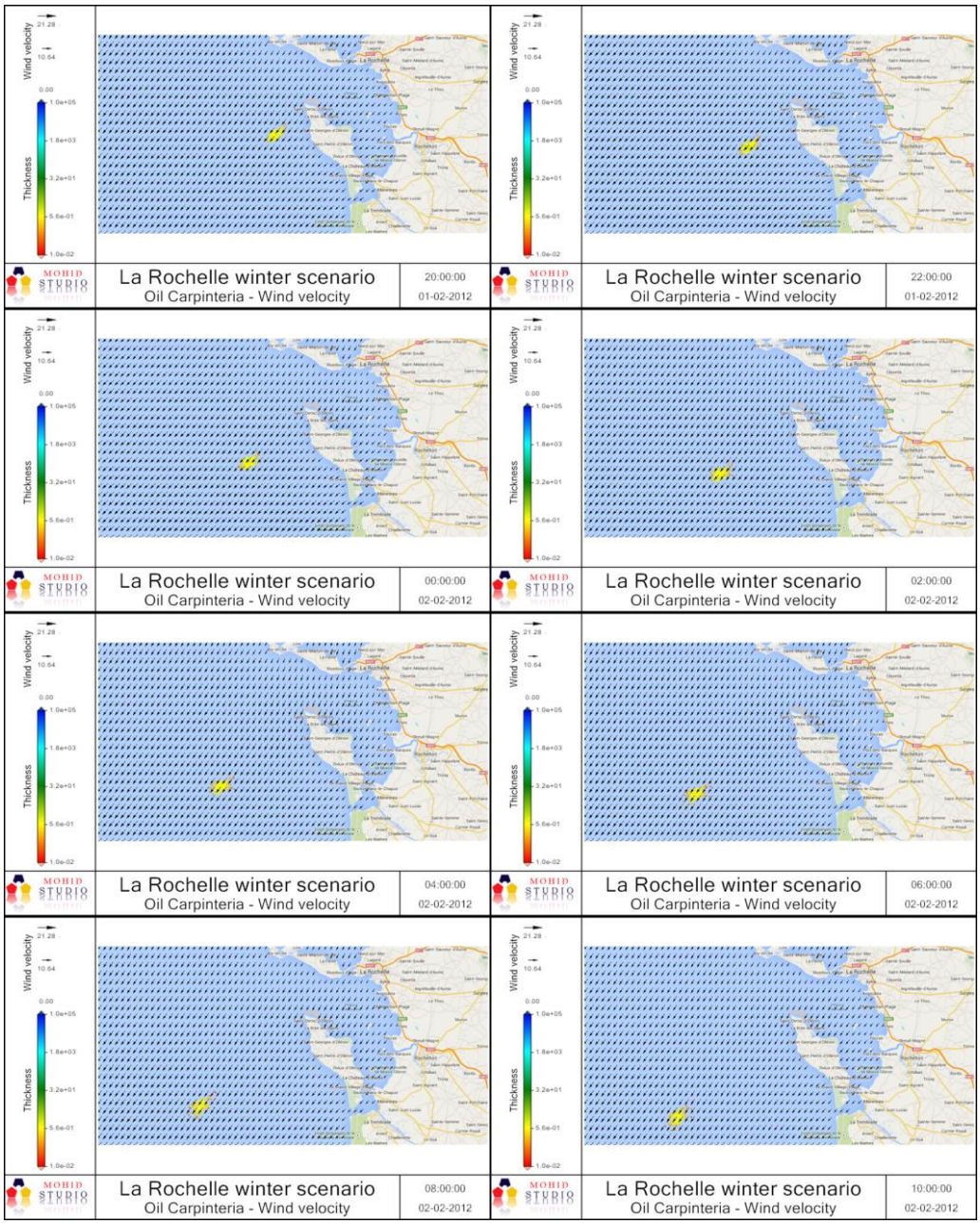
Wind velocity
21.28
10.64
0.00
Thickness
1.0e+05
1.8e+03
3.2e+01
5.6e-01
1.0e-02
MOHID STUDIO
La Rochelle winter scenario
Oil Carpinteria - Wind velocity
20:00:00
01-02-2012
La Rochelle winter scenario
Oil Carpinteria - Wind velocity
22:00:00
01-02-2012
La Rochelle winter scenario
Oil Carpinteria - Wind velocity
00:00:00
02-02-2012
La Rochelle winter scenario
Oil Carpinteria - Wind velocity
02:00:00
02-02-2012
La Rochelle winter scenario
Oil Carpinteria - Wind velocity
04:00:00
02-02-2012
La Rochelle winter scenario
Oil Carpinteria - Wind velocity
06:00:00
02-02-2012
La Rochelle winter scenario
Oil Carpinteria - Wind velocity
08:00:00
02-02-2012
La Rochelle winter scenario
Oil Carpinteria - Wind velocity
10:00:00
02-02-2012

Annex 4 – Scenario La Rochelle June 2012 (Hydrodynamic)

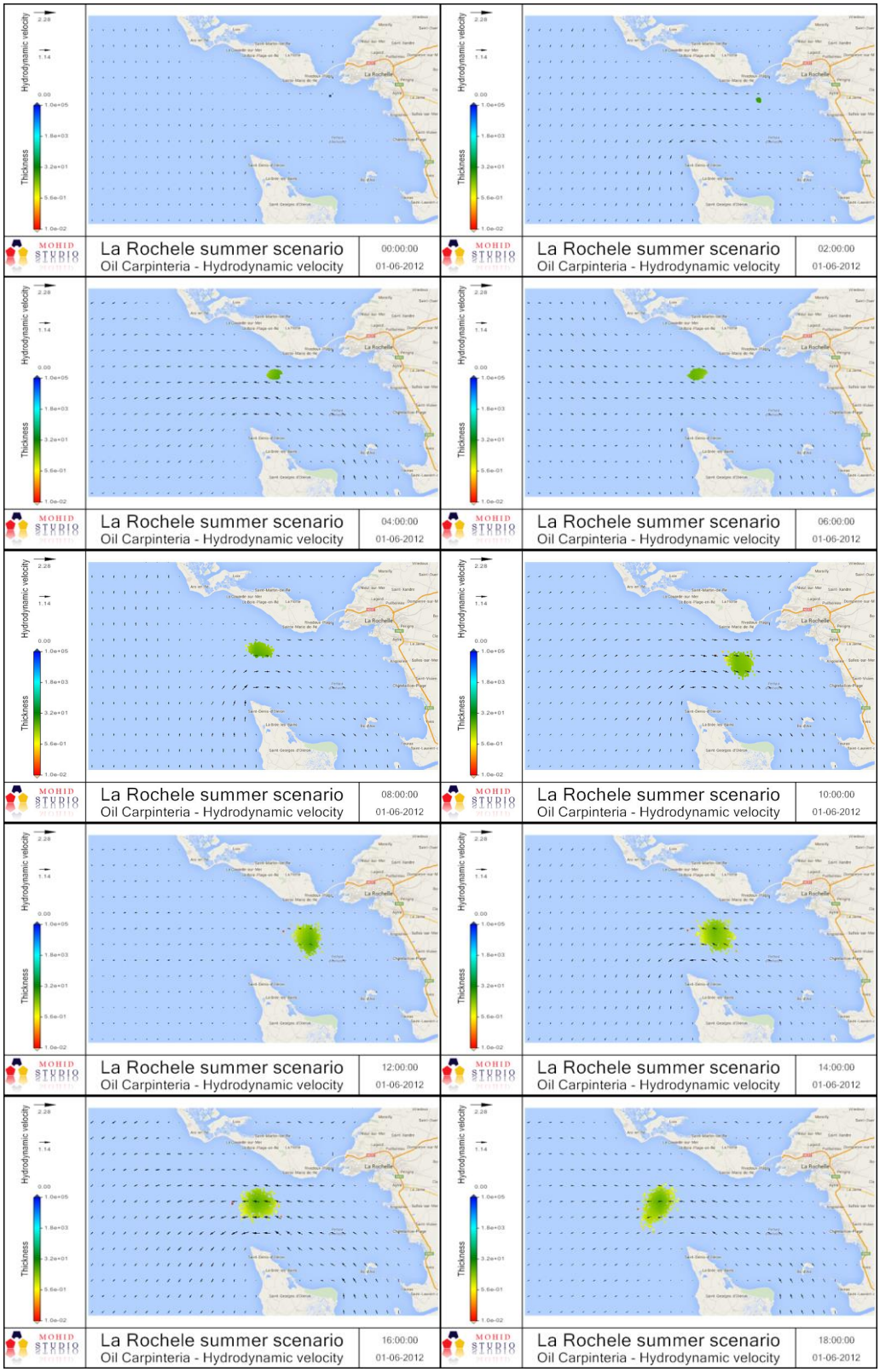

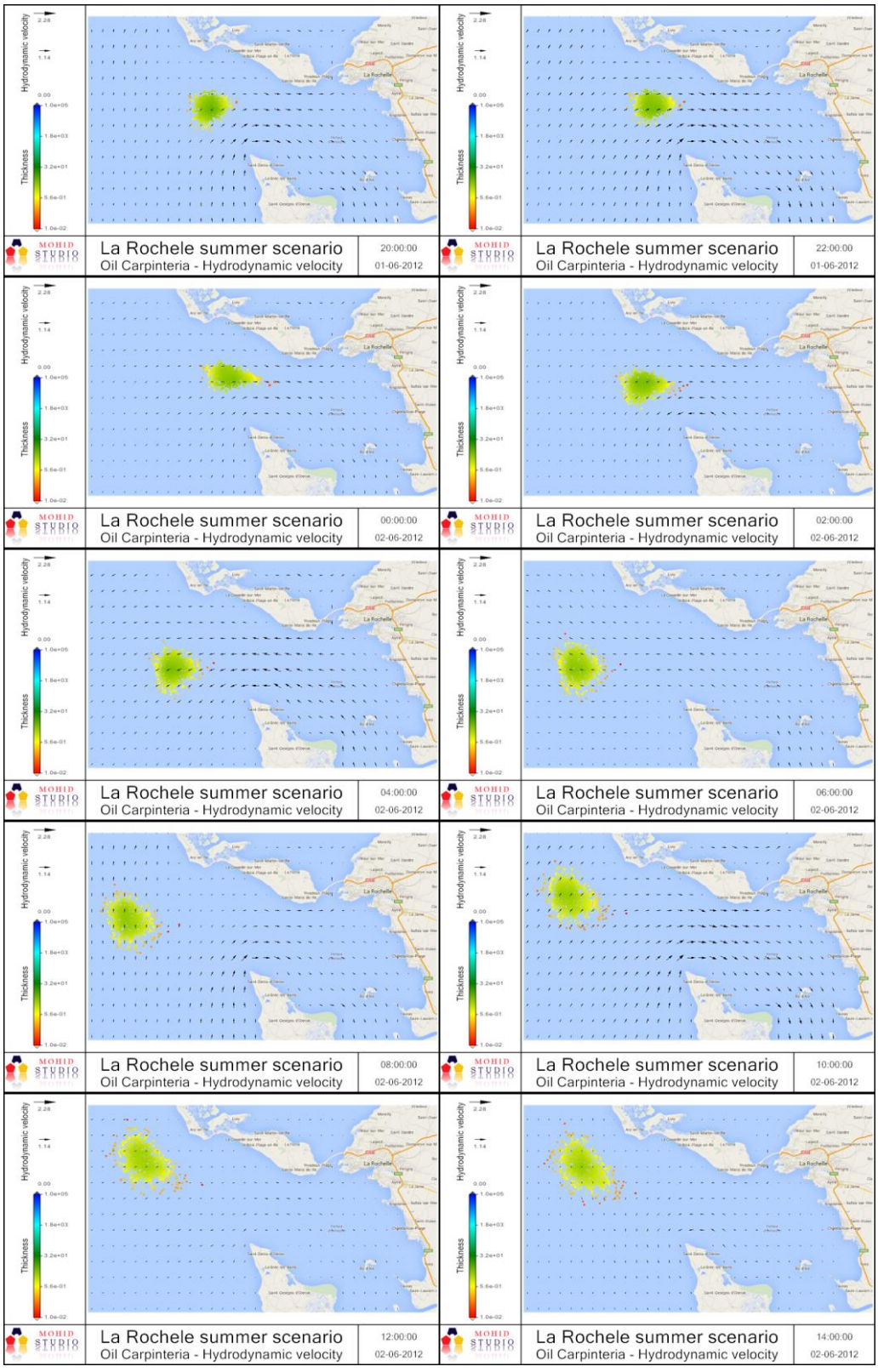
Hydrodynamic velocity
Thickness
La Rochele summer scenario
Oil Carpinteria - Hydrodynamic velocity
20:00:00
01-06-2012
La Rochele summer scenario
Oil Carpinteria - Hydrodynamic velocity
22:00:00
01-06-2012
La Rochele summer scenario
Oil Carpinteria - Hydrodynamic velocity
00:00:00
02-06-2012
La Rochele summer scenario
Oil Carpinteria - Hydrodynamic velocity
02:00:00
02-06-2012
La Rochele summer scenario
Oil Carpinteria - Hydrodynamic velocity
04:00:00
02-06-2012
La Rochele summer scenario
Oil Carpinteria - Hydrodynamic velocity
06:00:00
02-06-2012
La Rochele summer scenario
Oil Carpinteria - Hydrodynamic velocity
08:00:00
02-06-2012
La Rochele summer scenario
Oil Carpinteria - Hydrodynamic velocity
10:00:00
02-06-2012
La Rochele summer scenario
Oil Carpinteria - Hydrodynamic velocity
12:00:00
02-06-2012
La Rochele summer scenario
Oil Carpinteria - Hydrodynamic velocity
14:00:00
02-06-2012

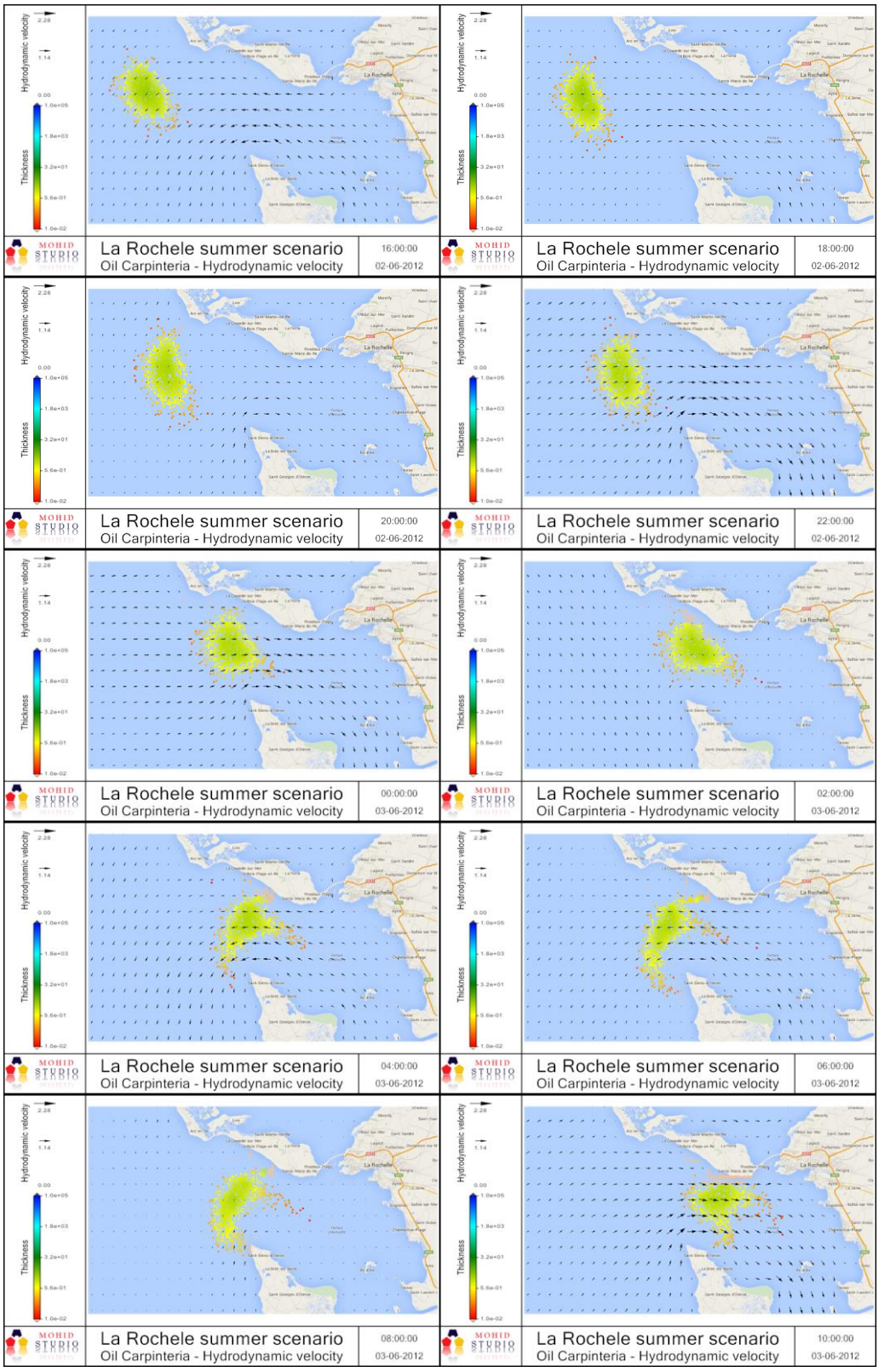
Hydrodynamic velocity
Thickness
La Rochele summer scenario
Oil Carpinteria - Hydrodynamic velocity
16:00:00
02-06-2012
La Rochele summer scenario
Oil Carpinteria - Hydrodynamic velocity
18:00:00
02-06-2012
La Rochele summer scenario
Oil Carpinteria - Hydrodynamic velocity
20:00:00
02-06-2012
La Rochele summer scenario
Oil Carpinteria - Hydrodynamic velocity
22:00:00
02-06-2012
La Rochele summer scenario
Oil Carpinteria - Hydrodynamic velocity
00:00:00
03-06-2012
La Rochele summer scenario
Oil Carpinteria - Hydrodynamic velocity
02:00:00
03-06-2012
La Rochele summer scenario
Oil Carpinteria - Hydrodynamic velocity
04:00:00
03-06-2012
La Rochele summer scenario
Oil Carpinteria - Hydrodynamic velocity
06:00:00
03-06-2012
La Rochele summer scenario
Oil Carpinteria - Hydrodynamic velocity
08:00:00
03-06-2012
La Rochele summer scenario
Oil Carpinteria - Hydrodynamic velocity
10:00:00
03-06-2012

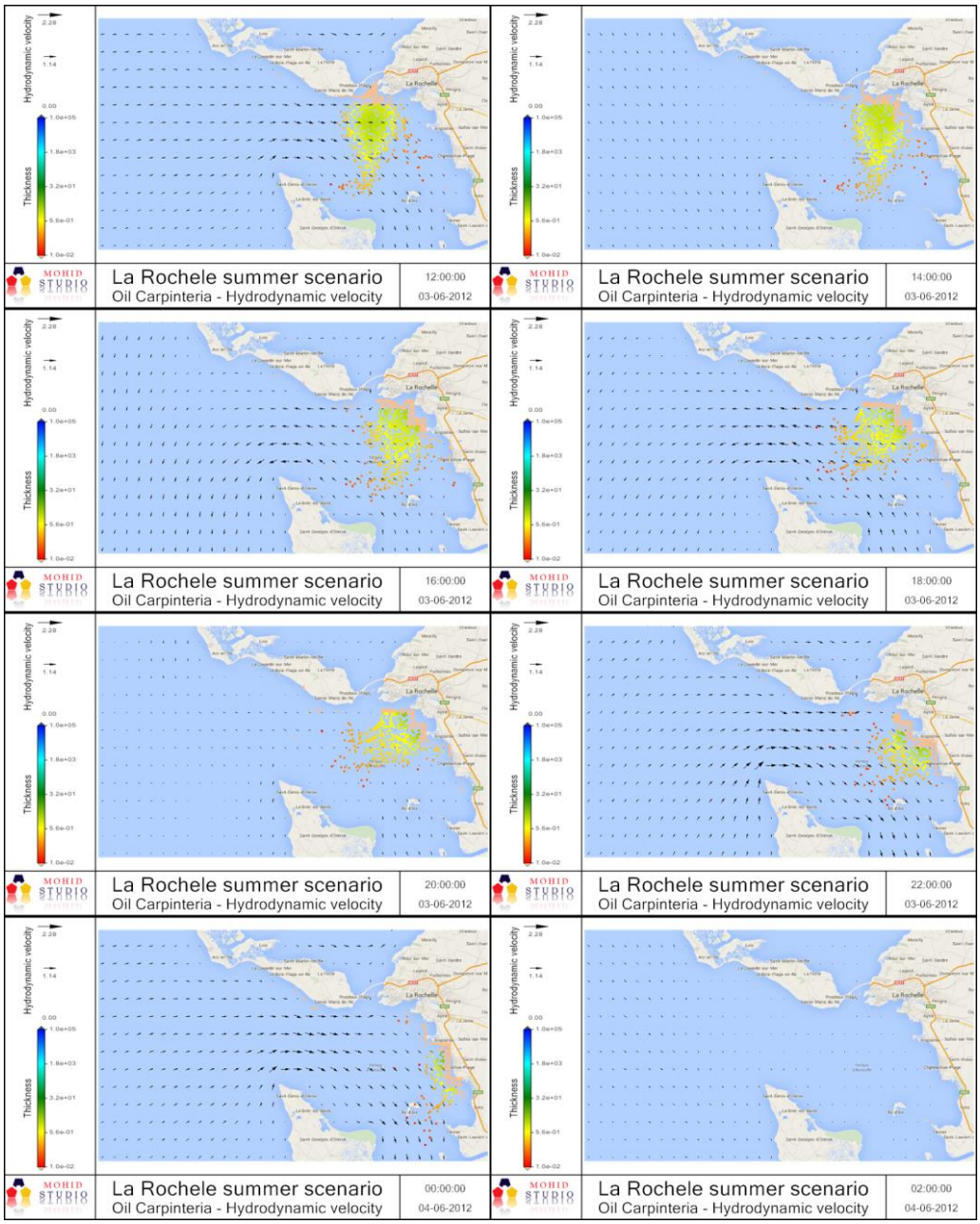
Hydrodynamic velocity
Thickness
MOHID STUDIO
La Rochele summer scenario
Oil Carpinteria - Hydrodynamic velocity
12:00:00
03-06-2012
La Rochele summer scenario
Oil Carpinteria - Hydrodynamic velocity
14:00:00
03-06-2012
La Rochele summer scenario
Oil Carpinteria - Hydrodynamic velocity
16:00:00
03-06-2012
La Rochele summer scenario
Oil Carpinteria - Hydrodynamic velocity
18:00:00
03-06-2012
La Rochele summer scenario
Oil Carpinteria - Hydrodynamic velocity
20:00:00
03-06-2012
La Rochele summer scenario
Oil Carpinteria - Hydrodynamic velocity
22:00:00
03-06-2012
La Rochele summer scenario
Oil Carpinteria - Hydrodynamic velocity
00:00:00
04-06-2012
La Rochele summer scenario
Oil Carpinteria - Hydrodynamic velocity
02:00:00
04-06-2012